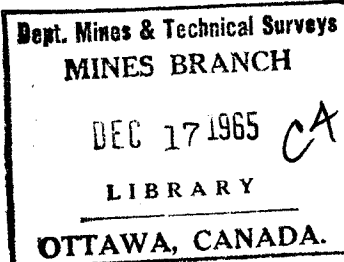CANADA

DESIGN AND CONSTRUCTION OF A FACILITY FOR RESEARCH ON THE INELASTIC BEHAVIOR OF GEOLOGIC MATERIALS

H. R. HARDY. JR.

DEPARTMENT OF MINES AND TECHNICAL SURVEYS, OTTAWA

MINES BRANCH

RESEARCH REPORT

R 165

FUELS AND MINING PRACTICE DIVISION

SEPTEMBER 1965
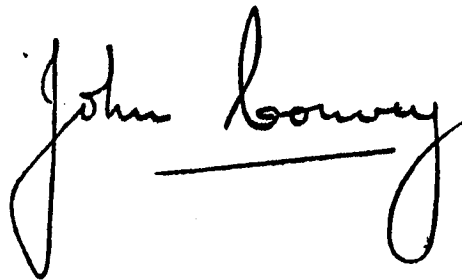
FOREWORD

The Mines Branch conducts long-term research programs on physical properties of rocks in the Physics Section of the Fuels and Mining Practice Division with the objective of applying the knowledge obtained in these continuous programs to practical problems. Thus, there is recognition of the importance of the time dependency of rocks in relation to the design of mine structures, but a suitable facility capable of accurate measurements and therefore requiring advanced control systems was not available until the author undertook the design and construction of the necessary apparatus.

It was a happy coincidence that the Virginia Polytechnic Institute accepted the study of the inelastic behavior of rocks as a thesis topic as part requirement for a higher degree. This research report, based on the section of the thesis text dealing with the constructional features of the facility, is published in the light of considerable interest shown by numerous enquiries on the equipment designed and constructed by the author.

John Convey,
Director,
Mines Branch.

Mines Branch Research Report R 165

DESIGN AND CONSTRUCTION OF A FACILITY FOR RESEARCH ON THE INELASTIC BEHAVIOR OF GEOLOGIC MATERIALS[*]

by

H.R. Hardy, Jr.[**]

- - -

ABSTRACT

This report describes the design and construction of a facility for research on the inelastic behavior of geologic materials. It includes the development of the following: a room-sized constant temperature enclosure capable of maintaining temperatures constant to $\pm 1/5^{\circ}$C; a programmable pneumatic-hydraulic axial loading system, which makes it possible to carry out creep, stress relaxation, constant rate of straining, constant rate of loading and cyclic loading experiments; and a system for accurate measurement and recording of strain, stress, confining pressure and temperature. Also included are details on the preparation and strain gaging of test specimens.

Direction des mines

Rapport de recherches R 165

CONCEPTION ET CONSTRUCTION D'UNE INSTALLATION POUR LA RECHERCHE SUR LE COMPORTEMENT NON ÉLASTIQUE DE CERTAINS MATÉRIAUX DES COUCHES GÉOLOGIQUES*

H. R. Hardy, Jr. **

RÉSUMÉ

Ce rapport décrit la conception et la construction d'une installation pour la recherche sur le comportement non élastique de certains materiaux des couches géologiques. Il touche à la mise au point de ce qui suit: un espace fermé de la dimension d'une chambre ordinaire où il est possible de maintenir une certaine température à $\pm$ 1.5 °C près; un système de compression axiale, pneumatique et hydraulique, qui permet d'exécuter un programme d'expériences sur le fluage, le relâchement des contraintes, la constance du taux de déformation, la vitesse de répartition des charges et les surcharges alternées; et enfin un système de mesurage précis et d'enregistrement des déformations, des contraintes, des pressions dynamiques et des températures. L'auteur donne également des détails sur la préparation et la mesure des déformations des éprouvettes.

---

*Ce rapport fait partie d'une thèse de doctorat soumise au Department of Engineering Mechanics, Virginia Polytechnic Institute, Blacksburg, Va., en juin 1965.

**Chargé de recherches, Section de la physique, Division des combustibles et du génie minier, Direction des mines, ministère des Mines et des Relevés techniques, Ottawa, Canada.

LIST OF FIGURES

LIST OF FIGURES (Cont'd)

LIST OF FIGURES (Concluded)

LIST OF TABLES

1.1 Introduction

The study of the mechanical properties of geologic materials was initiated in the Mining Research Section of the Fuels and Mining Practice Division, Mines Branch, Canadian Department of Mines and Technical Surveys, in 1951 as part of a fundamental study of ground stress in Canadian coal mines (4)[*]. The initial work was restricted to short-period tests on typical mine rock under uniaxial compressive stress, but, as the importance of the "time factor" became more obvious, studies were undertaken to investigate inelastic (time-dependent) behavior. These studies, which were initiated in 1957, consisted mainly of a comprehensive literature search on the subject, and the initial development of experimental facilities (20, 21). This research project was inactive during the period 1959-1961 due in part to the relocation of laboratory facilities.

In the fall of 1961 the project was reactivated with the proposed research program being broadly outlined as follows:

"To study experimentally the inelastic behavior of selected geologic materials and to analyse these experimental data using the concept of mechanical models and the analytical methods of visco-elasticity. In particular, to develop governing equations for these materials based on suitable laboratory experiments and valid at least within a range of stress, confining pressure, duration of loading, and temperature consistent with practical applications".

A more detailed discussion of the overall research program has been presented by the writer (Hardy (23)) in a recent paper.

The initial phase of this program involved the development of a suitable deformation facility and associated experimental techniques for conducting deformation experiments, under uniaxial compressive stress, on small laboratory sized specimens of rocks and minerals. The loading system, which is basically an "on-off" pneumatic-hydraulic servo system, was designed to provide a wide range of test modes. These allow creep, stress relaxation, constant rate of straining, constant rate of loading, and cyclic loading experiments to be carried out.

To date relatively few workers have undertaken detailed investigations into the inelastic behavior of geologic materials. This has been due in part to the many experimental difficulties that must be overcome if significant data are to be obtained. This report describes the design and construction of the final facility, and, as well, discusses the

---

[*]References are at the end of this report.

various experimental difficulties and the methods developed to overcome them. In all, the development of the final experimental facilities has taken approximately three years, and represents a total of approximately five man-years labour.

1.2 Test Area

1.2.1 Introduction

Early experiments by the writer (18) had indicated the necessity of conducting any fundamental static and quasi-static deformation experiments on geologic materials, particularly those under uniaxial stress, in a controlled environment. Such conditions are necessary due to the fact that the control and measuring systems, as well as the test materials themselves, are sensitive to temperature and humidity variations. For example, the temperature coefficients of a number of typical Canadian shales and sandstones (25) have been found to be in the range of 10-15 μs/^{o}C[*]. Thus a change in room temperature of 10°C would result in an error of 100-150 μs in the observed strain, which could be equivalent to the total time-dependent strain observed in a 10 day creep test. Many geologic materials are similarly sensitive to moisture. The design of a suitable test enclosure and temperature and humidity control system was begun early in 1961[**].

A number of other features were considered necessary for a satisfactory test area. These included the use of antivibration mounting bases for the loading frames to reduce as much as possible the effects of local vibration[+]; the development and installation of suitable electrical and pneumatic supplies to allow uninterrupted long period operation of the control and measurement systems independent of local power; and the installation of an extensive network of highly stable and well shielded electrical circuits for the control and monitoring systems. Figure 1 shows a general floor plan of the test enclosure and the surrounding area.

---

[*] For brevity "μs" is written for "microstrain", representing a strain of 10^{-6}.

[**] The initial design of the enclosure and the temperature and humidity control system was carried out by Dr. W. M. Gray of the Fuels and Mining Practice Division, Mines Branch, during the spring and summer of 1961 while the writer was in attendance at V.P.I.

[+] The building housing the test facility was located adjacent to a heavily travelled main street and was subject to vibrations from explosive studies and heavy machinery in adjacent buildings.
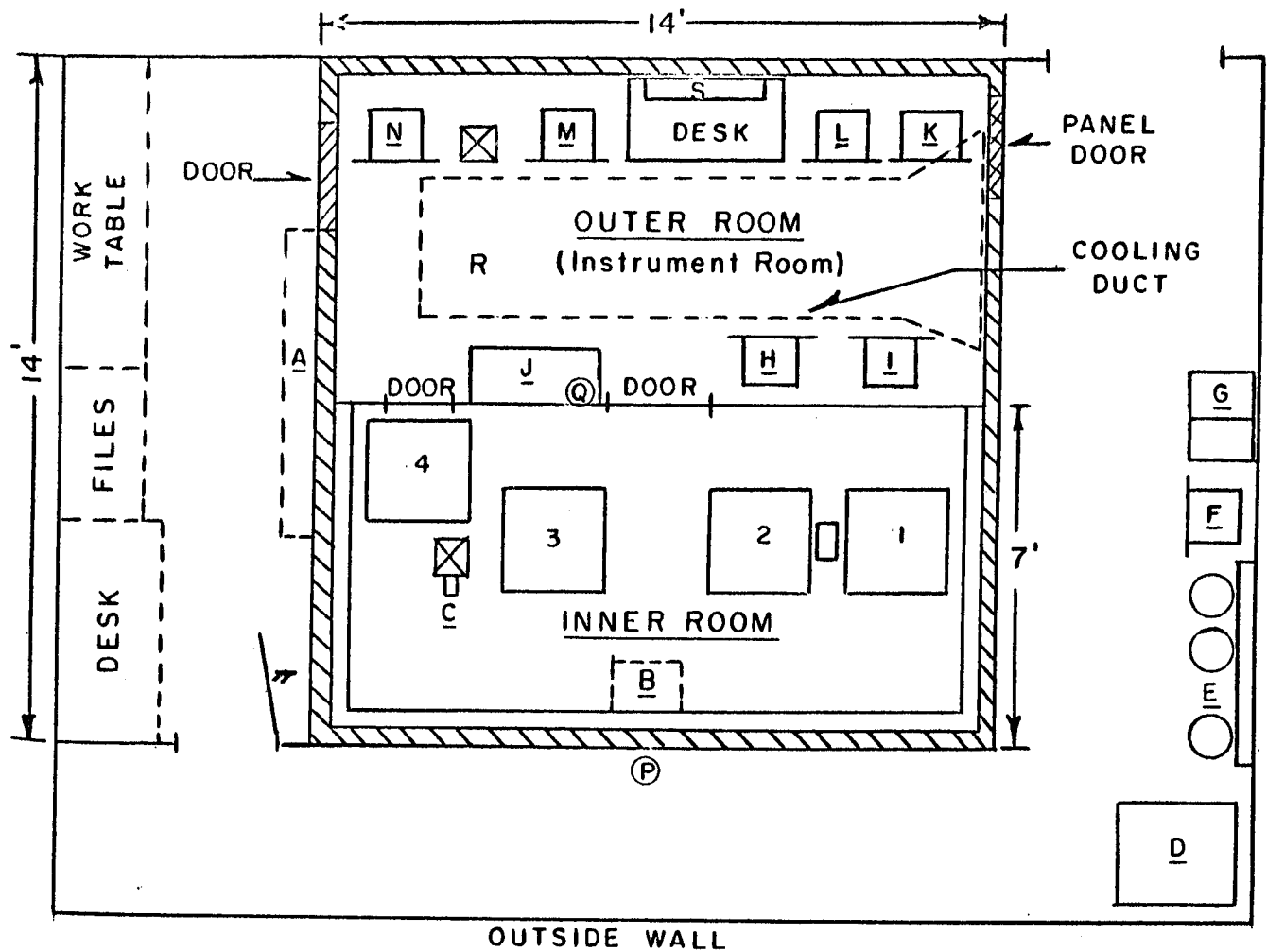
A - Temp. and Humidity Control Panel
B - Humidifier
C - Humidity Transducer
D - Compressor
E - Nitrogen Gas Supply
F - Standby Power and Battery Charger
G - Storage Batteries
H, I - Load and Pressure Control Racks
      (Type A Loading Machines)
J - 2-Channel "Fast" X-T Recorder

K - Operations Control Rack
L - Manual Readout Rack
M - 12-Channel "Slow" X-T Recorder
N - Y-XT Recording System

P - External Thermostat
Q - Room Thermostat
R - Duct Thermostat
1, 2, 3, 4 - Antivibration Bases

FIGURE 1 - Plan View of Test Enclosure.

1.2.2 The Enclosure

The location selected for the test area was a second storey laboratory area with a poured concrete subfloor that had originally supported heavy machinery. The base of the enclosure itself was constructed on the existing wooden floor, but concrete bases to support the heavy loading frames were poured directly onto the concrete subfloor. The test enclosure measures 14' x 14' x 10' high overall with a six foot hall on three sides and a three foot space between its roof and the existing ceiling. The structure consists of an outer insulated shell and a smaller inner shell as shown in Figure 2. Effectively, the inner shell is a room within a room, since the air in the outer shell circulates freely around it on all sides. The construction hence defines two areas, an inner room that houses the loading frames, and an outer room containing the control and monitoring systems.

The outer shell is approximately 14' x 14' x 10' high O.D. and was framed using wooden two-by-fours. A layer of foil vapour barrier was first placed on the existing floor, and the base constructed with the two-by-fours on edge lying east-west. The space between the framing was filled with rock wool insulating batts and a dust barrier consisting of a layer of heavy paper tacked over the framing to prevent loose rock wool fibres being picked up by the circulating air. A second set of two-by-fours on edge, running north-south was then erected. The inner floor of 3/4 inch plywood was then nailed to this set of two-by-fours leaving an open space seven inches wide across both ends. This allowed air to circulate through the airways formed by the top set of two-by-fours. Figure 2D illustrates some details of this construction. The wall framing was then erected followed by the roof and the center wall. The rough 110 V a-c wiring for lights and power outlets was installed at this stage. The roof and outer shell walls were then insulated with four-inch thick batts of rock wool, foil vapour barrier was applied to the outer side of the wall and roof, and these surfaces were sheeted inside and outside with 1/2 inch thick plaster board. Both sides of the center wall were sheeted with similar material. Figure 2E illustrates the construction used on the outer shell.

The main function of the inner shell was to form a vapour-tight seal around the inner room to provide an area where deformation experiments on materials subjected to various humidity conditions could be carried out. First the framework of the inner shell was erected. Holes were cut in the floor, and wells constructed to take the loading frame bases. Details of these wells are shown in Figure 2C. Where the construction of a well caused a serious blockage of the airways, an arched opening was made in the well panel (see Figure 2D, edge view) to allow the air to circulate around the bases once they were installed. At this stage of construction the joints on the inside walls and ceiling of the outer shell and the center wall were plastered. The inside walls and ceiling were then painted along with the inner shell framework. The loading frame bases were cast in position
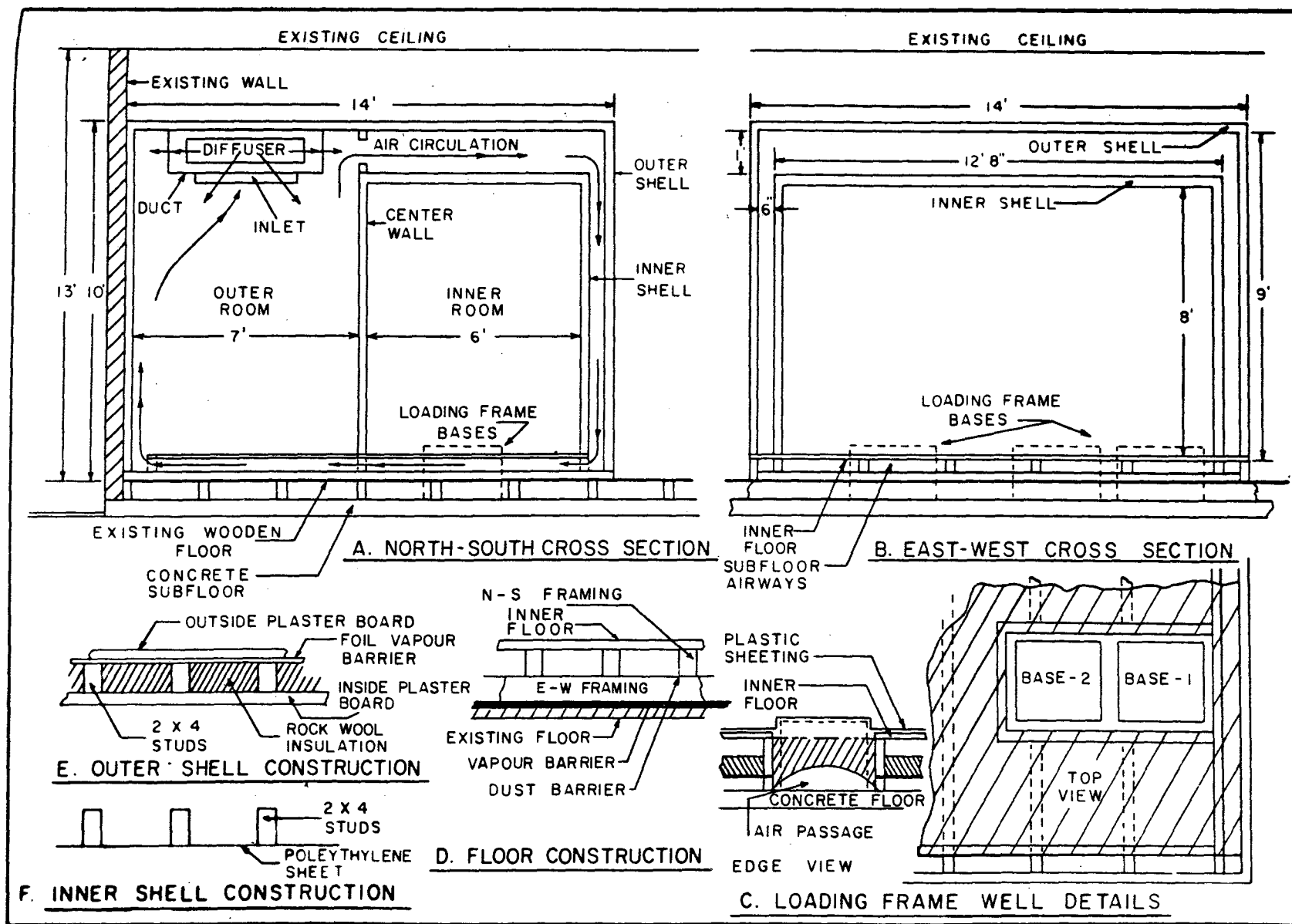
FIGURE 2 - Construction Details of Test Enclosure.

and the concrete allowed to cure for about two weeks. The walls, ceiling and floor of the inner shell were then covered with No. 6 gauge clear polyethylene sheet*, which was supplied in rolls six feet wide. This was attached to the inside of the inner shell frame using small flat-headed tacks after first applying a 3/4 inch strip of cloth masking tape+ over the sheet along each tacking line in order to prevent tearing.

The construction of the enclosure was completed by the installation of a heavy insulated door and removable door panel (see Figure 1 for location), the installation of corrugated rubber matting on the floors of the inner and outer rooms and the installation of lighting fixtures and 110 V a-c outlets.

1.2.3 Temperature Control System

The system used to control the temperature of the test enclosure is based on a design suggested by Solvason (45). Figure 3 illustrates the main features of the system. Basically it consists of a cooling section, a reheating section and an electrical control section. In operation, air from the outer room is drawn up into a duct (in the ceiling of this room) and passed through a set of cooling coils, which lowers its temperature below that of the outer room. This cooled air is then forced over a set of heating coils and its temperature raised to some higher value. The reheated air is passed out a diffuser at the far end of the duct where a fan mixes it with the existing room air. A series of five blower type fans**located around the perimeter of the center wall forces this mixed air over the roof and around the walls of the inner room. It finally returns to the outer room via the airways below the inner floor and the ducts along the north wall of the outer room. A ten-inch fan located in the inner room circulates the inside air to reduce thermal gradients to a minimum. Figure 2A illustrates the approximate air paths.

The degree of reheating of the cooled air is controlled by a motor driven Variac. The control motor is modulated by an electronic control bridge unit, which coordinates signals from three temperature sensing transducers.

---

* Coverall No. 6CG polyethylene sheet manufactured by Warp Bros., Chicago, U.S.A.

+ Tuck Tape, adhesive cloth tape, manufactured in Canada by Canadian Technical Tape Ltd., Montreal.

** Electrohome junior blower, Model 197-44-05-15B, capacity 100 cfm.
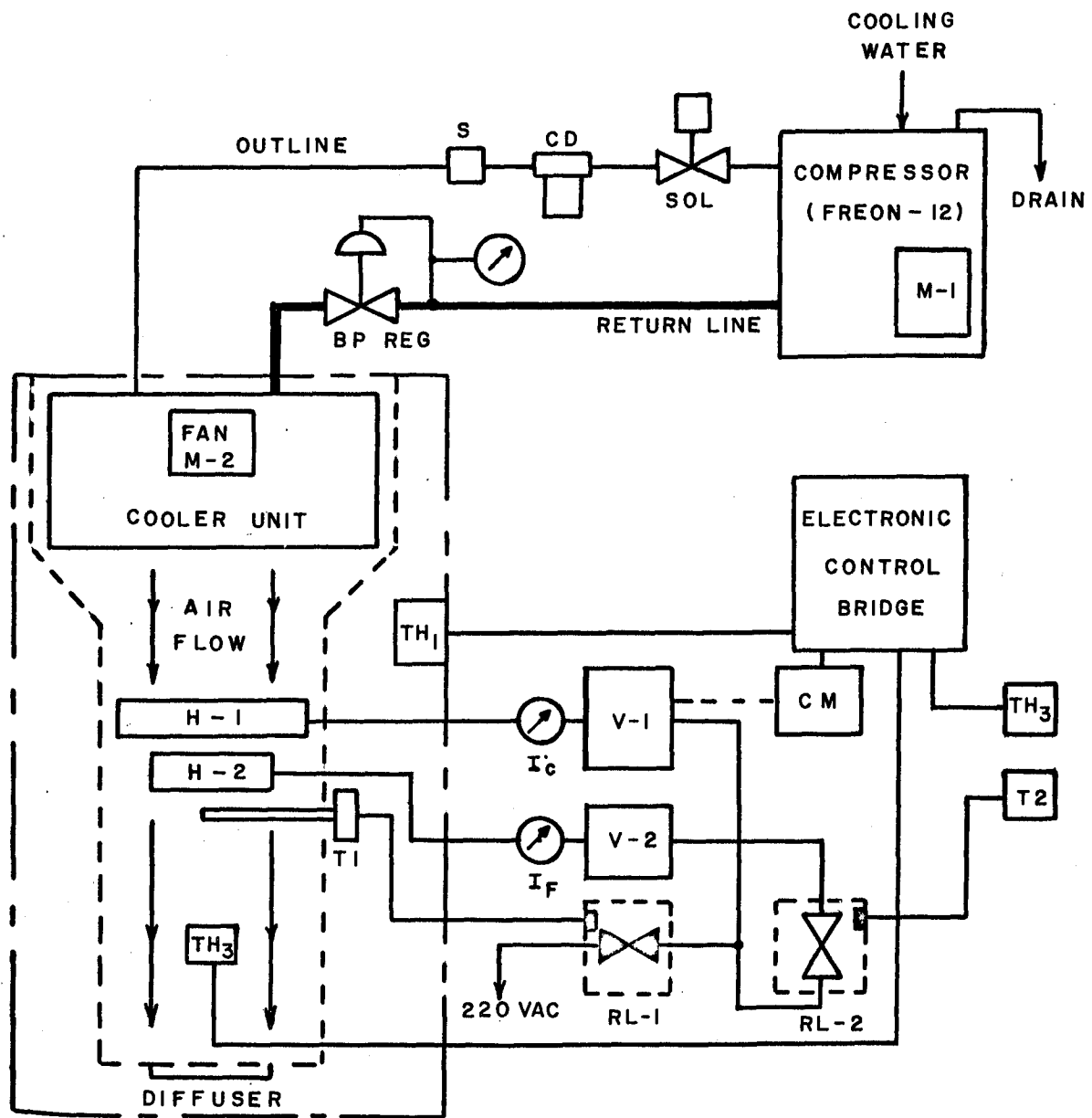
FIGURE 3 - Outline of Test Enclosure Temperature Control System.

After a period of time the temperature of the air circulating around the outside of the inner room reaches an equilibrium temperature. Due to the relatively low insulation provided by the polyethylene covering on the inner shell and the fact that very little heat is generated within it, the temperature of the inner room approaches that of the outer room, remaining however always slightly higher. The constancy of the inner room temperature, however, is always much greater than that of the outer room since it is a completely closed system.

The cooling system (see Figure 3) consists essentially of a water cooled compressor[*] (mounted on antivibration blocks and located about six feet from the test enclosure), which supplies Freon-12 to a cooler unit[+] mounted at one end of a large ceiling duct running the width of the outer room. The Freon liquid leaves the compressor through a normally closed solenoid valve (which opens when the compressor is operating), passes through a filter-drier unit[x] and an in-line sight glass[**] and is carried (via copper tubing, 1/4 in. O.D. x 0.030 in. wall) to the cooler unit in the inner room. There it passes through an expansion valve[++] and hence through the cooling coils. The Freon gas leaves the cooling coils via a back-pressure regulator[+++] and returns to the compressor (via 3/8 in. O.D. x 0.030 in. wall copper tubing). The liquid and the return lines are taped together and insulated in a common jacket over most of their length to increase efficiency and to prevent the condensation of water vapour.

The compressor operates continuously when the temperature control system is in use. The unit is cooled by tap water, which circulates through the compressor and leaves via a drain line to the sewer. The compressor motor is electrically interlocked with transducers, and the compressor is automatically shut-off if preset limits are exceeded. The compressor motor is electrically protected for overload and is interlocked with the fan motor in the cooler unit so that a failure of the fan motor will automatically shut the compressor off, thus preventing icing-up of the cooling coils.

---

[*] Kelvinator compressor, one ton capacity, Type No. 1151178, F-12 Charge 6 lbs, driven by a 1 HP, 1760 rpm, Delco motor, which requires 220 V a-c at 7 amps.

[+] Keeprite Roundell unit cooler, Model R375, rated at 373 Btu per degree, and 770 cfm.

[x] Sporlan filter-drier Type c-162

[**] Imperial sight glass Type 270C

[++] Detroit high temperature thermostatic expansion valve, 1/2 ton capacity, No. 71800.

[+++] Aminco back pressure regulator No. 1205, Type JV-FM-5/8, with attached 0-100 psi pressure gauge.

- 9 -

The reheating section of the system is illustrated in Figure 3 and consists of two sheathed heaters*, which span the air duct about two feet down-line from the cooler unit, and a set of Variacs and relays, which supply power to these heaters. The largest heater (H-1) is termed the control heater and is rated at 2000 watts. The smaller heater (H-2) is termed the fixed heater and has a rating of 1000 watts. The power supplied to H-1 and H-2 is controlled by two Variacs, V-1 and V-2 (230 volts, 10 amp and 5 amp capacity respectively), and monitored by two ammeters (I_c and I_f) in series with the heaters. The setting of V-1 is determined by the electronic control system and is automatically varied by the associated control motor (CM) so as to keep the room at a constant temperature.

The purpose of H-2 is to provide a certain fixed amount of heat to the duct air in order that H-1 will be capable of maintaining control over the full range of ambient temperature with the required accuracy. Under normal ambient conditions ($65°F < T_o < 110°F$) H-2 is not utilized. However, in the late spring and early fall and when trouble occasionally develops in the building heating system, the ambient temperature may drop below 65°F, heat losses through the walls of the enclosure increase, and additional heating capacity is required in the system. Relay RL-2** and thermostat T2***(located outside the enclosure) control the power to H-2. When the ambient temperature falls below 65°F, T2 closes RL-2 (which is normally open) supplying power to H-2 at a preset level determined by V-2. At an ambient temperature $T_o > 65°F$, RL-2 remains open.

To prevent overheating of the air duct in the event of a control system failure, a normally closed relay (RL-1)** was placed in series with the primary of V-1 and V-2 and an associated thermostat (T1)+ was located approximately two feet down-stream of the heaters. In operation this thermostat senses the temperature of the reheated air in the duct and, if it exceeds a preset limit, both heaters are shut-off. Since the room temperature was to be controlled at 22°C (approximately 72°F) and the thermostat used had a fixed differential^x of 12.5°C, a set point of approximately 38°C was selected. In this case, if the duct temperature rises above 38°C the heaters are shut off and remain off until the temperature drops to below 25.5°C.

---

* Both heaters are Chromalux brand, Finstrip iron sheathed heaters, H-1 -- 2000 watts, 230 volts, No. SEF-38, H-2 -- 1000 watts, 230 volts, No. SEF-19.
** Honeywell mercury switch-type relay, Type R879B.
*** Honeywell thermostat, Type T42B.
+ Honeywell Airstat controller Type LA219A, incorporating a bimetallic-operated mercury switch.
x The differential rating of a bimetallic strip-type thermostat is the number of degrees the temperature must fall below the set point before the switch contacts of the thermostat will reopen.

The electronic control section is illustrated briefly in Figure 3. It utilizes a Honeywell electronic controller[*], a modulating motor (CM)[x], which operates Variac V-1 and which in turn controls the amount of power to the control heater (H-1), and a set of three resistance-type thermostats[+]. The room thermostat (TH_1) is located on the wall of the inner room, the duct discharge thermostat (TH_2) is located in the air duct near the outlet diffuser, and the external space thermostat (TH_3) is located in the hall outside the test enclosure. Each of the thermostats is assigned a certain control authority[**].

The system operates as follows: on a call for heat from the room thermostat (TH_1) the control bridge becomes unbalanced and the modulating motor adjusts the Variac to provide more power to the duct heater. Since TH_1 has 100% authority, the motor could turn the attached Variac fully on, which would cause the room temperature to overshoot. However, TH_2 (authority 0-40%) senses the increased discharge temperature and tries to rebalance the control bridge; in so doing it starts shutting the Variac off. In other words, TH_2 tends to snub the action of TH_1 to prevent overshooting. A decrease in hall temperature is sensed by TH_3 (authority 0-40%), which is able to operate the control motor and increase the Variac output even if the room temperature is at the control point. Thus the system will compensate for the increased heat loss through the walls that will eventually result from the lower hall temperature. With this arrangement the actual room temperature and the temperature at TH_1 are precisely in phase and, as a result, offset in the system is eliminated. This type of correction is frequently referred to as anticipation compensation.

---

* Honeywell MD-791A electronic temperature control panel, Model W626A.

x Honeywell Modutrol motor, Model M905J.

+ TH_1 - Honeywell Thermostat, Model T7018C.
  TH_2 - Honeywell Thermostat, Model L7033A-5".
  TH_3 - Honeywell Thermostat, Model T7001A.

** The percentage authority is defined as the percentage of the total possible rotation of the control motor that is produced by an unbalance in the individual thermostats. For example assuming the motor is capable of a total rotation of 160 degrees, an unbalanced thermostat with a 20 per cent authority could produce a maximum angular rotation of 32 degrees.

A complete description of the system, wiring details, and the computation and check-out procedure used in the adjustment and calibration of the system will not be presented here since they are available in detailed form elsewhere[*].

During 1963 a number of studies were conducted on the constant temperature system in order to obtain optimum performance. A control temperature of 22°C was selected with TH_2 and TH_3 authorities of 10% and 30% respectively. Full time operation of the system commenced on May 30, 1964. Figure 4 illustrates the variation of ambient (hall) temperature (T_o) and the temperature of the outer room[x] (T_c) with time over a period of 22 days. In both cases temperature was measured with regular glass-stemmed thermometers, which provided an accuracy of $\pm$ 0.5°C and $\pm$ 0.1°C in the observed values of T_o and T_c respectively. On June 18, after approximately 18 days operation, a series of leaks developed in the cooling system necessitating a shut down. After repairs were made and the Freon circuits refilled, the system was started up again and ran continuously for some 36 days, at which time trouble developed in the compressor motor forcing another shut down. The system was started up again on July 24 and has been running continuously since (approximately 150 days). During this later period the ambient temperature range was found to be 18.9 to 33.3°C, whereas the outer room temperature varied only over the range 21.3 to 22.5°C. The mean and standard deviations of T_c and T_o over this period were found to be T_c = 22.0 $\pm$ 0.29°C and T_o = 24.8 $\pm$ 2.34°C. It should be noted that much greater stabilities were often observed over periods of up to 48 hours. The main stability problem remaining appears to be associated with the authority setting for TH_3. Originally an authority of 30% was used; this was subsequently reduced to 15% when short period outside temperature fluctuations were found to be affecting T_c. However, even with the 15% setting, it is found that a large increase in ambient temperature causes the control system to drop T_c too low. This situation is probably due in part to the very good thermal insulation of the outer shell. The behavior of the system with lower values of TH_3 authority is to be investigated.

---

[*] See the following engineering data available from Minneapolis - Honeywell Regulator Company, Minneapolis 8, Minn., U.S.A.
    Form 77-7316 - Engineering data for electronic control system W626A
    Form 77-7301 - Computations for electronic control system adjustments.
    Form 77-7507 - Check-out and testing data for electronic control system W626A.

[x] The majority of temperature stability experiments to date have been conducted with the door open between the inner and outer rooms. Since no effort is being made to control humidity in the inner room at present, this does not introduce any difficulties and simplifies experimental procedure.
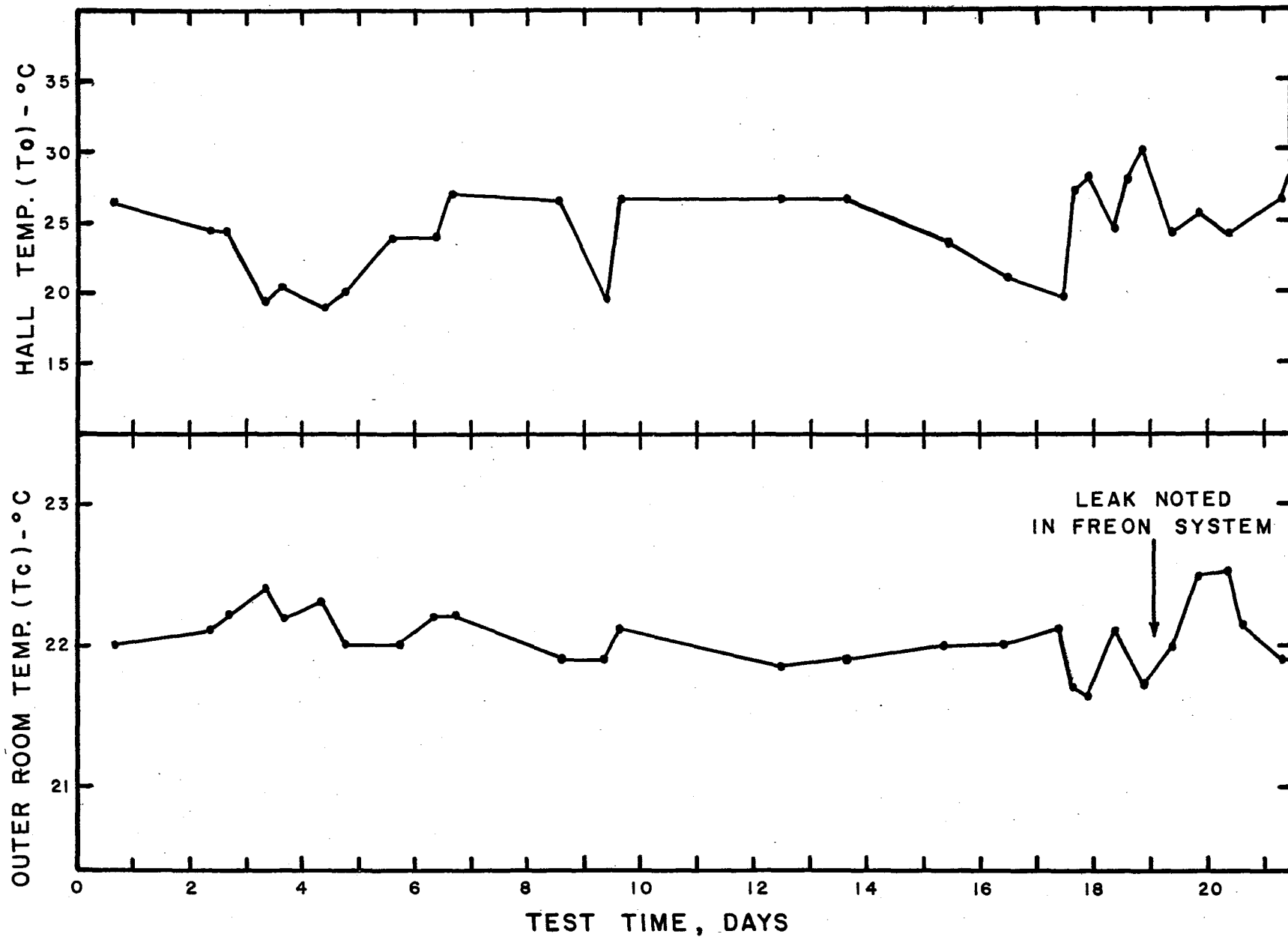
FIGURE 4 - Curves Showing the Variation of Ambient and Enclosure
Temperature with Time.

1.2.4 Humidity Control

As it was anticipated that in the future deformation experiments would be conducted on a number of evaporite minerals (NaCl, KCl etc.), which are particularly sensitive to moisture, the inner room was equipped so that its humidity could be accurately controlled. Humid air was generated by a simple humidifier unit* consisting of a large water-soaked wick, a water reservoir, and an associated air circulating fan. Dry room air is drawn in by the fan and passed out over the wick, where it picks up moisture. The water level in the reservoir is maintained automatically by a float-operated microswitch, which operates a solenoid valve in series with the water supply line to the unit. A humidity sensitive element** located in the inner room and an associated hygrometer controller[+] unit located outside the test enclosure control the operation of the humidifier fan. With this relatively simple arrangement it is possible to control the relative humidity of the inner room to $\pm$ 2%.

1.2.5 Antivibration Loading Frame Mounts

During construction of the test area, antivibration mounts were installed for support of the four proposed loading frames. Each mount consisted of large poured concrete blocks (18 in. x 24 in. x 24 in. high) weighing approximately 800 lbs supported on resilient pads, consisting of alternate layers of Isomode rubber[x] and 16 gauge aluminum, at the four corners. These pads rested on a multiple sandwich base consisting of alternate layers of 1/2-inch thick steel plate and 1/2-inch thick Ten-Test insulation board. Figure 5 illustrates the arrangement. This system has been used in the past by the writer (22) and has proven very satisfactory for removing much of the vibration resulting from local traffic and general building vibration.

1.2.6 Electrical Power Supply System

Since the axial load and confining pressure control systems and sections of the axial load, confining pressure and strain measurement systems must operate 24 hours a day over extended periods of time, it was necessary to provide a high capacity storage battery system

---

* Electrohome Humidette, Model A26.
** Hygrodynamics Inc. narrow range sensing element, Class A, Type 4-4820.
+ Hygrodynamics Inc. Hygrometer Controller, Model 15-3110.
x Available in Canada from Upton, Braden and James Co. Ltd., Montreal.
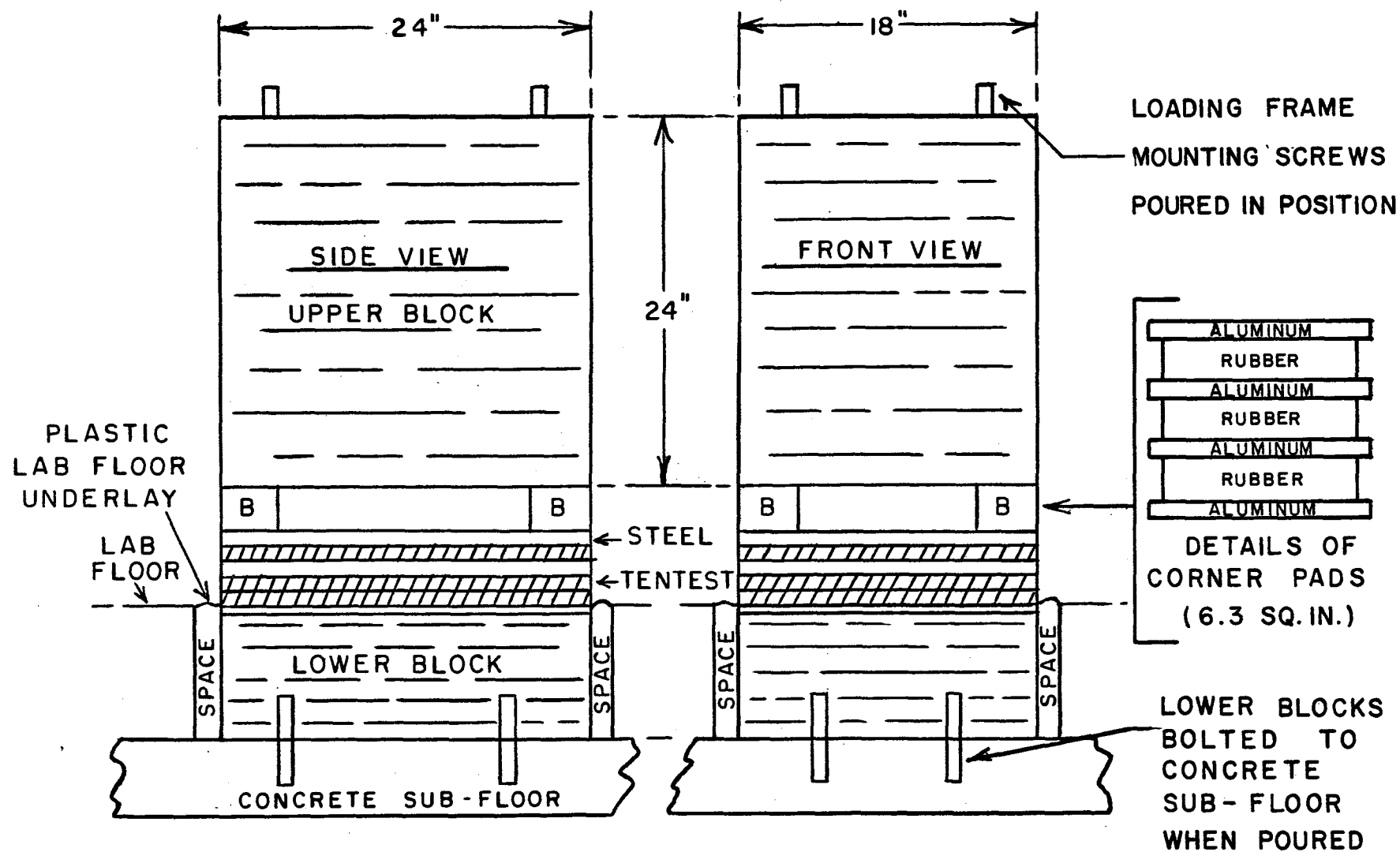
FIGURE 5 - Construction Details of Antivibration Loading Frame Mounts.

and a 110 V a-c standby system for operation of this equipment. Four six-volt, 220 ampere-hour storage batteries, arranged in two sets, provide a series of 2 and 6 V d-c lines for operation of control and measurement circuits and a 12 V d-c line for operation of a 110 V a-c 300 watt standby system. A separate 6 V d-c bias supply utilizing No. 6 dry cells is also included. An automatic battery charger and associated cycler unit insure that both sets of storage batteries are kept at full charge when the facility is not in use. During operation of the facility, the automatic charger is connected only to Battery Set B and a high current power supply is connected across Battery Set A to maintain it at full charge.

The standby unit, batteries and associated charging units are located in the hall outside the constant temperature enclosure. D-c and a-c distribution panels located in the outer room of the test enclosure monitor the active circuits and provide facilities for metering the voltage in each circuit. Figure 6 illustrates the arrangement of these power supplies and the monitoring facilities.

1.2.7 Pneumatic Supply System

A 2000 psi nitrogen gas supply system for operation of the Type-A axial loading and confining pressure systems is shown in Figure 7. The gas supply consists of eight standard nitrogen cylinders in two separate circuits of four each. One cylinder (primary supply) in each circuit is located in the outer room near the load and pressure control systems, and the other cylinders (secondary supply) are located in the hall outside the constant temperature room. The primary supply in the inner room eliminates the possibility of a high pressure drop between the secondary supply and the pressure control systems when a large volume gas flow is required. A system of valves allows individual nitrogen cylinders to be removed and replaced, and allows the primary and/or secondary gas supplies to be connected into or disconnected from the circuit. The pressure in the two circuits is monitored by dial type pressure gauges located both at the secondary supply (outside the constant temperature room), and on the gas distribution panel in the outer room. Inline filters with 25-50 micron sintered bronze elements are located at the input to the distribution panel.

1.2.8 Electrical Wiring

Since many of the control and monitor signals were in the 5-20 μv level, it was necessary to take very special care with all electrical wiring. All 110-220 V a-c power wiring was shielded where possible, and kept as far from control and monitor wiring as practical. All 110 V a-c power cables from wall outlets to various instruments utilized shielded cables and polarized connectors. In most cases cables carrying d-c power from the battery supplies were also shielded. All relay racks were grounded, via their individual 110 V a-c power cables, to the electrical ground of the building.
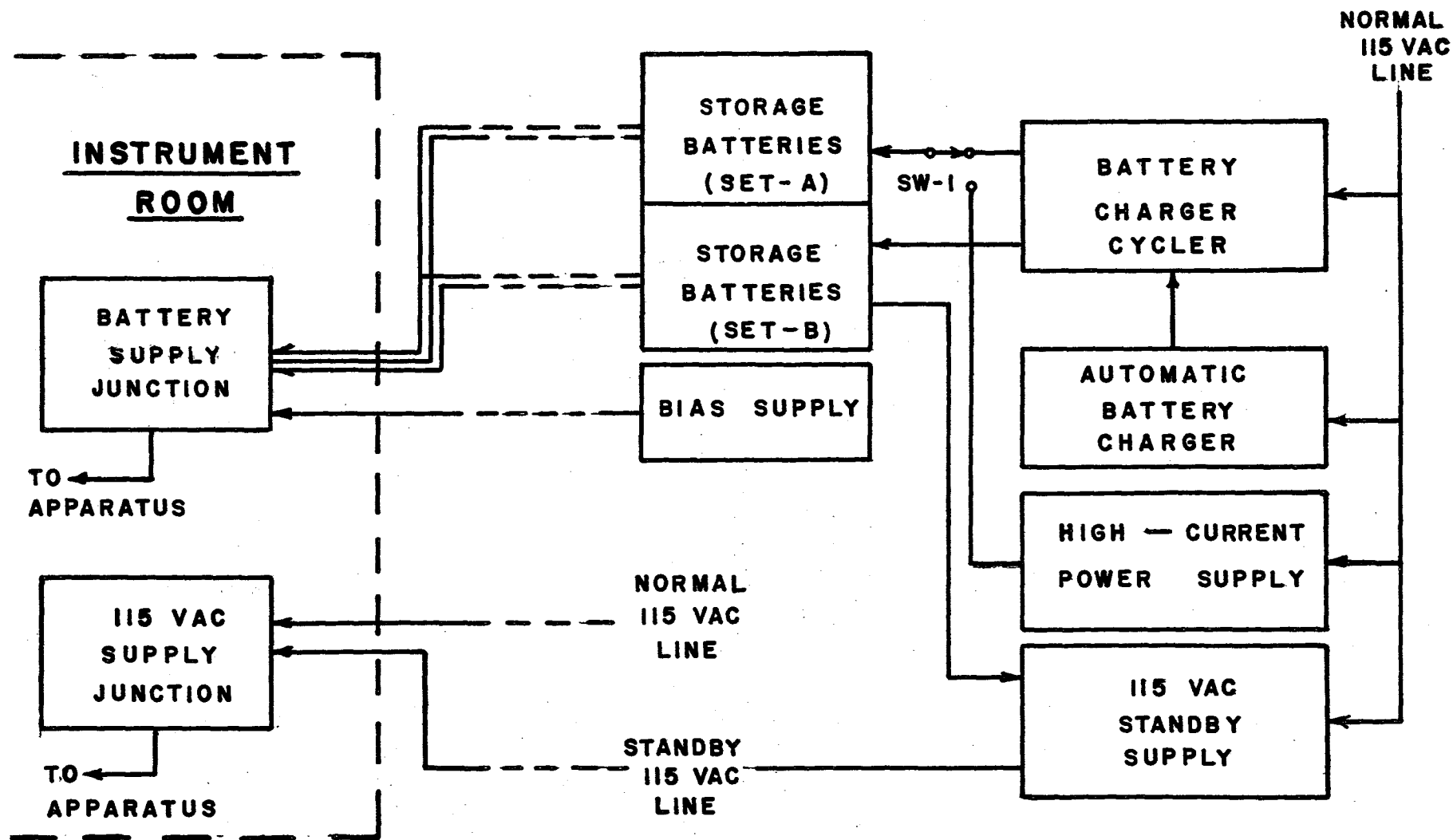
FIGURE 6 - Block Diagram of Electrical Power Supply System.

INSTRUMENT ROOM

BATTERY SUPPLY JUNCTION

TO APPARATUS

115 VAC SUPPLY JUNCTION

TO APPARATUS

STORAGE BATTERIES (SET-A)

STORAGE BATTERIES (SET-B)

BIAS SUPPLY

NORMAL 115 VAC LINE

STANDBY 115 VAC LINE

SW-1

NORMAL 115 VAC LINE

BATTERY CHARGER CYCLER

AUTOMATIC BATTERY CHARGER

HIGH — CURRENT POWER SUPPLY

115 VAC STANDBY SUPPLY

- 16 -
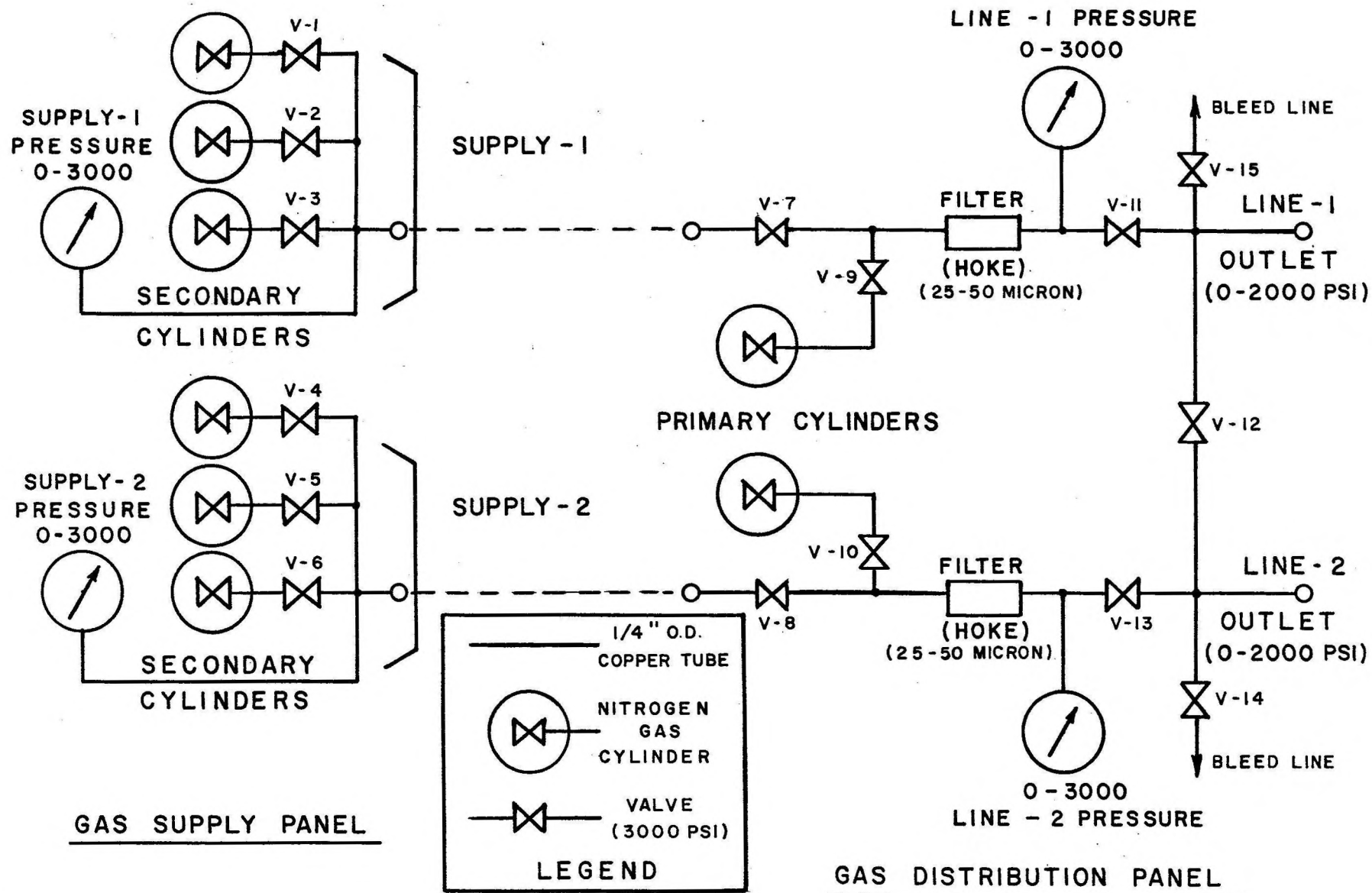
FIGURE 7 - Circuit of Pneumatic Supply System.

Shielded cables were used for all control and monitor signals. In most cases the longer cables were terminated at both ends on terminal strips located in steel junction boxes, while shorter cables connected these lines to the various pieces of apparatus. The cable shields themselves were connected to the electrical ground of the building and the junction boxes were grounded via the cable shields. Most low level signals (up to 10 MV) were carried in individual cables to prevent interference. All cables were permanently tied or clamped in place.

1.3 Axial Loading System

1.3.1 Loading Frames

In the past many workers studying time-dependent pro-perties of geologic materials have utilized lever type loading systems to axially load cylindrical test specimens (e.g., Fairhurst (9), Hardy (18), Phillips (38), Price (39), etc.). Such systems may have an apparent advantage due to their basic simplicity, but they do not provide the highly stable loading conditions required to determine significant deformation parameters. The loading system finally developed by the writer is based on the design of a load maintaining system described by Hardy and Larocque (24). It consists of a loading frame incorporating a single acting hydraulic ram with an attached load cell and an associated control system that monitors the ram thrust or the specimen strain and adjusts the input pressure to the ram so that the ram thrust or specimen strain varies in accordance with an established loading program. Such a system is generally referred to as a feedback control system.

Figure 8 shows a photograph of two of the axial loading frames mounted on antivibration bases in the inner room of the test enclosure. The loading frame consists of an upper and a lower steel platten (15-$\frac{1}{2}$" x 15-$\frac{1}{2}$" x 1-$\frac{1}{2}$" thick), which are tied together by four heavy steel rods (1-$\frac{1}{2}$" diameter). These rods are threaded at both ends to provide adjustment of the working space between the plattens and to allow the plattens to be adjusted perfectly parallel. A modified Blackhawk 50 ton hydraulic ram* is threaded into the upper platten and locked into position by an upper and a lower locking ring. A strain gage type load cell is attached to the lower end of the ram piston to monitor the thrust. Figure 9 shows a close-up view of one of the loading frames with a specimen loading jig in position between the load cell and the lower press platten.

---

* The Blackhawk hydraulic ram Type RC-210 has an effective piston area of 11.045 sq in., an outside diameter of 5 in. and a 6 in. stroke. Modification involved the removal of an attached handle, and the cutting of a 5"-12 UN thread on the outside diameter of the ram body over a length of approximately 7 in.

FIGURE 8 - Two Axial Loading Frames Mounted on Antivibration Bases in Inner Room.
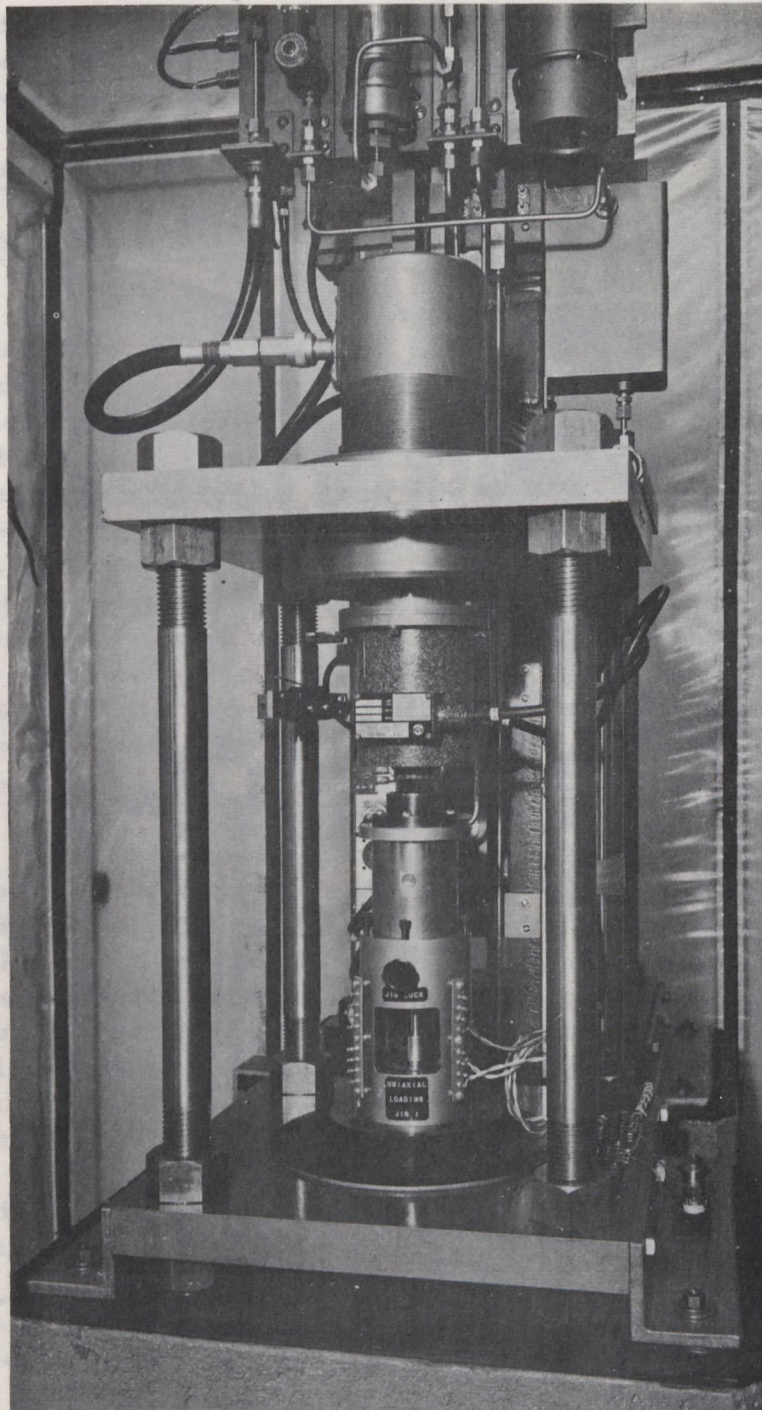
FIGURE 9 - Close-Up View of Loading Frame with Specimen
Loading Jig in Position.

1.3.2 Feedback Control Systems

The description and analysis of feedback control systems is presented in detail in many recent texts (e.g., Ahrendt and Savant (1), Truxal (47), and Thaler and Brown (46)). Figure 10A shows the arrangement of the basic feedback control system. It consists of a process to be controlled, a controller, a programmer, a feedback transducer, and a summing network. The input programmer puts out a signal (R), which is designed to be an analog of the desired process state, and the feedback transducer puts out a signal (-B) proportional to the actual process state. These two signals are applied to the summing network and the error signal E = (R - B) applied to the input of the controller. In operation, the controller adjusts the process state so that the error signal (E) to the controller is a minimum. Under optimum conditions the process state will accurately follow the input program. Feedback control systems have been developed that utilize pneumatic, hydraulic, mechanical and electrical signals. Using appropriate transducers, mixed systems that incorporate a number of types of signals may be designed.

Figure 10B shows a block diagram illustrating the form of the feedback system developed for carrying out rock deformation experiments. Here the "process" consists of the loading of a test specimen under various test modes, the controlled variables being specimen stress (σ) and strain (e). By selection of the appropriate input program and feedback transducer the following test modes may be obtained:

(i)   Controlled strain rate ---------------------------- (CER)

(ii) Controlled stress rate ----------------------------- (CSR)

(iii) Constant strain (stress relaxation experiment) --- (CE)

(iv) Constant stress (creep experiment) ------------- (CS)

(v)   Incremental --------------------------------------- (I)

(vi) Cyclic -- (CY)

Depending on the time scale and the desired control quality, two types of controllers may be utilized. These are classed as "continuous" and "on-off" types. In the "continuous-type" controller the rate of correction of the controlled variable is proportional to the error signal (i.e., the difference between the actual value and the required value of the controlled variable). However, in the case of the "on-off" type controller only two states are possible. The controller is normally in the "off" state and can only be switched into the "on" state if the error signal exceeds some definite level. Hence the rate of correction of the controlled variable is independent of the magnitude of the error in the controlled variable. Under this condition the actual value of the controlled variable will tend to oscillate about the required value. If rapid changes in the controlled variables (σ and
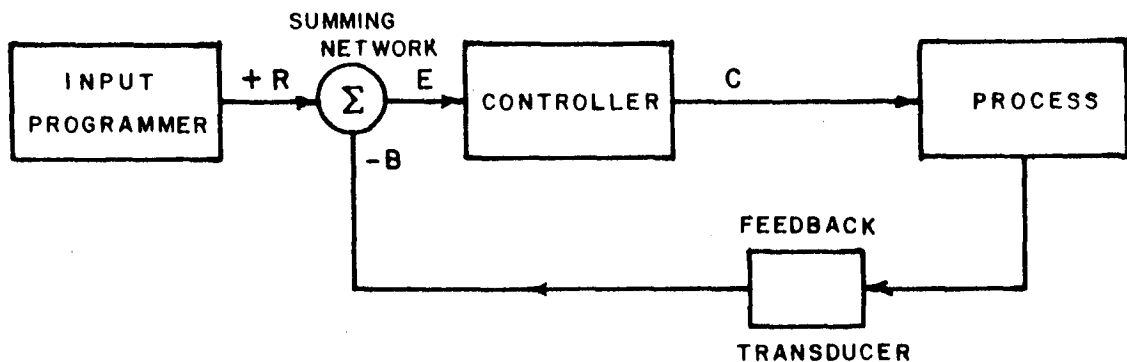
R – INPUT PROGRAM SIGNAL
B – FEEDBACK SIGNAL
E – ERROR SIGNAL (R–B)

A. BASIC FEEDBACK CONTROL SYSTEM
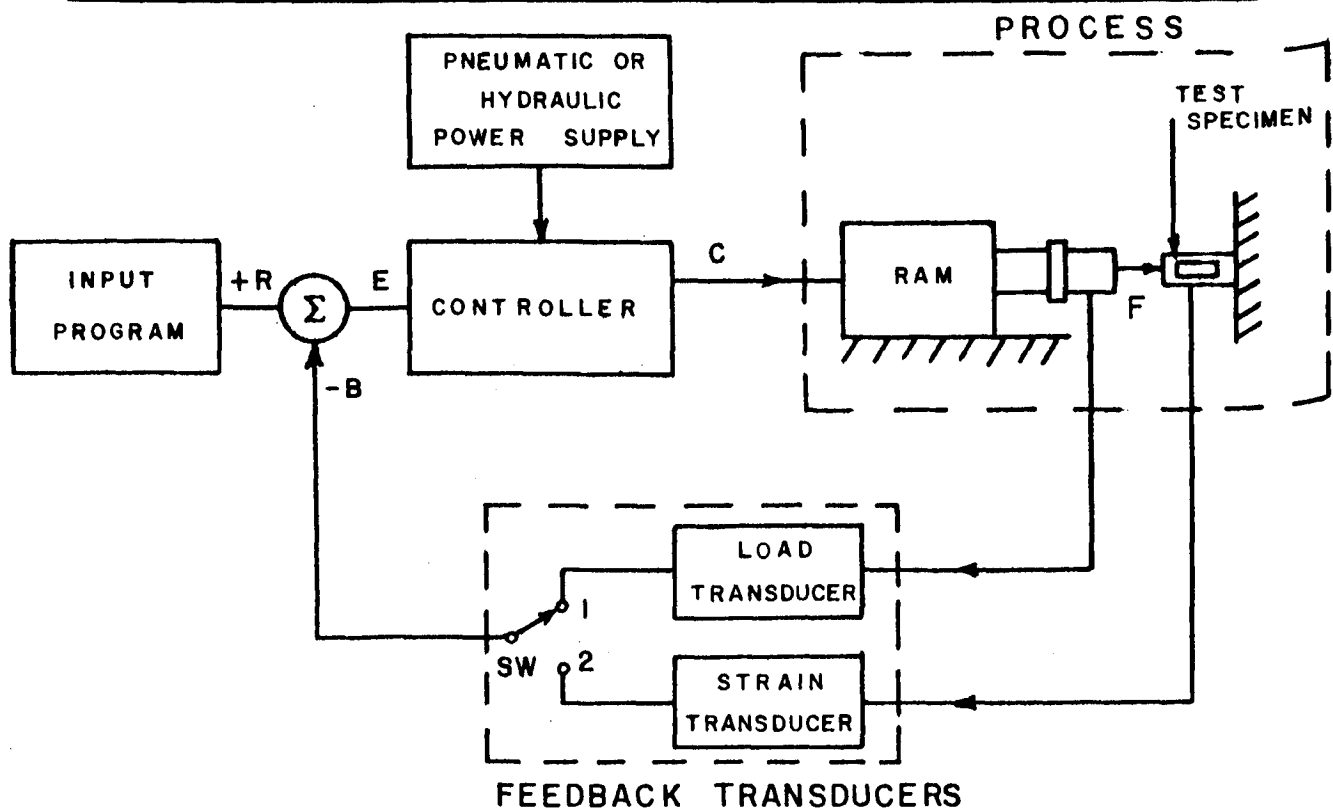
B. SIMPLIFIED BLOCK DIAGRAM OF CONTROL SYSTEM FOR ROCK DEFORMATION EXPERIMENTS

FIGURE 10 - Block Diagrams of a Basic Feedback Control System And a Control System for Rock Deformation Studies.

e) are required, a "continuous"-type controller must be utilized, whereas if only slow changes are involved a simpler "on-off" type may be used.

Since it was decided that initial deformation experiments would be conducted over relatively long periods of time that would involve either fixed or slowly varying controller variables, it was decided that the "on-off" type control system would be the most practical. The loading system utilizing this control system and the loading frame discussed earlier will be referred to for convenience as the Type-A loading system. It should be noted that some time was spent in designing and in initially developing a loading system incorporating a "continuous" type controller to be used in experiments at higher loading rates. This system is referred to as the Type-B loading system and is still under development.

1.3.3 Type-A Loading System

Figure 11 shows a simplified block diagram of the Type-A loading system. Since the system has both stress and strain feedback available, it is capable of operating in any of the test modes described earlier. To illustrate the operation of the system, let us consider that it is connected in the constant stress (CS)*, and that the axial specimen stress (σ_{zz}), as measured by the load cell, is below the control point ($\sigma_{zz}(c)$). Since σ_{zz} is below the control point, the pneumatic controller will be in the "load-on" state, which will allow gas to flow from the regulator unit to the primary side of the separator. As a result, the oil pressure on the secondary side of the separator will rise, increasing the pressure in the hydraulic ram and raising σ_{zz}. The load cell, placed between the ram and the test specimen, senses the magnitude of the applied load and provides a feedback signal (-B) to the control bridge that is proportional to $\sigma_{zz}(c)-\sigma_{zz}$. The resulting output voltage from the control bridge (ΔV), which is proportional to -B, is fed to the electronic controller, which in turn operates the pneumatic controller. Now as σ_{zz} approaches $\sigma_{zz}(c)$, ΔV tends to zero and the electronic controller switches the pneumatic controller into the "off" state, shutting off the flow of gas to the separator. If $\sigma_{zz}(c)$ is exceeded, the resulting feedback voltage triggers the pneumatic controller into the "unload-on" state, which allows gas to bleed out of the separator reducing σ_{zz}.

---

* Note that in the CS-mode the programmer output remains constant for a particular value of stress, and the control mode selector will be set for stress feedback. The unit marked ZB-1 in the stress feedback line is a zero balancing unit to enable the output voltage of the load cell to be set to zero when the applied load is zero.
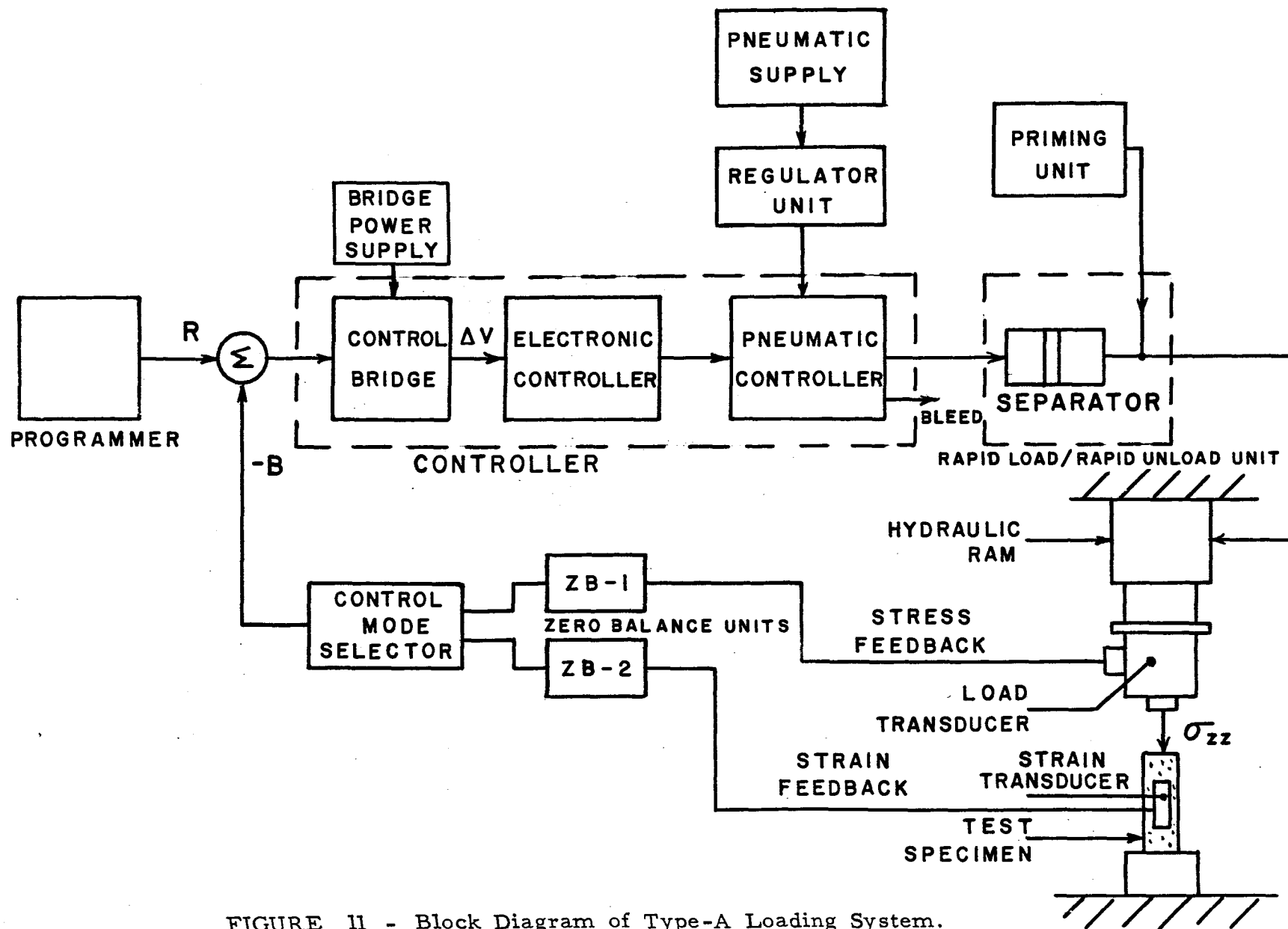
FIGURE 11 - Block Diagram of Type-A Loading System.

Operation in the other various test modes will be similar. For example, if a controlled rate of straining is required, strain feedback will be employed and the programmer will provide a signal corresponding to the required strain vs time function.

Basically the system may be divided into two sections, namely a pneumatic/hydraulic section and an electronic section. The former consists of the pneumatic controller, its associated regulator unit, the rapid load/rapid unload unit (RL/RUL) containing the separator and its associated priming unit, and the hydraulic ram. The latter consists of the electronic controller, the control bridge, the programmer, and the feedback transducers and associated circuitry. Figure 12 is a photograph that shows in the foreground two racks containing the load control system.

1.3.4 Pneumatic/Hydraulic Section

Figure 13 shows details of the pneumatic/hydraulic (p/h) section of the system. The regulator, pneumatic controller and priming unit are located in the outer room (see Figure 12). The RL/RUL unit is located near the hydraulic ram in the inner room, as shown in Figure 16. In most cases standard hydraulic fittings* , valves** and tubing+ rated for at least 2000 psi were used in the construction of this equipment.

(i) Pneumatic Controller

Figure 13 shows the pneumatic circuit of this unit. It contains two solenoid valves++, the loading valve (V-5), and the unloading valve (V-8), which control the gas pressure on the primary side of the separator. These valves are activated by electrical signals from the

---

* Weatherhead, Ermeto-type steel fittings rated at 15,000 psi were used in most applications.

** Manual valves used throughout the system were Hoke, Type 270N equipped with nylon stem tips.

+ 1/4" O.D. steel tubing rated at 10,000 psi was used in most applications. Where long distances or difficult bends were involved standard 1/4" O.D. soft copper tubing was employed (e.g., between the pneumatic controller and the RL/RUL unit). No failures have been observed with such installations even in cases where pressures of up to 2000 psi have been maintained over periods of at least two years.

++ ASCO, Type 8262-99 solenoid valves, rated at 3000 psi, and fitted with 6 V d-c solenoid coils.
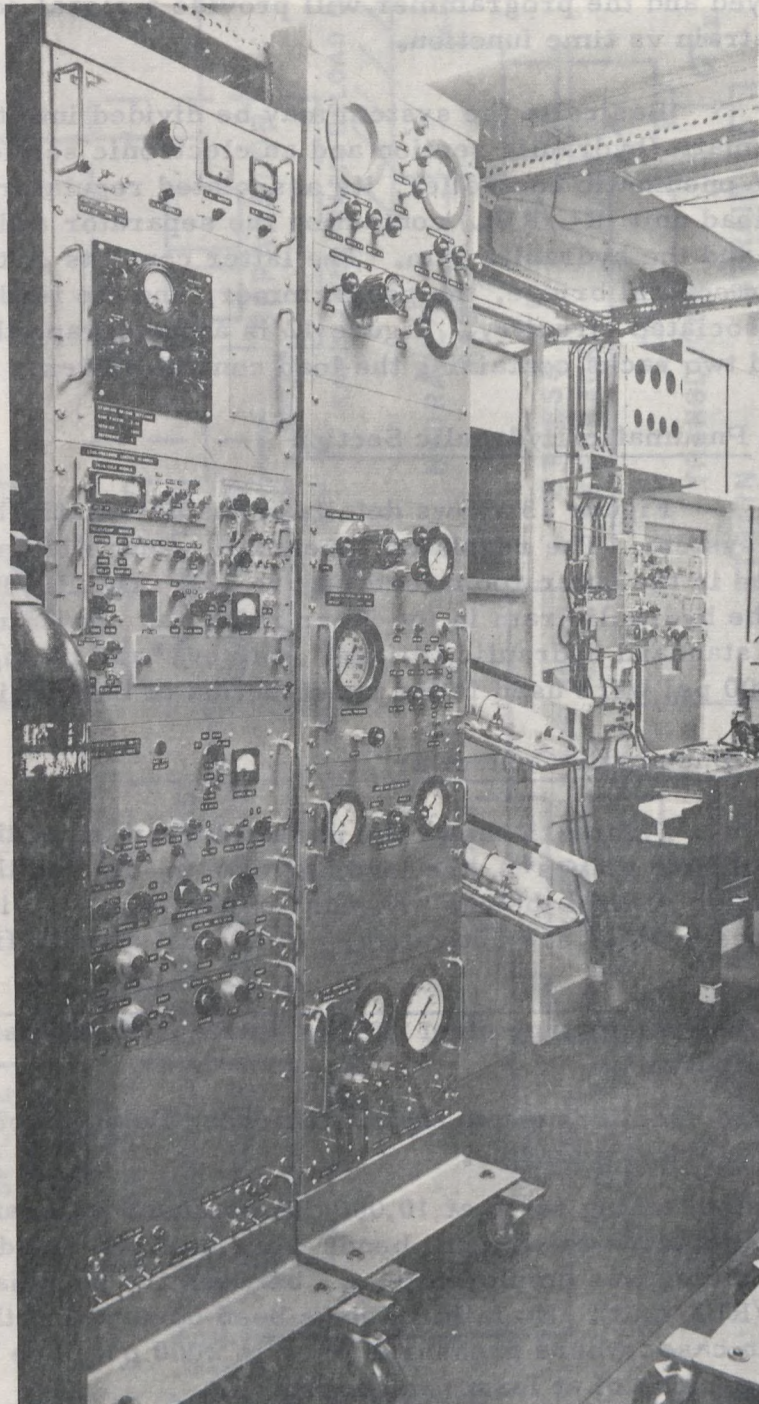
FIGURE 12 - Photograph Showing in the Foreground Two Racks
Containing the Load Control System.
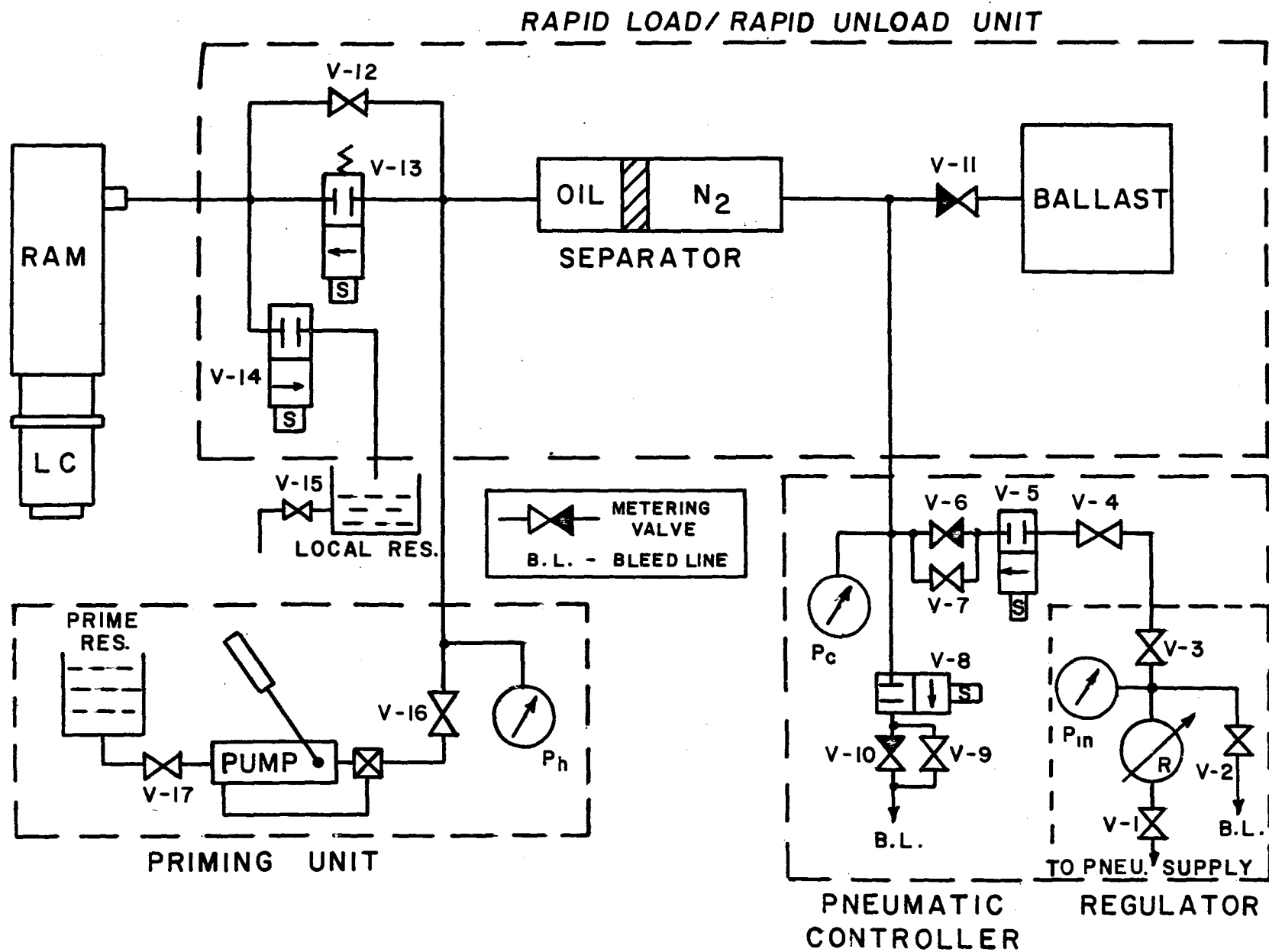
FIGURE 13 - Circuit of Pneumatic/Hydraulic Section of Control System.

electronic controller. Micrometer-type metering valves* (V-6 and V-10) in series with the solenoid valves allow the gas flow during loading and unloading to be finely adjusted to obtain optimum control. For some operations it is desirable to have full gas flow and for these cases by-pass valves (V-7 and V-9) are included. The pneumatic control pressure (P_c), which corresponds to the gas pressure on the primary side of the separator, is monitored by a large 0-3000 psi gauge included in the controller. Figure 14 shows two views of the completed controller.

The electrical wiring diagram of the controller is shown in Figure 15. The controller has a number of control modes as selected by Switch SW-1, namely: auto, manual and remote. Normal operation is in the auto-mode in which case the loading and unloading solenoid valves are energized by the electronic controller via Connector CON-2**. During certain experimental operations it is necessary to operate the load or the unload valves manually. This is accomplished by putting the controller in the manual-mode and activating the loading or unloading valves using Switches SW-3 or SW-2 respectively. In this mode, power to operate the solenoids is obtained from the external storage battery supply via Connector CON-3.

The operation of the solenoid valves is interlocked with other parts of the control system so that in the event of certain system failures the controller will "fail-safe". Relays RL-1 and RL-2 are connected in such a way that an interlock signal must be applied to Connector CON-4 before they will operate normally. In the event of certain system failures, this interlock signal is lost and in this case the unload solenoid valve will automatically be energized and the loading solenoid valve will be prevented from operating. Switch SW-4 (pos. 2) provides a temporary override of the interlock to allow various adjustments to be made to the system. Other parts of the circuit do not pertain to the present description and will not be discussed further here.

---

*Hoke, Type 2RB280 metering valves with attached vernier handwheels.

**Note that Connector CON-2 is labeled "From Scanner". This refers to a special arrangement that is utilized when more than one loading frame is being operated from a single electronic controller. When only one loading frame is being used this connection would go directly to the output of the electronic controller.
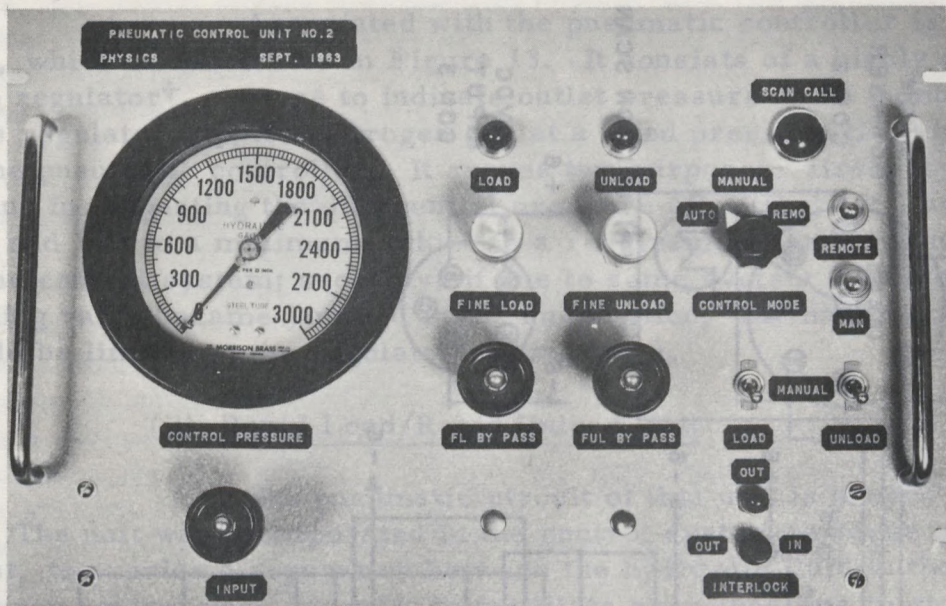
A.   Front View of Pneumatic Controller Unit.
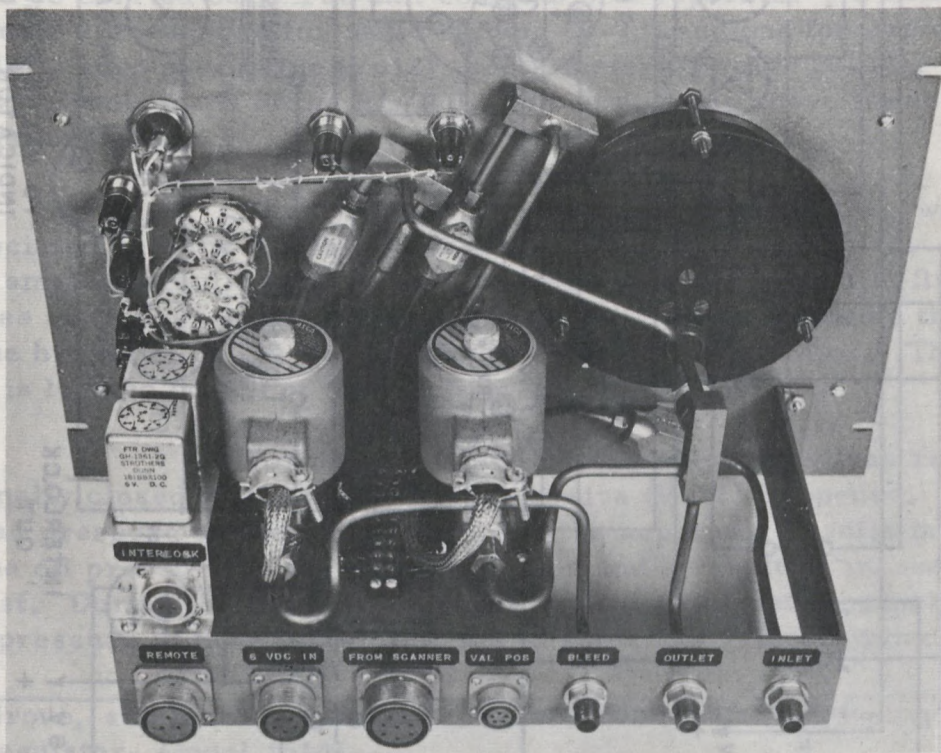
B.   Rear View of Pneumatic Controller Unit.

FIGURE   14 - Two Views of Completed Pneumatic Controller Unit.
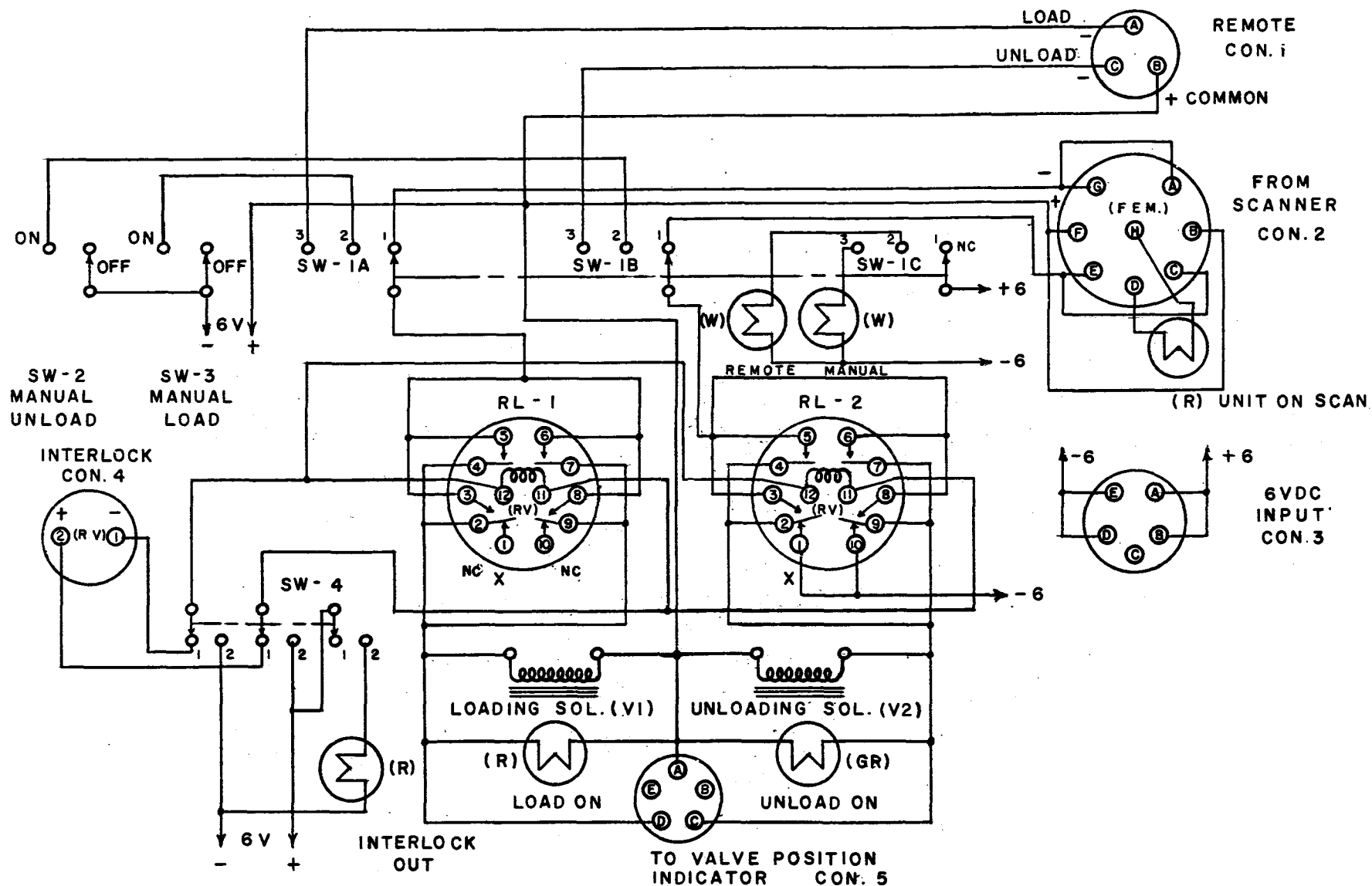
FIGURE 15 - Circuit Diagram for Pneumatic Control Unit.

Associated with the pneumatic controller is a regulator unit, which is illustrated in Figure 13. It consists of a highly stable spring-type regulator[+], a gauge to indicate outlet pressure and a number of valves. This regulator supplies nitrogen gas at a fixed pressure (P_{in}) to the input of the pneumatic controller. It serves two purposes: first, it provides a means for adjusting the differential pressure $\Delta P = (P_{in} - P_c)$ across Valves V-5 and V-6 to a minimum, which is a requirement for optimum operation of the control system; secondly, if due to some system malfunction the loading valve became jammed in the on-position, the maximum ram pressure would be limited to the regulator setting (P_{in}).

(ii) Rapid Load/Rapid Unload Unit

The pneumatic circuit of this unit is presented in Figure 13. The unit was incorporated in the control system to serve three purposes. First, to provide a separation between the hydraulic fluid in the ram and the nitrogen control gas, secondly to facilitate slow, positive motion of the ram during alignment and preloading of the test specimen, and thirdly to provide an arrangement whereby rapid loading and unloading of the test specimen could be carried out. The unit consists of a separator[*], a ballast tank, two solenoid valves[**](one for rapid loading (V-13) and one for rapid unloading (V-14)), a by-pass valve (V-12), and a metering valve (V-11). Figure 16 shows a photograph of the RL/RUL unit in position above the loading frame in the inner room.

The hydraulic circuit of the priming unit, which is associated with the RL/RUL unit, is also shown in Figure 13. It consists of a small hydraulic hand pump[++], a reservoir for hydraulic fluid[+++], a series of valves, and a pressure gauge (P_h), which indicates the pressure of the hydraulic oil on the secondary side of the separator. The priming unit is located on one of the racks in the outer room.

For normal operation the solenoid valves remain in the normally closed state and the by-pass valve (V-12) is opened. Any increase in gas pressure on the primary side of the separator results in an increase in the oil pressure on the secondary side and a resulting increase in ram thrust. During the initial stages of a typical deformation experiment the gas pressure in the separator is set to some low value (approximately 50 psi)

[+] Grove, small volume, high pressure, combination reducing and relief regulator, Model 15LH.

[*] Sprague, Model 60010 accumulator with a volume of approximately 25 cu in. and rated at 4000 psi.

[**] Hoke solenoid valves, Type - B90D-120C rated at 2000 psi and fitted with 6 V. d-c solenoid coils.

[++] Blackhawk hand pump, Model P-39.

[+++] Blackhawk hand pump oil, Type HF-47.
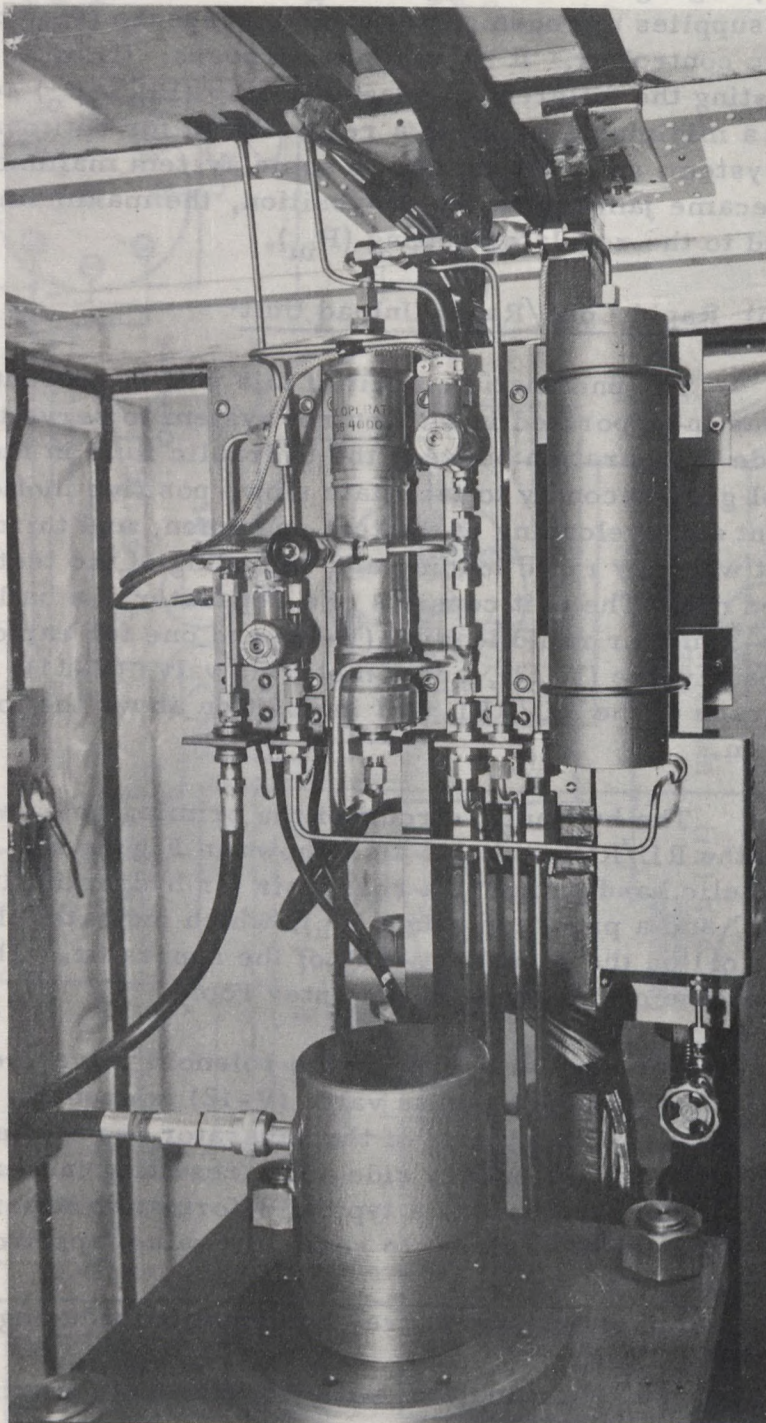
FIGURE 16 - Photograph of Rapid Load/Rapid Unload Unit
in Position above Loading Frame.

and the ram piston slowly lowered into contact with the specimen loading jig using the hand pump in the priming unit. Once in position, Valve V-16 is closed isolating the RL/RUL unit from the priming unit. A ballast cylinder, having an internal volume of approximately 35 cu in., is included in the circuit to improve the load stability of the system when it is operating in the constant stress or constant strain mode. Its effect on the system may be increased or decreased by adjustment of the metering valve (V-11).

When rapid loading experiments[x] are to be carried out, Valve V-12 is shut off. Valve V-13 is remotely opened and the system pre-loaded as just described for normal operation. Once the specimen has been preloaded, V-13 is shut-off. The gas pressure on the primary side of the separator is increased to a specific level after which V-5 in the pneumatic controller is shut off and the control system clamped in an inactive mode. To initiate rapid loading, V-13 is remotely opened causing the ram pressure to rise suddenly and come to equilibrium with the pressure on the secondary of the separator. When the specimen stress just reaches the control point, the control system is unclamped and normal operation of the system is re-established.

1.3.5 Electronic Section

(i) Electronic Controller

The electronic controller performs a number of important functions. First, it accepts the low level, unbalance signals (ΔV) from the control bridge and converts these to high level signals for operation of the loading and unloading solenoids in the pneumatic controller. In this respect it performs the function of an amplifier. Secondly, it contains a number of logic circuits that insure that correct sequencing of the loading and unloading valves is maintained (e.g., the loading valve must be closed before the unloading valve can be opened). Thirdly, additional logic circuits are included so that the controller will "fail-safe" (e.g., failure of a critical section of the controller will automatically put the controller into the neutral position, where both loading and unloading valves will be closed).

Figure 17 shows a block diagram of the controller. The low level output signal from the control bridge enters the controller via the galvanometer signal conditioning circuit (GSC), shown in Figure 18. The output of this circuit is connected to the coil of a light spot type galvano-meter in the galvanometer-photocell unit (GPU). This circuit allows the polarity of the galvanometer input signal to be selected (SW-4), provides a manual galvanometer sensitivity control (SW-1) and includes circuitry for

---

[x] A number of additional electronic units are involved in the operation of the rapid loading system. Since this system has not yet been employed in actual deformation experiments, further details of these electronic units will not be presented here.
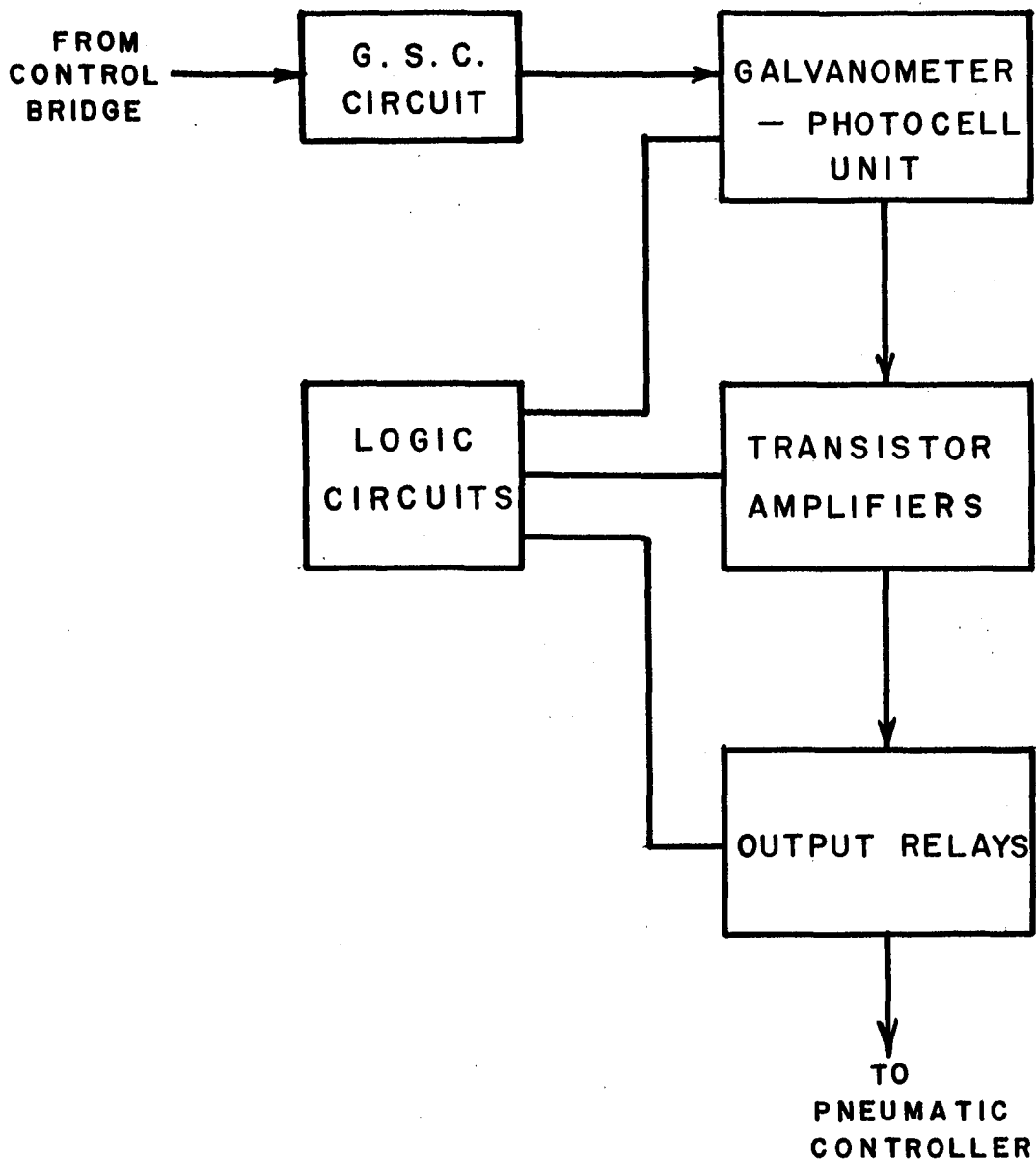
FIGURE 17 - Block Diagram of Electronic Control Unit.
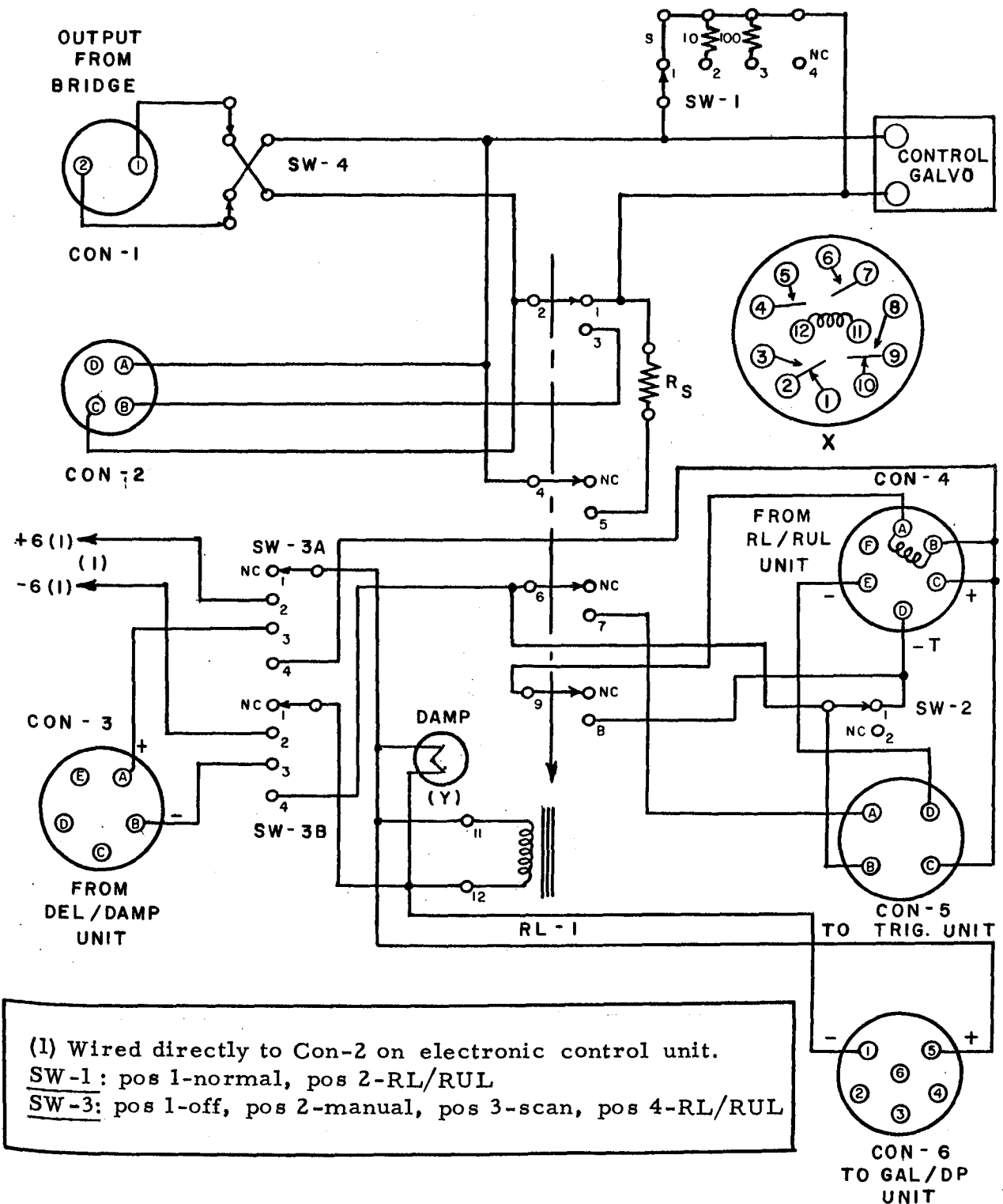
FIGURE 18 - Circuit Diagram for Galvanometer
Signal Conditioning Circuit.

manually or automatically shunting the galvanometer system. Switch SW-3 selects the various shunting (or damping) modes. In Position-1 the galvanometer is connected directly to the output of the control bridge via Connector CON-1. In Position-2 Relay RL-1 is activated; this removes the input signal, and shunts the galvanometer with R_s. The other shunting modes are activated by signals from various external systems such as the RL/RUL system. These are connected to the GSC circuit via Connectors CON-3, -4, -5 and -6.

A circuit diagram of the main section of the controller is given in Figure 19. Details of this section are discussed by Hardy and Larocque (24) in a recent paper, hence its operation will be outlined only briefly here. The bridge unbalance signal (ΔV) causes the light spot galvanometer in the GPU to deflect an angle α that is proportional to the magnitude and the sign of the unbalance. For example, if the load were above the control point the unbalance signal would be positive in sign and the galvanometer would deflect in a counter clockwise direction. A series of three photocells are located as shown in Figure 19. If the control bridge unbalance continues to increase to $+ \Delta V_\beta$, where the angle of deflection becomes $\alpha = +\beta$, then Photocell C-1 will be illuminated generating an output signal (E_1). This signal is amplified and in turn closes Relay R-1, which energizes the unloading solenoid valve in the pneumatic controller. As the load begins to decrease, ΔV decreases and when $\alpha < \beta$ the loading valve is turned off. If, however, the load increases too rapidly, it may overshoot the control point, ΔV will become negative in sign, and the galvanometer will deflect clockwise. If it reaches a level of $-V_\beta$, where $\alpha = -\beta$, Photocell C-3 will be illuminated, which will result in Relay R-3 closing and the loading solenoid valve in the pneumatic controller being opened. In effect the electronic controller is a highly sensitive relay circuit. For $\Delta V \geq |V_\beta|$ either the loading or unloading solenoid valve will be open depending on the sign of ΔV. For $\Delta V < |V_\beta|$ both valves will be closed. The controller therefore has a dead-band of 2 ΔV_β, which places a limit on the control precision of the overall system. The relative importance of the magnitude of the dead-band depends on the gain in the feedback loop and the control bridge. For example, consider that the system is operating in the constant stress (CS) mode, and that a change in specimen stress $\Delta \sigma_A$ results in an unbalance signal ΔV_A at the input of the electronic controller. If it is desired to control the stress to within a value $\Delta \sigma_A$, then it is necessary that $\Delta V_A \geq \Delta V_\beta$. Since $\Delta V_A = GK \Delta \sigma$, where G is the gain of the control bridge, and K is the sensitivity of the feedback transducer in volts/psi stress, the importance of the dead-band may be reduced by having large values of G and K.

The central photocell in the GPU is associated with one of the logic circuits. This circuit prevents either solenoid valves being energized until the other is de-energized. The light spot galvanometer is illuminated by a bulb (B-1) containing two separate filaments. In the event of a failure of the active filament an associated logic circuit switches the second filament into operation.
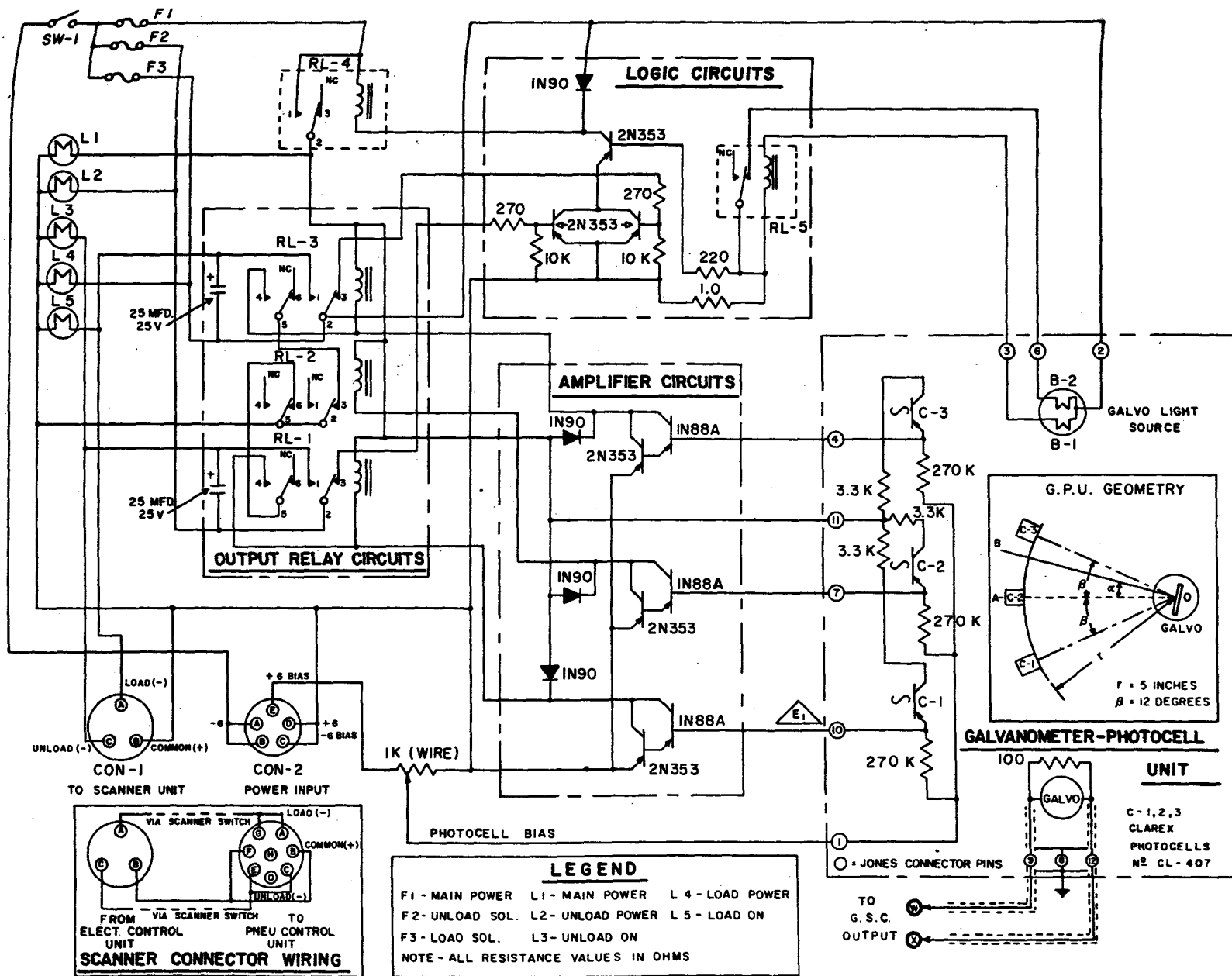
FIGURE 19 - Circuit Diagram for Main Section of Electronic Controller.

A series of tests was conducted to check on the sensitivity of the electronic controller. In particular, the critical input current (I_c) that would just deflect the galvanometer through the angle $\pm\beta$ (and hence trigger the solenoid valves) was measured for different settings of the galvanometer sensitivity control (SW-1, see Figure 18). The results are shown in Table 1. Figure 20 shows a number of views of the completed controller. Figure 20B shows a top view of the unit including the inside of the galvanometer-photocell unit.

TABLE 1

Controller Sensitivity

Switch Position	Shunt Resistance	I_c
	Ohms	μ amps
1	0	28, 000
2	10	27
3	100	5
4	infinity	2. 4

(ii) Control Bridge

The control bridge serves two purposes; first it supplies an excitation voltage to the bridge circuits in the feedback transducers, and second it amplifies the low level unbalance signals from these transducers to a higher level for activation of the electronic controller. The design and merits of various types of control bridges are described in detail by Hetenyi (26). The control bridge used was a Baldwin Type-K strain indicator modified for use with external four-arm bridge transducers. This was mounted in a standard relay rack panel. The rear of the unit was enclosed in a thick walled (1/4 in.) aluminum box, which was insulated by a one inch layer of glass wool and enclosed by an outer steel case attached to the rack panel. This arrangement was utilized in an attempt to stabilize the system from short term temperature variations. Some sections of the indicator were rewired to enable all electrical connections to be made at the rear of the unit. A signal (ΔV), denoted as the control bridge unbalance, was obtained by a parallel connection across the existing panel galvanometer in the indicator. This was brought by shielded cable to a connector at the rear of the unit.

In its original form the Type-K indicator operated from a set of self-contained A and B batteries. Since it was necessary that the bridge operate continuously for long periods of time, these batteries were replaced by a regulated A and B power supply operated from the 110 V a-c lines. Figure 21 shows the circuit of this supply.
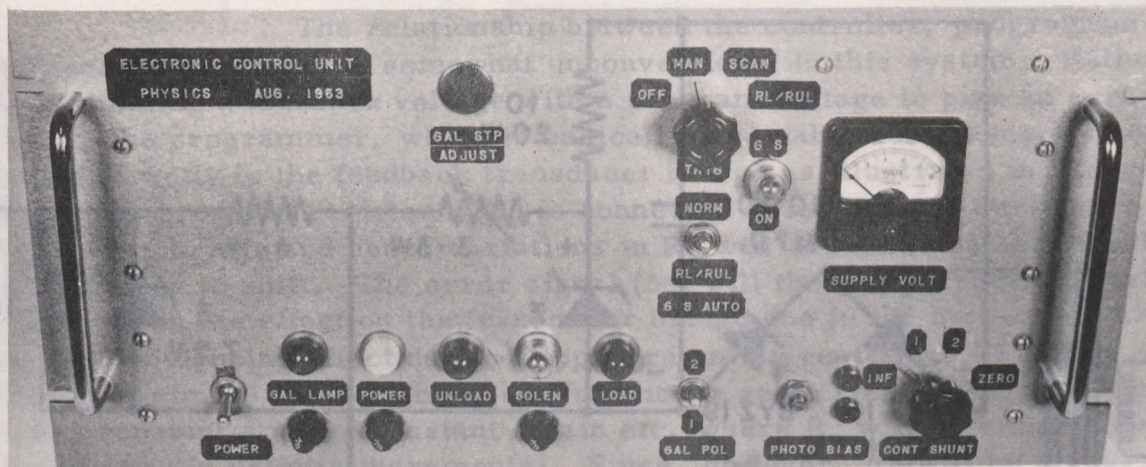
A.   Front View of Electronic Controller.
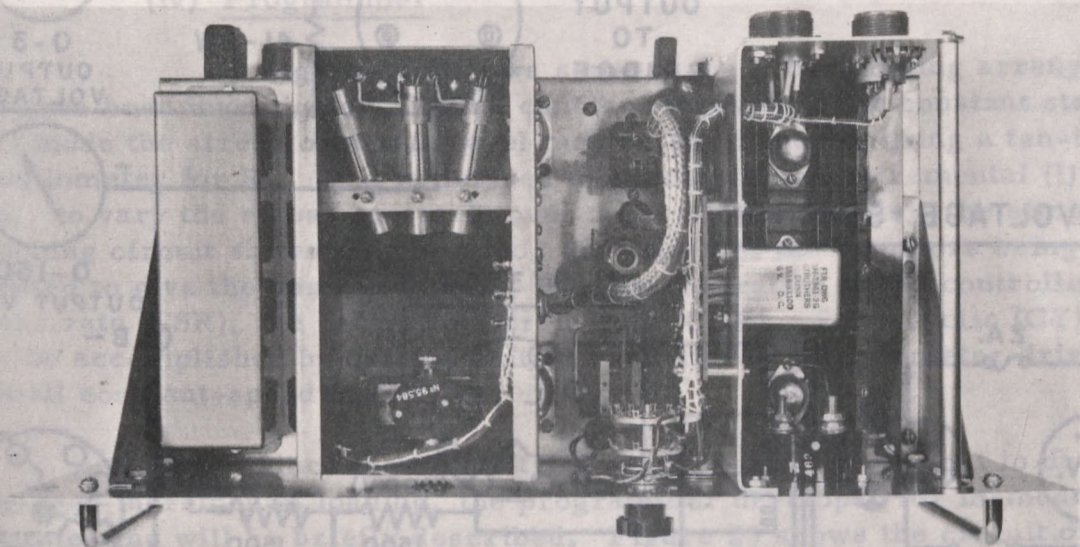
B.   Top View of Electronic Controller (section at left
contains the galvanometer-photocell unit).

FIGURE   20 - Photographs Showing a Number of Views
of Completed Electronic Controller Unit.

LOW VOLTAGE SECTION
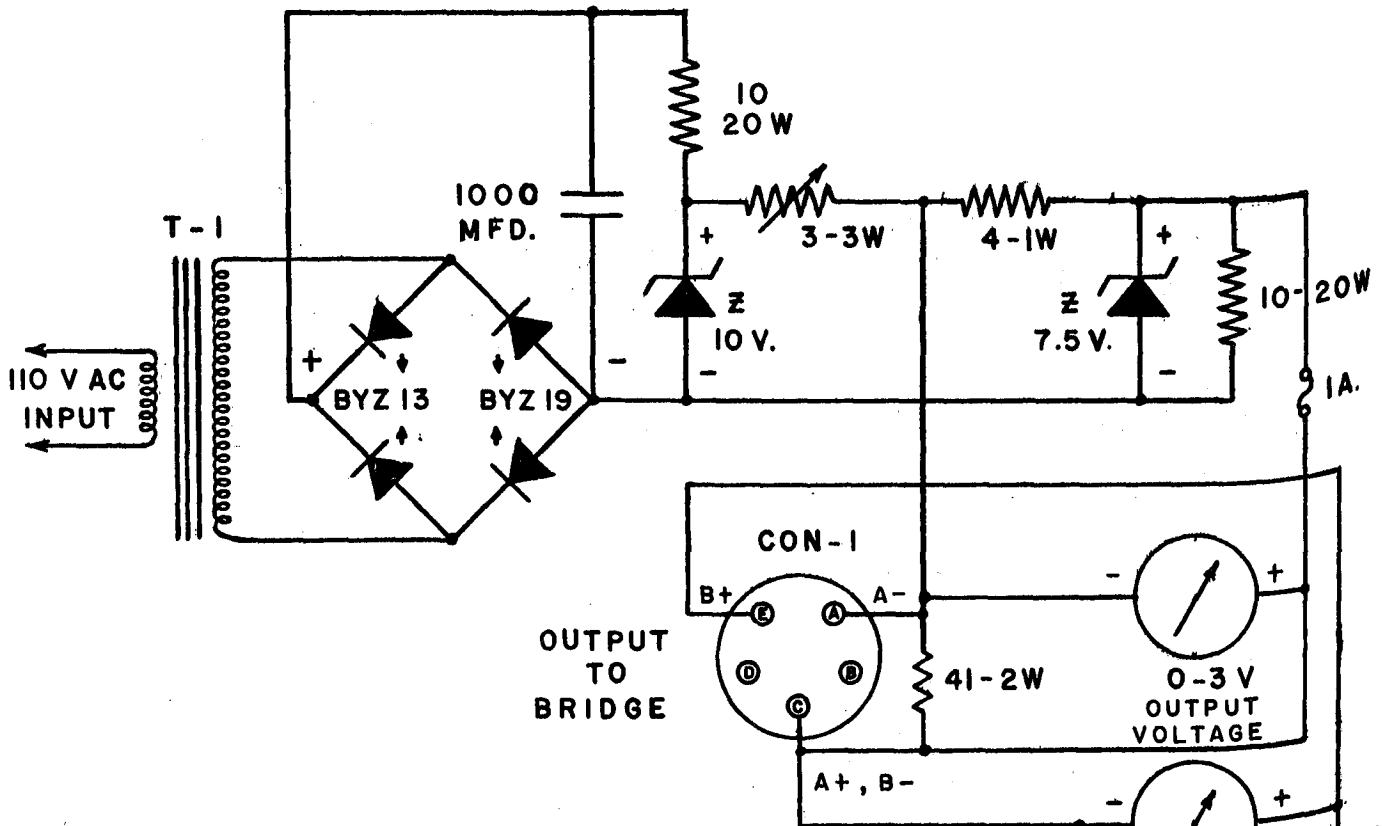
HIGH VOLTAGE SECTION
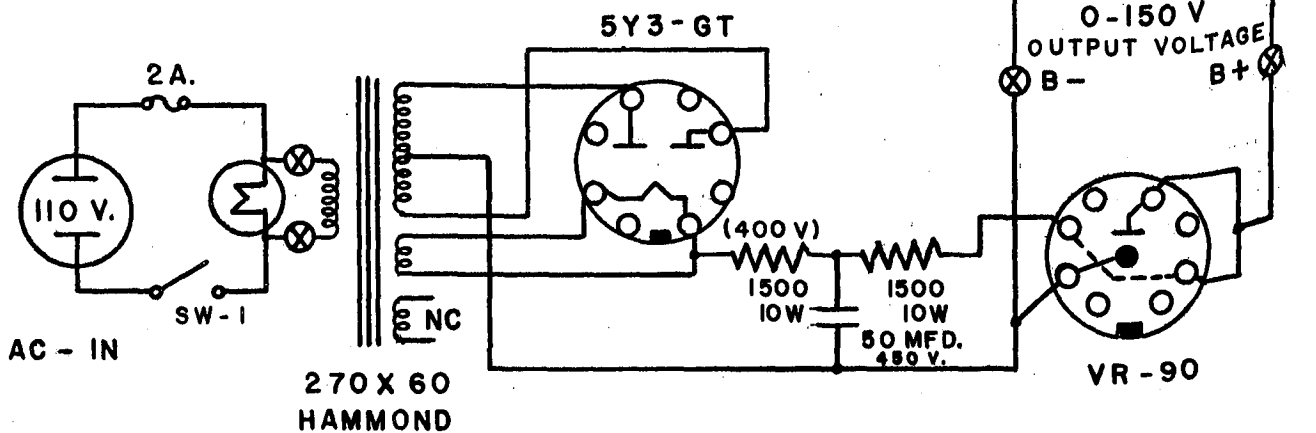
NOTE - ALL RESISTANCE VALUES GIVEN IN OHMS

FIGURE 21 - Circuit Diagram for Regulated Bridge Power Supply.

(iii) Programmer and Feedback Section

The relationship between the controller, programmer and feedback sections is somewhat unconventional in this system. Rather than summing a feedback voltage with a program voltage to give an error signal, the programmer, which is basically a variable resistance, is connected directly to the feedback transducer bridge as illustrated in Figure 22A. The program resistance R_v is connected across one of the arms of the transducer bridge and hence variations in R_v will cause the balance condition of the bridge to shift. The error signal (Δe) will thus be proportional to the difference in the effect on the transducer bridge due to the measured variable, and the unbalancing effect due to the programming resistor. This type of system is simple and relatively convenient for some type of programming (e.g., constant stress, constant strain etc. where R_v will be either constant or will vary in definite increments). Since, however, Δe will be a non-linear function of R_v*, programming of continuous variations in the controlled variable (e.g., constant rate of stressing) requires the use of special non-linear potentiometers.

(iv) Programmer

Figure 22B shows some of the programming arrangements that have been investigated. In the constant stress (CS) or constant strain (CE) mode the stress or strain level may be set manually using a ten-turn potentiometer for R_v. If it is desired to operate in the incremental (I) mode (i.e., to vary the stress or strain over a set of fixed levels), the simple switching circuit shown may be used, the values of the resistors being selected to give the desired levels. Finally, operation in the controlled stress rate (CSR), the controlled strain rate (CER), or the cyclic (CY) mode may be accomplished by using a suitable non-linear potentiometer driven by a small constant-speed motor.

Since the majority of experiments carried out to date have used incremental loading, the programmer developed for IS-mode programming will be briefly described. Figure 23 shows the circuit of the IS-mode programmer. It consists of the galvo damping circuit, the valve control circuit and the program circuit. A function switch (SW-1) coordinates the operation of the unit. In Position-1 the system is inactive; in Position-2 the system is active (or set) with one of the programming resistors connected across one of the arms of the feedback transducer bridge. Under these conditions the control system will maintain the stress constant at a value

---

* See standard equations for balance conditions in a four-arm Wheatstone bridge, e.g., Hetenyi (26).
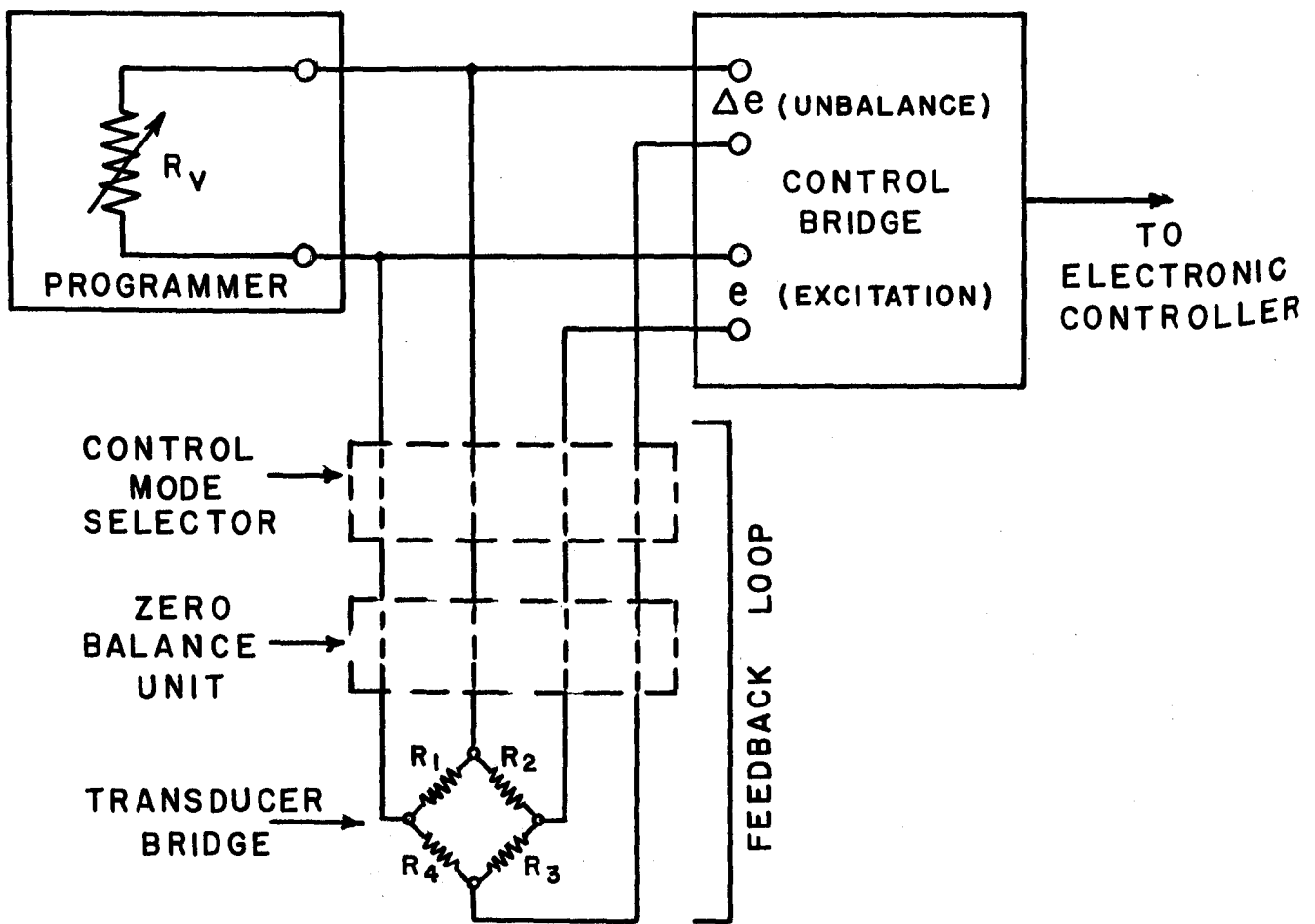
A. RELATIONSHIP OF PROGRAMMER TO FEEDBACK LOOP

a) CS/CE   b) I   c) CSR/CER/CY
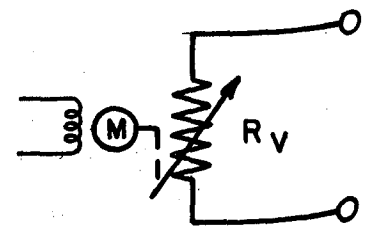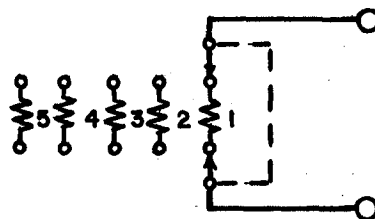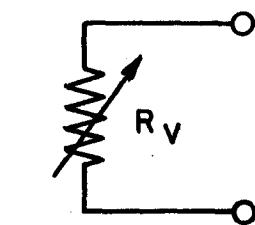
B. TYPES OF PROGRAMMING MODES

FIGURE 22 - Diagram Illustrating Details of Programming Arrangement.
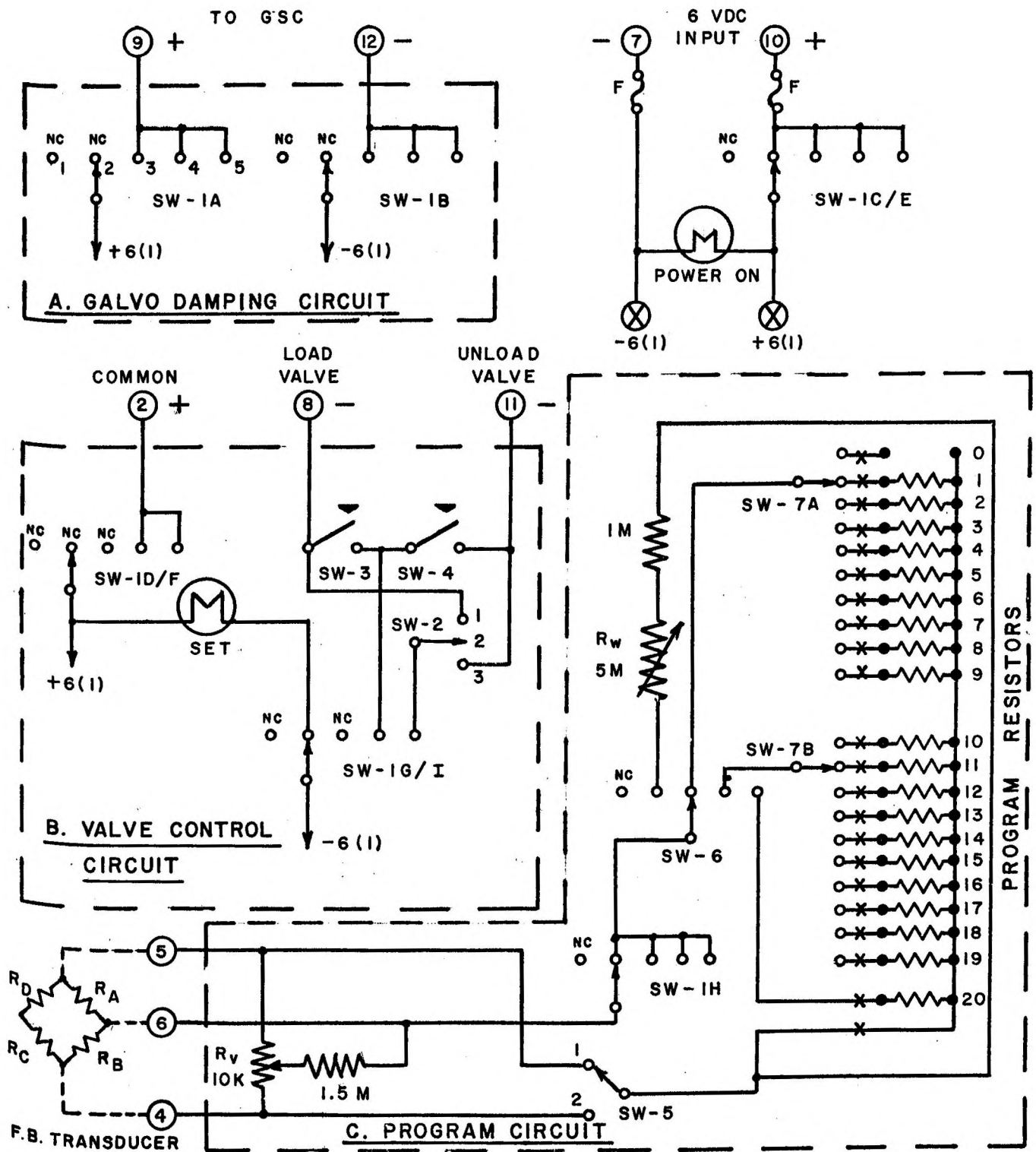
FIGURE 23 - Circuit Diagram of IS-Mode Programming Module.

determined by the particular programming resistor (selected by SW-5, SW-6 and SW-7). For example, the circuit diagram shows the programming resistor R_1 shunted across the arm R_A of the feedback transducer bridge. To increase the control stress to the next higher level, Switch SW-1 is first placed in Position-3, which damps the control galvanometer, SW-7 is shifted to Position-2, SW-1 is then placed in Position-4, and Switch SW-4 may now be used to open the loading solenoid valve in the pneumatic controller and allow the stress to rise. Observation of the panel galvanometer on the control bridge indicates when the system is approaching balance at the new level and at that time Switch SW-1 is placed back in Position-2. The unloading sequence follows the same order. Figure 24 shows two views of the completed IS-mode programmer module.

The program (or calibration) resistors each consist of an approximate resistance in series with a trimming potentiometer. Final adjustment of the particular values are made using a calibration chart with the controller connected into the actual control system. For convenience, each set of resistors and their associated trimming potentiometers are mounted on a plug-in card, as shown in Figure 25. Various loading programs, covering different ranges and with different increments, may be designed, each being constructed on its own plug-in card. Table 2 gives the calculated values of the program (calibration) resistors in Program 64/4, which was utilized for initial incremental studies on Wombeyan marble[*]. It should be noted that, since this material does not show appreciable inelastic behavior until a stress level of approximately 6500 psi, the initial stress increments in the program are large up to this level.

(v) Feedback Section

•The feedback section consists of a stress (load) transducer, a strain transducer, two zero balance units to allow adjustment of the two transducers, and a control mode selector that allows either stress or strain feedback to be selected.

Stress feedback is obtained by a Baldwin Type-C strain gage type load cell with a capacity of 20,000 lb, attached to the piston of the hydraulic ram. The load cell employed is a double bridge type that provides two separate outputs. One is used to provide the feedback signal in the control system, the other is fed to the measurement system to enable the specimen stress to be accurately monitored. These cells are calibrated to

---

[*] Initial experiments, using the facility, have been conducted on Wombeyan marble. This material is macroscopically homogeneous and isotropic, fairly coarse-grained (average grain size about 1.0 mm in diameter) and of high purity.

A. Front View of Program Module.
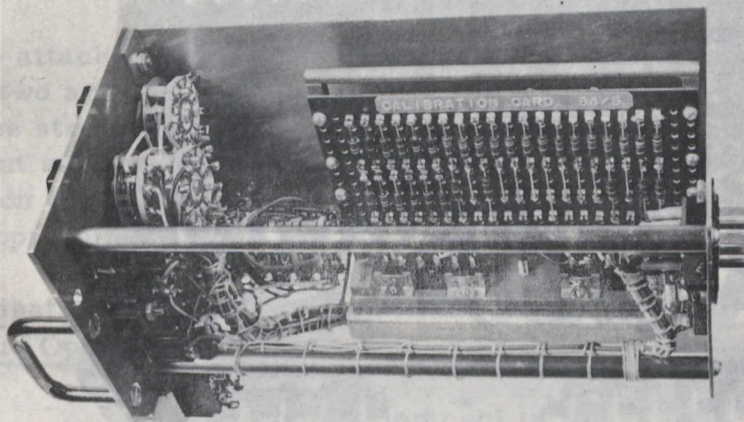
B. Side View of Program Module.

Figure 24 - Photographs Showing Two Views
of Incremental Mode Programmer.
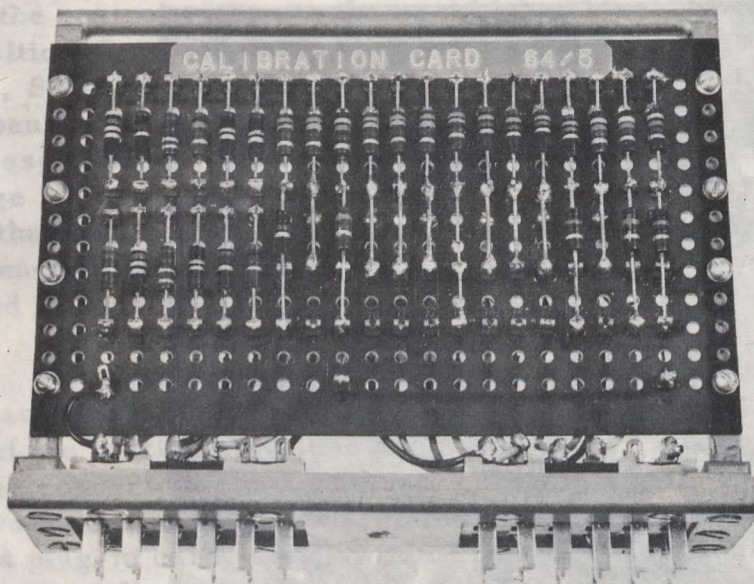
A. View of Plug-In Card Showing Fixed Resistors.
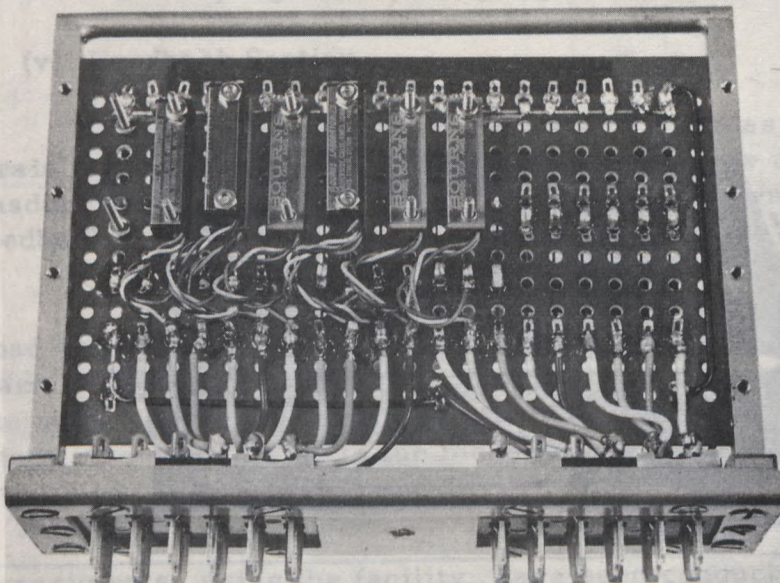
B. View of Plug-In Card Showing Trimming Potentiometers.

FIGURE 25 - Photographs of Load Program Plug-In Cards.

TABLE 2

Details of Program (Calibration) Card 64/4 used for Initial
Incremental Loading Studies on Wombeyan Marble

Switch Pos*	Load lb	Specimen Stress** psi	Program Resistor Ohms	Switch Pos*	Load lb	Specimen Stress** psi	Program Resistor Ohms
0	0	0	-	11	4400	9,944	71.8K
1	500	1130	625K	12	4600	10,396	68.7K
2	1000	2260	320K	13	4800	10,848	65.8K
3	2000	4520	158.8K	14	5000	11,300	63.3K
4	3000	6780	106.9K	15	5200	11,752	60.8K
5	3200	7232	98.6K	16	5400	12,204	58.1K
6	3400	7684	92.8K	17	5600	12,656	55.9K
7	3600	8136	87.8K	18	5800	13,108	54.1K
8	3800	8588	83.0K	19	6000	13,560	52.2K
9	4000	9040	79.1K	20	6200	14,012	50.6K
10	4200	9492	75.1K	--	--	--	--

*Refers to setting of Switches SW-6 and SW-7.
**Based on test specimen with a diameter of 0.750 in.

give an output of 2 MV per volt excitation at an applied load equivalent to
their capacity. The 20,000 lb cell employed has a sensitivity (K) of $0.6\mu V/lb$
(or $0.27\mu V/psi$ on a specimen with a diameter of 0.750 in.) with an excitation
voltage of 6 volts.

Strain feedback is obtained from a single resistance type
strain gage attached to the test specimen. This gage and a similar dummy
gage form two arms of a four-arm bridge arrangement, the output of which
provides the strain feedback signal. It is planned to modify this bridge
arrangement so that two arms of the bridge are strain sensitive. In this
configuration the strain sensitivity of the transducer will be increased by a
factor of approximately two.

1.4 Investigation of the Completed Axial Loading System in
Various Operating Modes

During the development of the system and after its
completion a series of studies was made on its operation. These included
an investigation of the behavior of the hydraulic ram, investigation of zero
drift effects in the load feedback transducer (load cell), investigation of the
effect of various parameters in the pneumatic control unit (in order to obtain
optimum stability in the constant stress (CS) mode), studies of stability in
the CS-mode, investigation of the behavior of the system in the incremental

stress (IS) mode, and finally the investigation of a simple method of loading at a constant rate of stress.

1.4.1 Behavior of the Hydraulic Ram

The hydraulic ram used in the axial loading system had an effective piston area of 11.045 sq in. Thus a ram pressure of 1000 psi would be expected to produce a ram thrust of 11,045 lb if the ram piston was friction-free. Since, however, some friction must necessarily be present as a result of the piston packing, a series of experiments was carried out to study the relationship of ram thrust to ram pressure. In these experiments the ram thrust was measured by a 20,000 lb load cell and ram pressure by a 0-3000 psi pressure gauge, which could be read to $\pm$ 7 lb. Figure 26A shows graphically the results of a number of experiments. The relationship appears to be linear for ram pressures greater than 100 psi. However, the curve does not appear to pass through zero, indicating the presence initially of an internal restoring force of approximately 600 lb. The slope of the curve, which should be equal to the area of the ram piston, was found to be approximately 10.7 sq in. This value differs from the quoted effective piston area (11.045 sq in.) by approximately 3 per cent, which is within the experimental error. The maximum ram thrust obtainable from this system is approximately 20,800 lb, which is developed at a ram pressure of 2000 psi (the maximum available nitrogen supply pressure).

Since the majority of the initial deformation experiments were to be conducted at relatively low axial loads (0-6000 lb), the behavior of the ram at these lower levels was further investigated. Figure 26B illustrates the variation of observed versus calculated ram thrust for two different experiments. The calculated ram thrust was determined from the measured ram pressure and the quoted effective ram area. The curve appears linear (region A-B) for ram thrusts above 550 lb, having a slope of approximately 1.0. Below this level (region O-A) the slope of the curve decreases to a lower value and the projected curve appears to pass through zero. It is suggested that the behavior in the region O-A is associated with packing friction and possibly with the extension of an internal spring, which serves to return the ram piston to its initial position when the piston pressure is reduced.

The behavior of the hydraulic ram in the region of interest (600-5000 lb) was found to be linear and reproducible. In this region the measured ram thrust was found to be approximately 450 lb lower than that calculated from the applied ram pressure. The anomalous behavior at ram thrusts below 600 lb is not considered important in the present application.
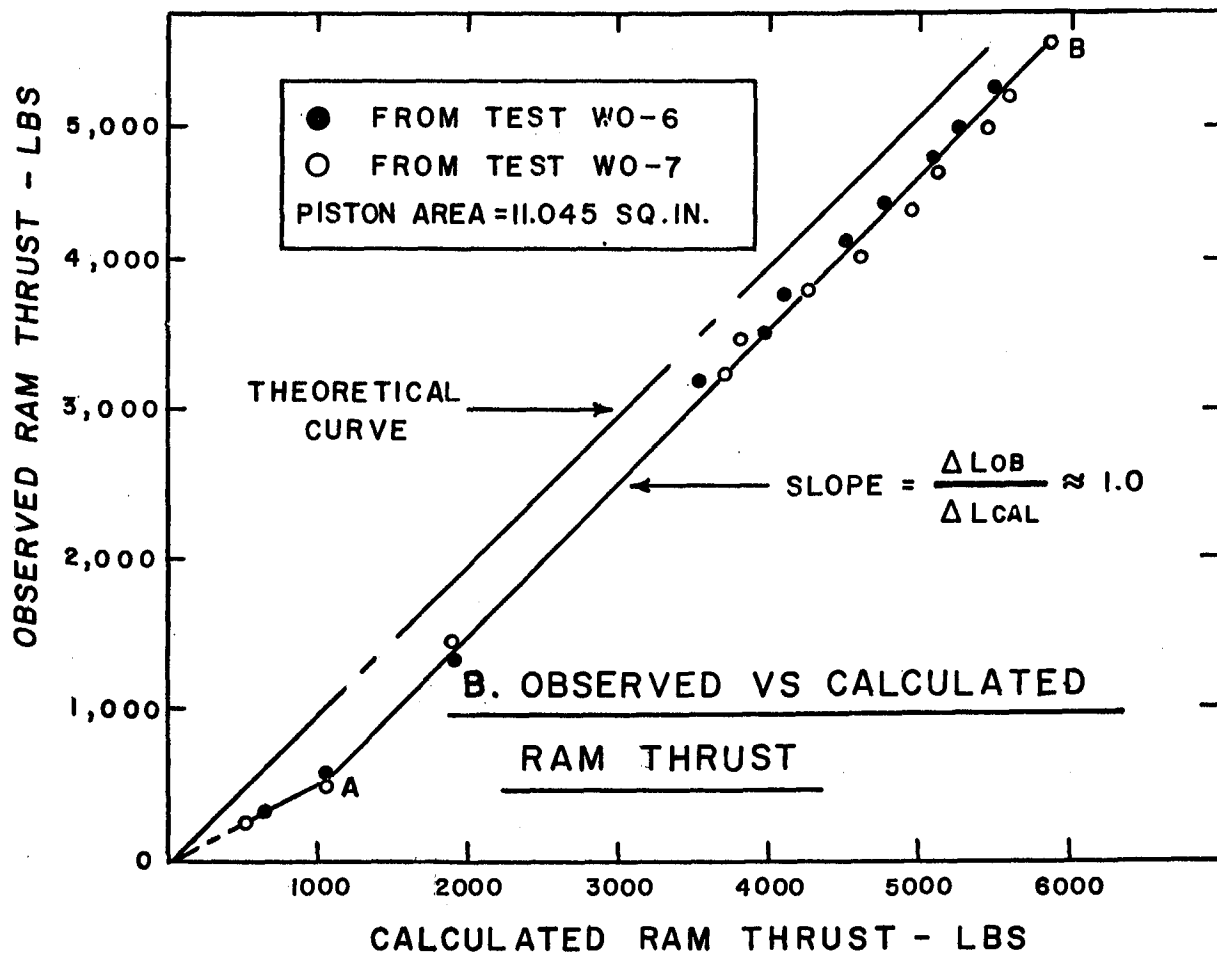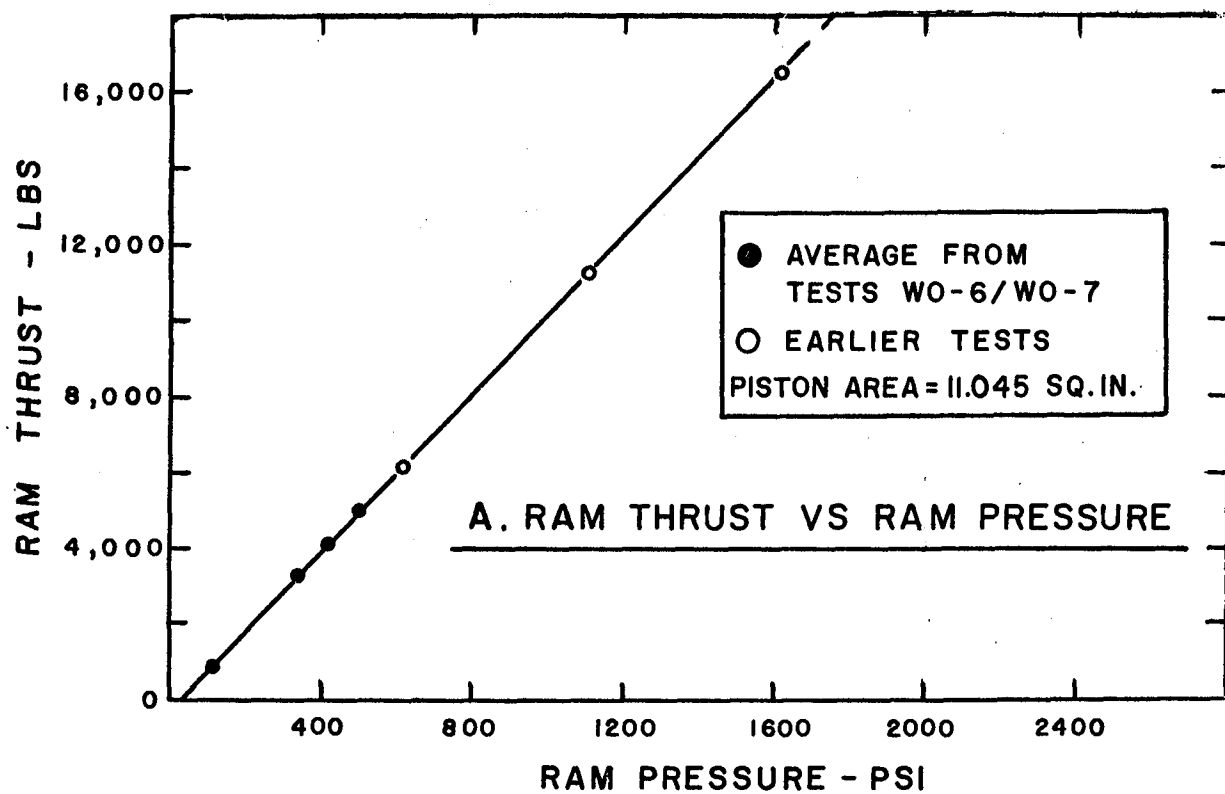
FIGURE 26 - Curves Illustrating Behavior of Hydraulic Ram.

1.4.2 Constant Stress Mode

(i) Load Cell Zero Drift

The stability of the control system in both the CS- and IS-modes depends on the stability of the load cell. Since no experimental method could be conceived to determine this stability during actual loading conditions, indirect means were adopted to estimate its magnitude. These consisted of studying the zero drift of the load cell over a period of time under no-load conditions, and investigating the zero drift produced after a period of sustained loading. It should be noted that all studies presented refer to a 20,000 lb Baldwin Type-C load cell. Table 3 lists the data from a number of these experiments.

All measurements of equivalent load variation quoted in Table 3 were made using a 12-channel printing recorder with no external amplification. From past experience it was determined that the charts from this recorder could be read to $\pm$ 1/10 of a small division, which corresponds to an experimental error of $\pm$ 8.5 lb.

TABLE 3

Load Cell Zero Drift Data

Test	Reference	Temperature	Average Load*	Test Period	ΔL**	$\Delta \sigma$+
		°C	lb	Hours	lb	psi
A	(WO-4)	22 $\pm$ 0.2	ZERO	20	$\pm$ 8.5	$\pm$ 19.3
B	(64-7)	22 $\pm$ 0.2	ZERO	48	$\pm$ 8.5	$\pm$ 19.3
C	(WO-4)	22 $\pm$ 0.2	2600	$1\frac{1}{2}$	- 8.8	- 20
D	(WO-6)	22 $\pm$ 0.2	3500	5	- 9.2	- 21
E	(WO-7)	22 $\pm$ 0.2	3500	5	- 25.2	- 55
F	(WO-2)	22 $\pm$ 0.2	4700	2	+ 26.0	+ 59

*In some experiments the load was maintained at various levels for a period of time. The value quoted is an average of these levels.

**Value quoted is load equivalent to observed maximum deviations from initial zero value.

+Value quoted is stress due to ΔL acting on a specimen with a diameter of 0.750 in.

The zero drift under no-load conditions (Tests A and B) was found to vary randomly about a relatively constant mean. The maximum limits of this variation being of the order of $\pm$ 8.5 lb. These variations are within the limits of the experimental error of the measurement system. The values of zero drift observed after the application of various sustained loads (Tests C-F) represent the difference between the initial and the final zero load levels. These measurements represent displacements; hence, if $-17 \leq \Delta L \leq + 17$ lb the variations will be within the experimental error. This is certainly the case for Tests C and D. Tests E and F lie slightly outside the range of experimental error, which may indicate that there has been a small zero drift, but the fact that the drift is positive for one test and negative for the other would suggest that the estimated value of experimental error was too low.

For the experiments carried out to date it appears that the load cell zero is stable to within approximately $\pm$ 13 lb, which compares closely with the calculated experimental error of $\pm$ 8.5 lb.

(ii) Optimization of the Pneumatic Controller

The pneumatic controller contains a number of parameters that must be adjusted to provide optimum control. These are (see Figure 13) the settings of the loading and unloading micrometer valves* (V-6 and V-10), the differential pressure ($\Delta P = P_{in} - P_c$) across the loading valve (V-6), and the ballast volume. The effects of these various parameters were investigated in considerable detail**, but only a brief review of these studies and the conclusions will be presented here.

In the CS-mode the optimum control conditions are defined as "those conditions that result in the axial applied load remaining as nearly constant as possible with time". The typical variation of applied load with time is shown diagrammatically in Figure 27A. It consists of a cyclic variation about the control point (L_c). The control point (L_c) for convenience is defined as the average load level based on the peak values, namely $L_c = (L_{max} + L_{min})/2$. The load fluctuation ($\Delta L(F)$) is defined as the peak to peak value of the fluctuation, namely, $\Delta L(F) = (L_{max} - L_{min})$. Table 4 illustrates the results of a number of typical tests conducted over short periods of time for various settings of the parameters. Figure 27B illustrates a section of a typical load versus time curve. The short period disturbance on this recording is due to background noise in the measurement system.

---

*The settings of the loading and unloading micrometer valves are abbreviated as LV and ULV. For example, the statement LV = 11 means that the loading valve is set at 11.

**During the period December 1963-September 1964 a number of experiments were carried out. These include Test Series 63-6 and 64-13. The detailed data and results of these tests are held by the writer.

A. TYPICAL LOAD VERSUS TIME VARIATION (NO DRIFT)

B. SECTION OF A TYPICAL LOAD VERSUS TIME RECORD

C. LOAD VERSUS TIME VARIATION WITH DRIFT
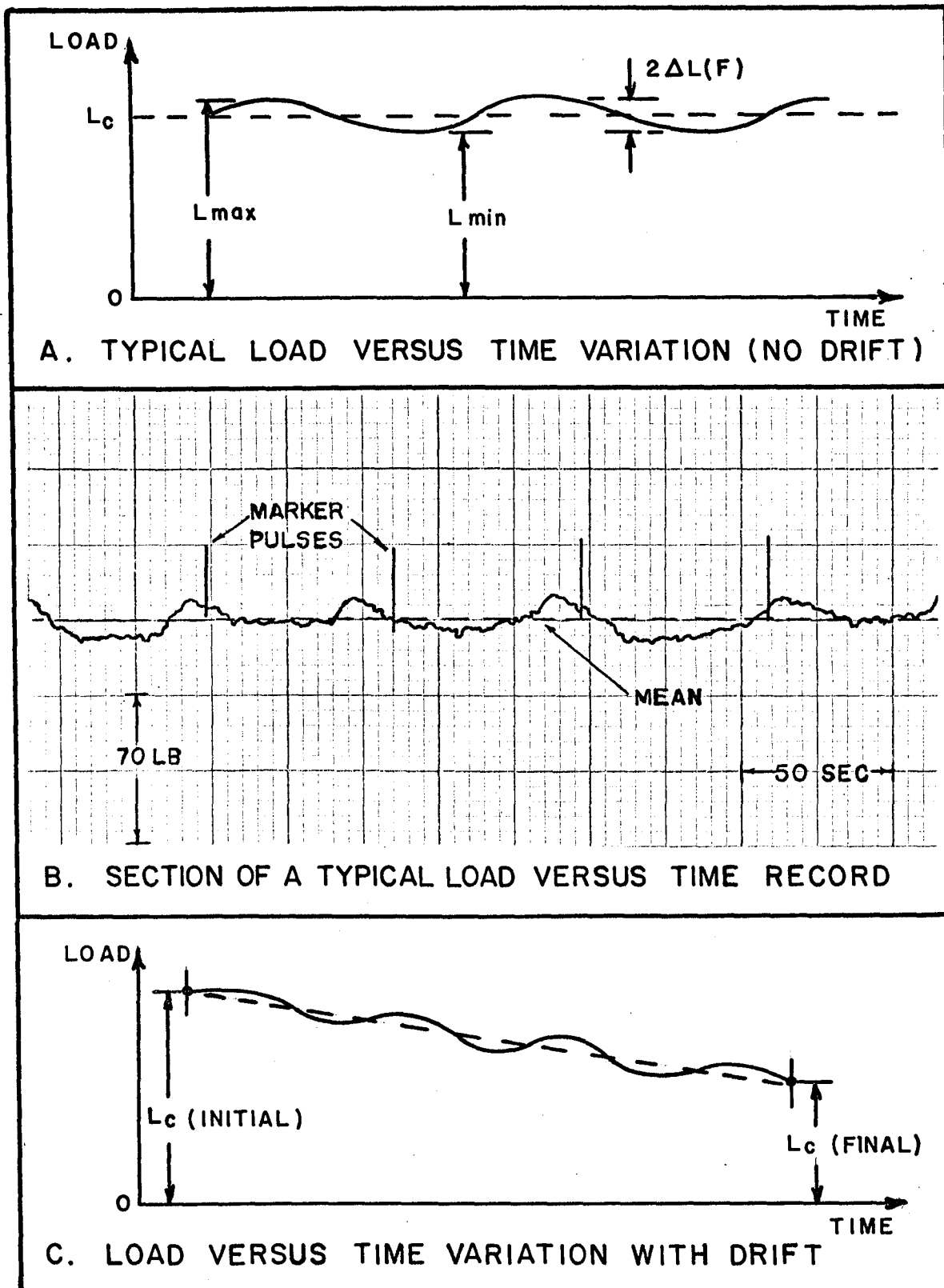
FIGURE 27 - Curves Illustrating Behavior of Control
System Operating in CS-Mode.

TABLE 4

Variation of Load Fluctuation with Various Parameters

(Control System in CS-Mode)

Test	P_c*	Control Parameters			L_c	$\Delta L(F)$	$\dfrac{\Delta L(F)}{L_c} \times 100\%$
		ΔP*	LV**	ULV**			
	psi	psi	Valve – Setting	Ballast	lb	lb	
A	700	100	11	4	out	7830	222	2.8
B	700	100	9	4	out	7830	156	2.0
C	700	100	7	4	out	7830	102	1.3
D	700	100	5	4	out	7830	22	0.3
E	700	100	7	4	in	7830	31.2	0.4
F	700	100	5	4	in	7830	13.2	0.17
G	700	100	5	3	in	7830	22.8	0.29
H	700	100	4	3	in	7830	4.5	0.06
I	480	100	4	4	in	5297	8.2	0.16

* P_c and ΔP values are approximate.

** LV and ULV settings quoted are in terms of the smallest calibrated divisions on the valve micrometer. Each division corresponds to a rotation of 36 degrees.

The results of these tests have indicated the following:

(1) The smaller the value of ΔP the less sensitive the control system is to the LV setting. The lowest possible ΔP is therefore desirable. However, when using low values of ΔP care must be taken to ensure that the regulator controlling ΔP is sufficiently stable to maintain the desired value.

(2) The lowest load fluctuations are attained with the ballast cylinder in the system.

(3) In general, the lowest load fluctuations are obtained with the lowest values of LV and ULV settings. The lower limit of the LV setting is determined by the natural leakage of the system. The response time of the system is also a function of the LV and ULV settings. If these are too low, the system will require an undesirably long time to come back into a stable condition if unbalanced significantly from the control point by a disturbance*. In general, a LV and ULV setting of 4.0 has been found to be the most satisfactory.

(4) It has been generally found that the percentage load fluctuation $(\Delta L/L_c) \times 100\%$ decreases with increasing load level. It is felt that this is due in part to the fact that frictional effects in the hydraulic ram and the separator become less important at higher load levels, and that the overall control system is only sensitive to load fluctuations greater than $\pm \Delta L(\alpha)$. The value of $\Delta L(\alpha)$ depends on the design of the galvanometer-photocell unit in the electronic controller, the sensitivity of the load cell, and the overall gain of the system. It is, therefore, a constant independent of load level; thus its effect on the percentage fluctuation will be of less importance at the higher load levels.

Based on these studies, the optimum conditions given in Table 5 are employed when operating in the CS-mode:

TABLE 5

Optimum Control Conditions
(CS-Mode)

Ballast	-	IN
ΔP	=	100 psi
LV	=	4.0
ULV	=	4.0

* This condition is undesirable when incremental loading is being carried out and will be discussed later in this section.

For these settings the load fluctuation ($\Delta L(F)$) appears to be less than $\pm$ 15 lb for experiments conducted over periods of time up to 10 hours.

(iii) Load Drift

The load drift ($\Delta L(D)$) of the control system is defined as the variation of the average load level (L_c) with time, namely $\Delta L(D) = L_c$ (final) - L_c (initial). Figure 27C illustrates a case where there appears to be a linear load drift. Table 6 presents load drift data from a number of deformation experiments conducted at different load levels and for various periods of time. The magnitude and the direction of the load drift do not appear to be dependent on the load level or on the duration of the test, although it may be significant that the largest load drift (+ 35 lb) observed in Test G was associated with the longest test duration (1481 minutes). The other observed load drifts are within the limits of load cell drift ($\pm$ 13 lb) determined experimentally and quoted earlier in this section.

TABLE 6

Values of Load Drift Obtained from a Number of Deformation Experiments

Test	References	Time	L_c	$\Delta L(D)$	$\dfrac{\Delta L(D)}{L_c}$ x 100 %
		Minutes	lb	lb	
A	(WO-3)	165	4420	0	0
B	"	113	5270	0	0
C	"	606	5620	0	0
D	(WO-4)	51	4850	+8.9	+0.18
E	"	170	5700	-26	-0.46
F	"	128	5930	0	0
G	"	1481	5930	+35	+0.59
H	(WO-5)	22	3960	-9.3	-0.23
I	"	37	5100	+2.2	-0.04
J	"	44	5340	+24.3	-0.46
K	(WO-6)	34	4150	+2.7	+0.07
L	"	38	4970	-3.5	+0.07
M	"	38	5270	-15.5	-0.29

1.4.3 Incremental Stress Mode

The IS-mode of operation makes it possible to rapidly raise or lower the load control level between two preselected values. To date its main purpose has been in incremental creep experiments. Here it is necessary to carry out creep experiments on the same specimen over a preselected range of load levels. To obtain significant data from such experiments it is necessary that the shift from one load level ($L_c(1)$) to the next ($L_c(2)$) be carried out as rapidly as possible. This is accomplished by first shunting the control galvanometer in the electronic controller, setting the load level selector switch in the IS-mode unit to the new required level, manually raising the control pressure (P_c) to the correct value, and finally removing the control galvanometer shunt and allowing the load control system to settle at the new level ($L_c(2)$).

Figure 28A illustrates the form of the load versus time disturbance produced during such an incremental load change. Three important parameters (see Figure 28A) are associated with this type of operation, namely: the loading time (T_L), the setting time (T_s), and the load overshoot ($\Delta L(O)$). Optimum operation in this mode requires that T_L be as small as possible while still maintaining T_s and $\Delta L(O)$ within certain limits. If an attempt is made to obtain very low values of T_L (which requires the control pressure to be raised very rapidly), it is found that both $\Delta L(O)$ and T_s become excessive (see Figure 28B). If an attempt is made to maintain $\Delta L(O)$ and T_s at too low a value, T_L will necessairly be excessively large (see Figure 28C).

The results of a large number of experiments have indicated that with care it is possible to carry out incremental loading experiments within the range of conditions listed in Table 7.

TABLE 7

Optimum Operating Conditions
(IS-Mode)

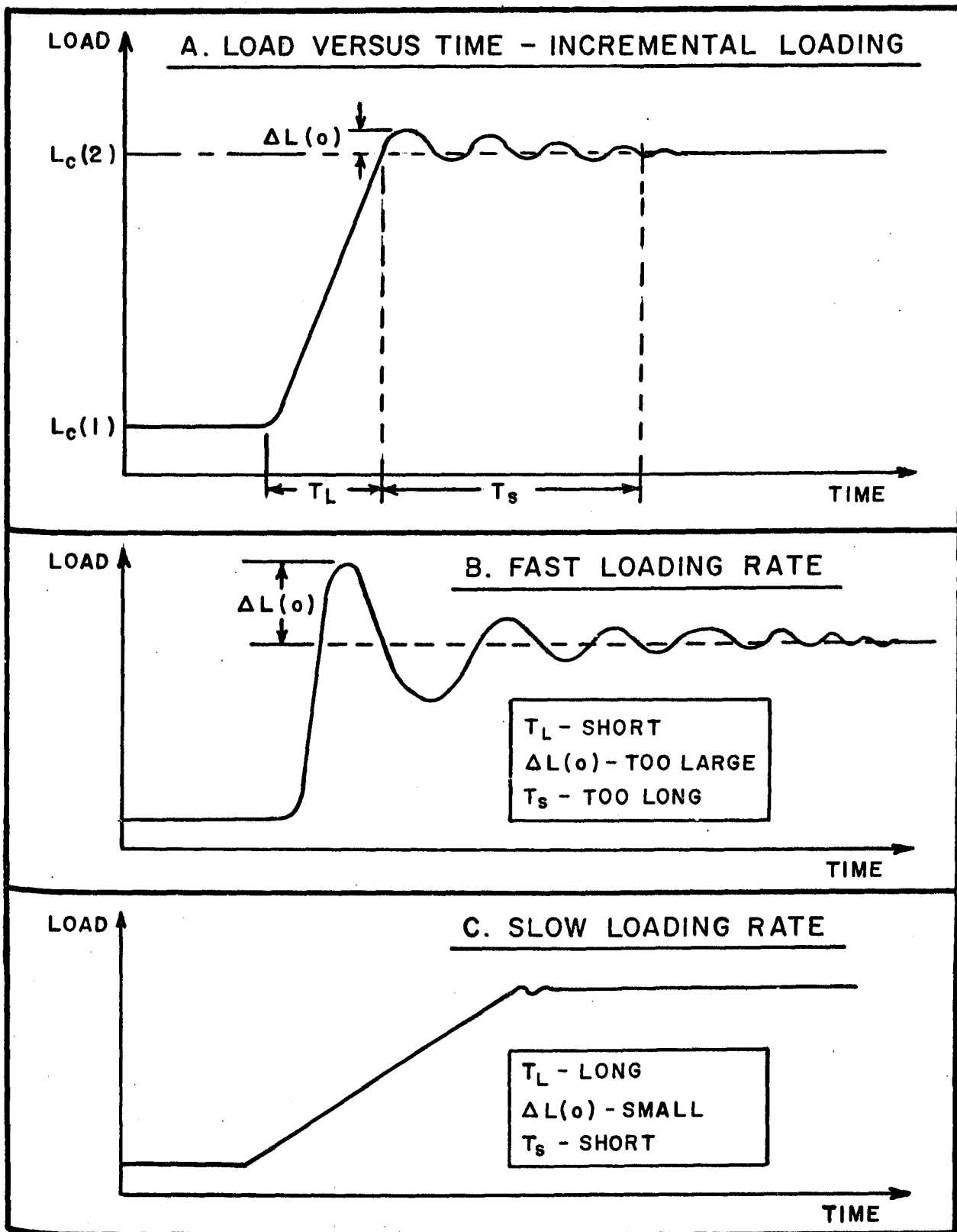| Factor	Range
ΔL	100 - 500 lb
L_c	2000 - 6000 lb
T_L	4 - 6 sec
$\Delta L(O)$	4 - 20 lb
T_s	100 - 300 lb

FIGURE 28 - Curves Illustrating Behavior of Control
System Operating in the IS-Mode.

The reproducibility of the various load levels was also investigated, using the load data obtained from two separate experiments (WO-6 and WO-7). It was found that the average error was only $\pm$ 10 lb, which was well within the possible error ($\pm$ 13 lb) due to load cell drift.

1.4.4 Constant Stress Rate Mode

A simple method for carrying out deformation experiments at an approximately constant stress rate (constant loading rate) was investigated. In this method only the pneumatic control unit was used; the remainder of the feedback control system was not employed. A nearly constant rate of loading was obtained by manually opening the loading solenoid valve (V-8, Figure 13) and allowing gas at the supply pressure to flow via the micrometer metering valve (V-10) to the separator, thus increasing the hydraulic pressure and the ram thrust. Figure 29A shows a simplified drawing of the pneumatic circuit.

A short series of experiments was carried out to check on the range of loading rates ($\dot{L}$) obtainable and their linearity. In all cases a supply pressure of 1000 psi was used, and load versus time curves were obtained for various settings of the micrometer loading valve. Figure 29B illustrates diagrammatically a typical load versus time curve. The data for these experiments are presented in Table 8.

From the results it appears that the method is satisfactory. A wider range of loading rates and an extended linear region should be possible if the ballast cylinder is disconnected from the circuit and if higher supply pressures (up to 2000 psi being available) are employed. It should also be noted that a number of unloading experiments were also carried out. Here the gas pressure in the system was bled off at a rate that was also determined by a micrometer metering valve. It was found, however, that under these conditions the load versus time curves were very non-linear over most of their range.

1.5 Stress, Strain and Confining Pressure Measurement System

1.5.1 Strain Transducers

The strain transducer itself presents a problem to which the final solution may be at best a compromise. In metals testing, strain gages directly attached to the test specimen and clip-on type gages using differential transformers have been widely used for uniaxial testing. Transducers using capacitance-type elements, vibrating wire elements, as well as a number utilizing various sonic and optical principles have also been employed. The majority of these methods are difficult and inconvenient to apply to testing of basically brittle geologic materials due to difficulties in specimen preparation and to the attachment of the transducer to the test
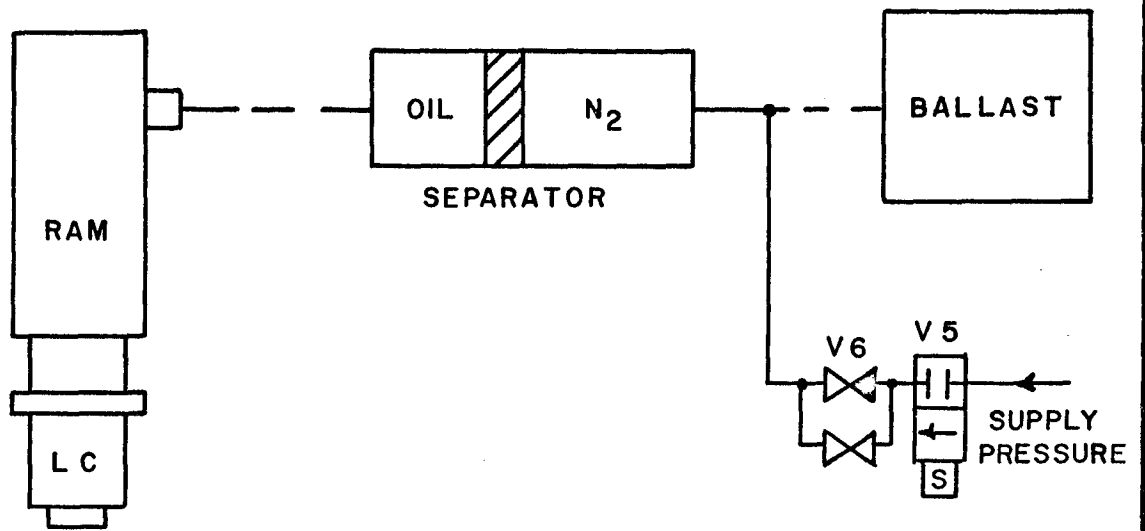
A. SIMPLIFIED PNEUMATIC CIRCUIT
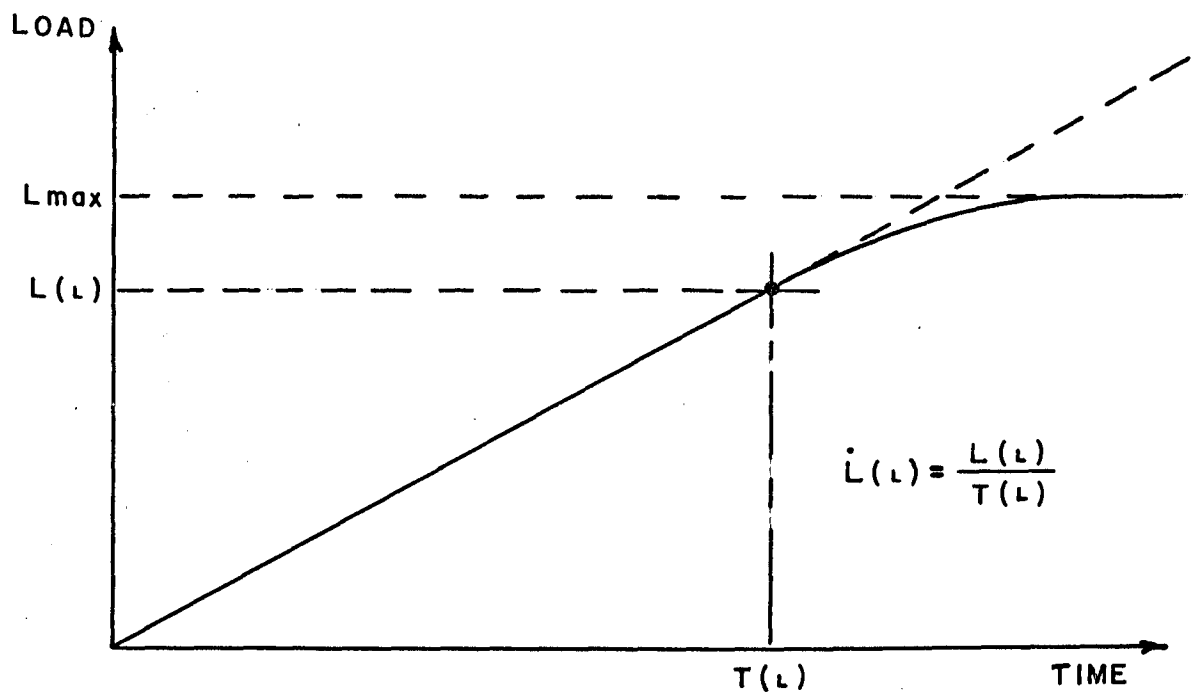
B. TYPICAL LOAD VERSUS TIME CURVE

$$\dot{L}(\iota) = \frac{L(\iota)}{T(\iota)}$$

FIGURE 29 - Outline of a Simple System for CSR-Mode Operation.

TABLE 8

Behavior of a Simple System for Obtaining an Approximately
Constant Rate of Loading

Test	Reference	Supply Pressure	LV* Setting	L_{max}**	$L(\mathfrak{t})$+	$\dfrac{L(\mathfrak{t})}{L_{max}}$ x 100%	$\dot{L}(\mathfrak{t})$++ lb/sec
		psi		lb	lb		
A	(64 - 15A)	1000	3.5	11,600	9,650	83	5.4
B	(64 - 15C)	1000	4.0	11,600	8,700	75	15.0
C	(64 - 15D)	1000	6.0	11,600	7,000	60	62.0

* LV settings quoted are in terms of the smallest calibrated divisions on the valve micrometer. Each division corresponds to a rotation of 36 degrees.

** L_{max} is the maximum load obtained in the test.

+ $L(\mathfrak{t})$ is the load at which the load versus time curve starts deviating from linearity.

++ $\dot{L}(\mathfrak{t})$ is the loading rate determined from the linear region of the load versus time curve.

specimen. Furthermore, it is desirable that the method used for the present uniaxial studies be equally applicable to future triaxial experiments.

Geophysicists and engineers involved in the study of the mechanical properties of geologic materials have utilized a number of methods of strain measurement both for uniaxial and triaxial tests. In uniaxial tests at the Mines Branch, early experiments (19) utilized an optical-mechanical system known as the Martens Mirrors apparatus. This system was time consuming and did not lend itself to recording. Later experiments utilized wire-type strain gages bonded directly to the specimen and, more recently, foil-type strain gages have been employed. However, at present the majority of routine short period uniaxial tests on geologic materials at the Mines Branch utilize an axial strain gage type compressometer and a transverse differential transformer type extensometer clamped to the test specimen. These were modified from the original design of Leeman and Grobbelaar (30, 31), and have proven very successful for short period test work. Recently Hunt (27) utilized this type of compressometer in a series of creep experiments on salt. The compressometer appeared to function in a well behaved manner over a 24 hour period to a maximum strain level of approximately 500 μs; however, it was not possible to assess the actual stability of the transducer by such indirect means.

A number of methods have been utilized by various workers in which specimen strain was determined by measurements of loading piston displacement. Griggs (12), Handin (15) and Robertson (40) have measured loading piston displacement by means of dial gages. Griggs and Handin (13) and Handin (15) have also used dial gages with attached precision potentiometers to give displacement data in a convenient form for recording. Handin (16) and Donath (7) have used differential transformers to measure piston travel. A recent paper by Serdenzecti and Boozer (42) illustrates their use of linear potentiometers for the same purpose. The capacitance-type strain transducer developed by Papirno (35) or some modified form of unbonded strain gage might also be applied. The latter concept has been under consideration by the United States Bureau of Reclamation for some time.

Although methods involving the measurement of piston displacement have proven more or less satisfactory for experiments where large strains (up to 10%) are involved, their use in experiments where small strains (maximum 0.5%) and small strain increments (0.001%) are of interest would probably be unsatisfactory in most cases. First, there is the problem of the interface between the specimen and the loading piston, secondly, the stability and accuracy of the necessary mechanical arrangement, and, finally, the degree of resolution of the transducer itself.

Even with extremely fine polishing of specimen end-surfaces, the actual surface will contain a large number of asperities, and under a compressive load such a surface will compress rapidly upon initial loading due to failure or to the development of plastic deformation in the individual asperities. It is obvious that strain measurements based on deformation measurements made across such a surface (as would be the case if relative motion of the loading piston was being considered) would be seriously in error, particularly at low loads.

Secondly, the mechanical stability and the accuracy of an external strain measuring system, although not too difficult to achieve in large strain experiments, become major difficulties when small strains are being considered. It is also important to remember that transducers such as potentiometers have an upper limit in their resolution based on the size and spacing of their resistive elements, and this limits their use to displacement increments of 100 μs or greater. Although such elements as capacitance- and differential transformer-type strain gages are capable of higher resolutions, there would be considerable difficulty in obtaining suitable mechanical stability in the overall deformation measuring device.

It is felt at the moment that the use of electric resistance strain gages attached directly to the test specimen offers the most convenient and reliable method of strain measurement. Their geometry and small size make it possible to mount a number on each specimen to provide data on possible specimen bending and on strain uniformity during the experiments. Considering future triaxial studies, this type of strain transducer offers no difficulty with regard to specimen jacketing, mechanical stability, or end-effects. However, this type of transducer does introduce another factor, namely the effect of confining pressure on the strain gage element itself. Brace (3) has investigated this effect in detail for confining pressures up to 150,000 psi. In his experiments Brace utilized three axial strain gages mounted at 120° apart around the circumference of the test specimen. This enabled him to determine the average axial strain and the maximum axial strain due to bending. Following discussions with Brace (2), it was decided to apply the same strain measurement procedure in the writer's experiments.

1.5.2 General Description of Measurement System

After considerable consideration it was decided to utilize measurement transducers[*] based exclusively on electric resistance strain gages. As a result load (stress) measurements are made using Baldwin load cells, specimen strains are measured by foil-type strain gages attached directly to the test specimen, and in future triaxial experiments confining pressures will be monitored by Baldwin pressure cells. The choice of this form of instrumentation has been influenced by the convenience in size and operation of the equipment, by the fact that the theory and application of strain gage measurement are well developed, and by the commercial availability of the equipment.

Figure 30 shows a block diagram of the overall measurement system. A general view of the system is shown in Figure 31. A system for very accurate monitoring of room and specimen temperatures, using thermocouples, is also included in the "Slow" Y-T recorder system. This system will be discussed in more detail in a later section. Load, confining pressure, strain, and temperature are converted to electrical signals by the appropriate transducers at the test area. These signals are carried by cable from the test area in the inner room to junction boxes and switching units in the outer room. Readout facilities here consist of,

    (1) a manual readout system,
    (2) a 12-channel "Slow" Y-T recorder system,
    (3) a 2-channel "Fast" Y-T recorder system, and
    (4) a single channel Y-XT recorder system.

The first three systems are mainly utilized for constant stress (CS) and constant strain (CE) experiments with the Type-A loading system. These experiments require the recording of rapidly changing phenomena at various stages of the experiment. For example, in CS experiments the Fast Y-T recorder may be employed to obtain curves of the two variables, axial strain and axial load, versus time during initial loading. Once the load is fully applied (or removed in the case of unloading) and the transient strain rate is sufficiently reduced (after approximately 20-60 minutes), the transducers associated with these two variables may be switched to the Slow Y-T recording system for display. Finally, when the strain rates become very low (after perhaps 24 hours) these transducers may be switched to the manual readout system. Such as arrangement provides convenient and accurate data during all stages of the experiments.

---

[*] Most strain gage transducers are classed as either four-arm (4A) or two-arm (2A) transducers. This refers to the fact that the transducer itself contains either a full four-arm bridge circuit, or a two-arm bridge circuit with the remaining two arms of the bridge being either remote from the transducer or in the measuring instrument itself.
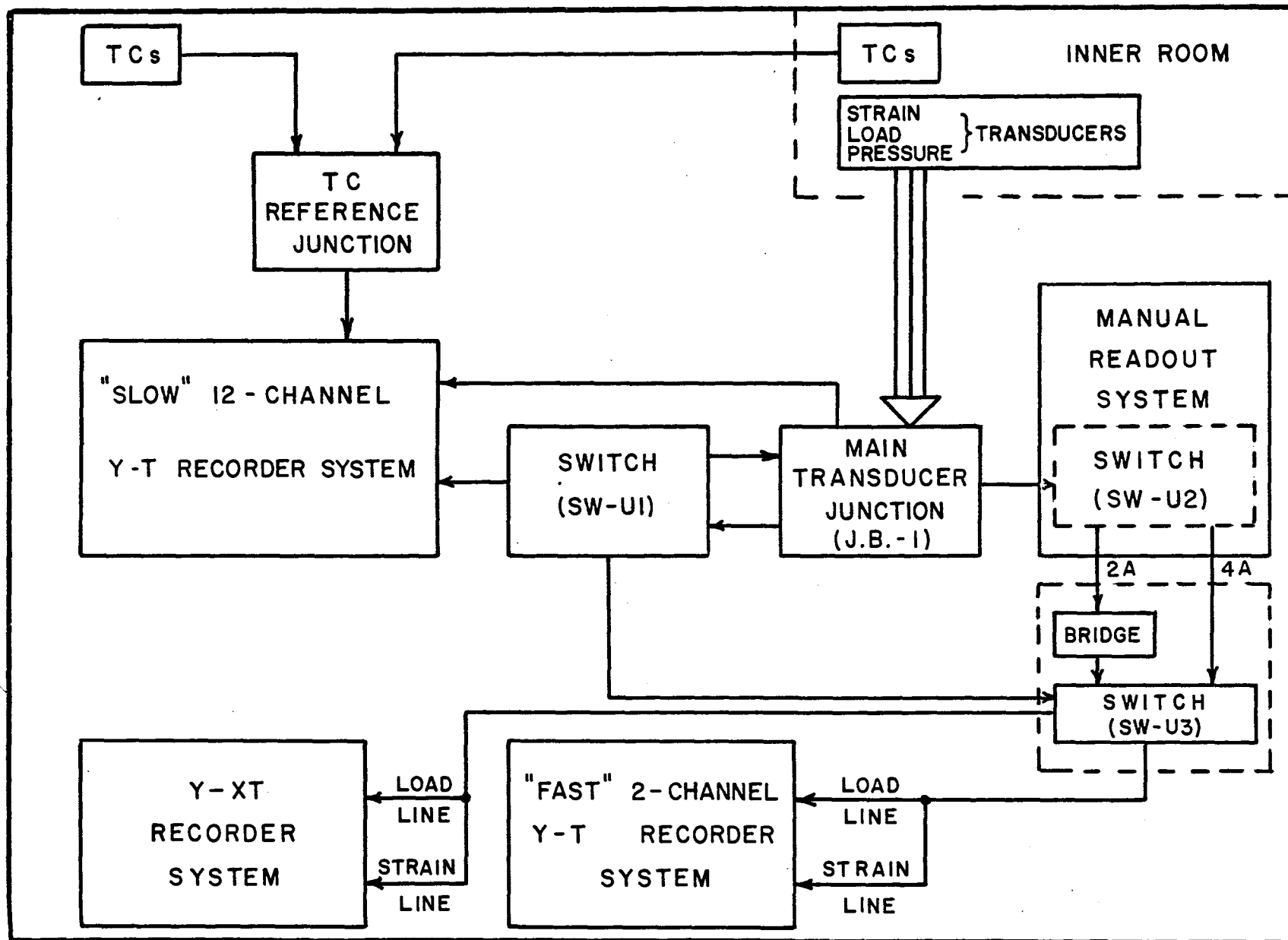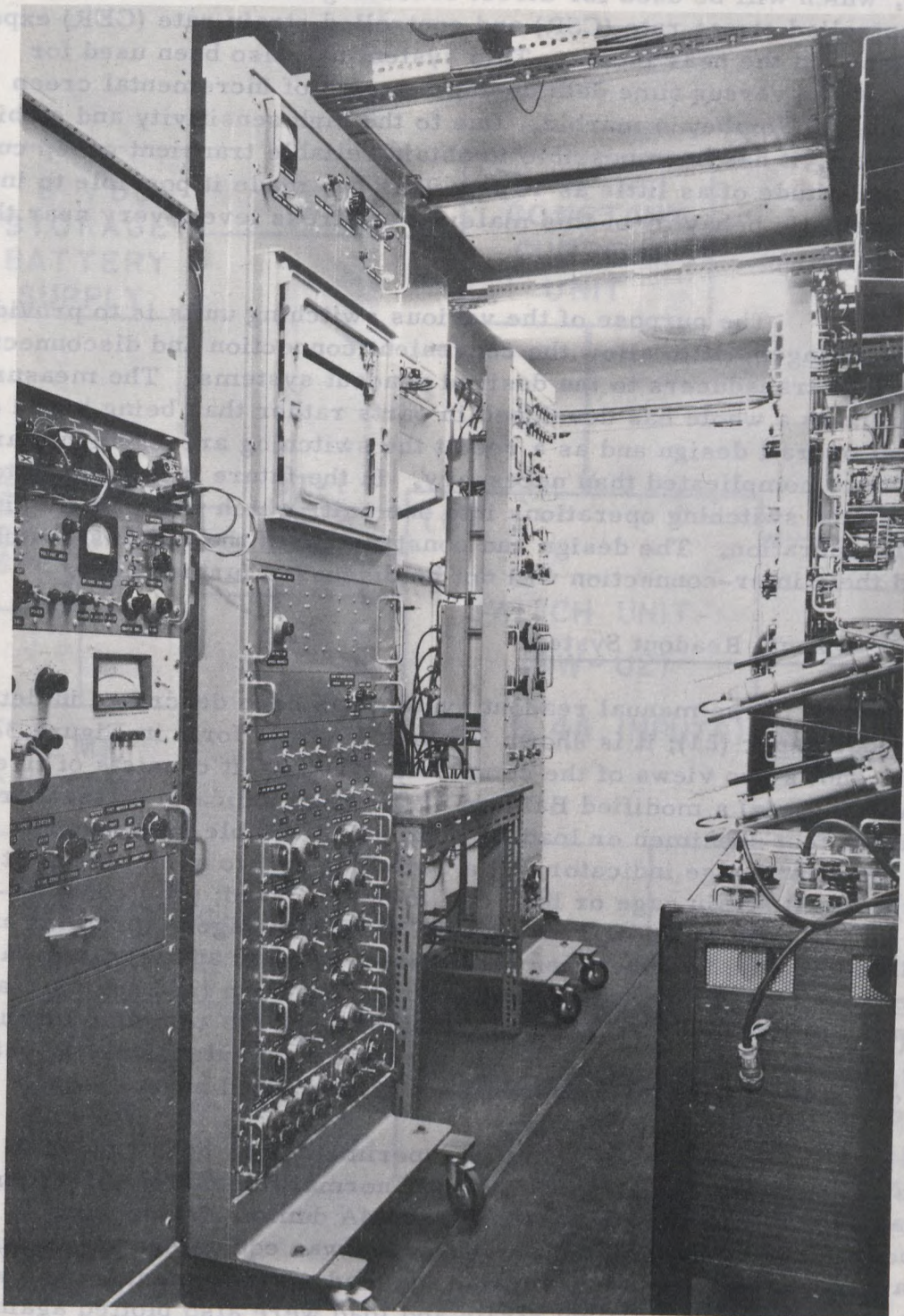
FIGURE 30 - Block Diagram of Measurement System.

FIGURE 31 - Photograph Showing General View of Overall
Measurement System.

The fourth system incorporates a single channel Y-XT recorder, which will be used for direct recording of stress-strain curves during controlled stress rate (CSR) and controlled strain rate (CER) experiments planned in the near future. This system has also been used for recording strain versus time data during a series of incremental creep experiments on Wombeyan marble. Due to the high sensitivity and stability of this system, it has been possible to obtain reliable transient creep curves having a magnitude of as little as 10 μs. This has made it possible to investigate the inelastic behavior of this material at stress levels very near the "elastic limit".

The purpose of the various switching units is to provide a flexible arrangement to allow the convenient connection and disconnection of the various transducers to the desired readout systems. The measurement system as a whole has developed in parts rather than being based on an original overall design and as a result the switching arrangements are perhaps more complicated than necessary. In the future it is planned to consolidate the switching operations into one unit, which will greatly simplify wiring and operation. The design and construction of the various switching units and their inter-connection will not be discussed further here.

1.5.3 Manual Readout System

The manual readout system has been described in detail in a previous paper (21); it is shown in block diagram form in Figure 32. Figure 33 shows two views of the completed system. It consists of five principal units: (a) a modified Baldwin strain gage indicator to measure strain in the test specimen or load cell; (b) an adjustable power supply to operate the strain gage indicator; (c) a switching unit to select the particular specimen strain gage or load cell to be observed; (d) a constant-current unit to pass a d-c current through all strain gages (specimen and load cell) during the time between strain observations; and (e) a standard specimen unit containing a set of highly stable two-arm (2A) and four-arm (4A) dummy bridge units to check on the stability of the complete manual readout system. Since the system has not been used extensively as yet, details of its design and operation will not be described here.

A series of stability experiments has been conducted on this system over a two week period (under normal fluctuations in room temperature and humidity) using the 2A and 4A dummy bridge units as references. The standard deviation observed was equivalent to ± 3.8 μs in the strain measurements and ± 10 lb in the load measurements. The variations in the observed equivalent strain and load were also plotted against room temperature and, although considerable scatter was evident, there appeared to be a strong dependence on temperature. Assuming a linear dependence, the variation of the equivalent strain was found to be approximately 3 μs per degree Celsius. This system to date has not been used for
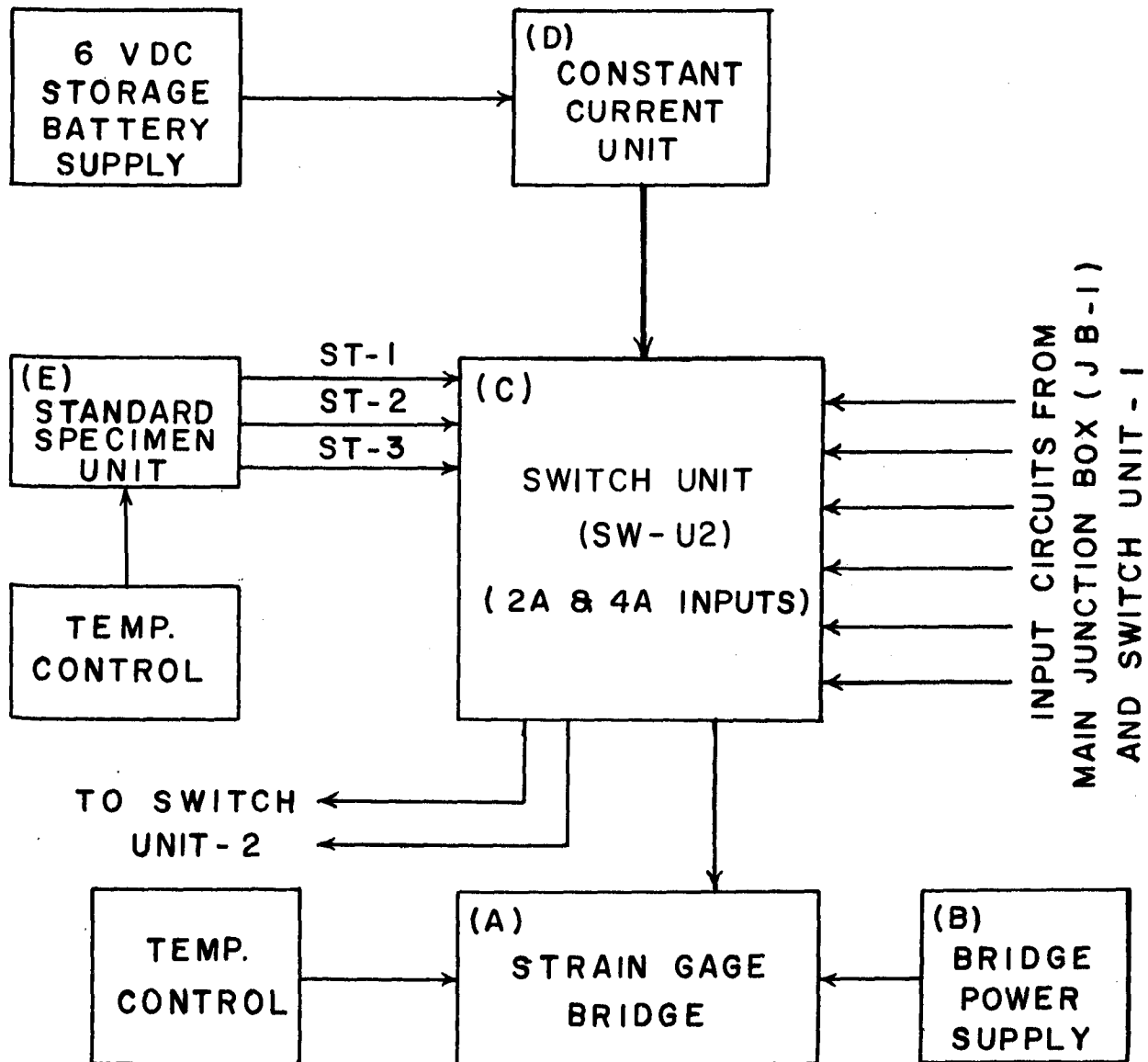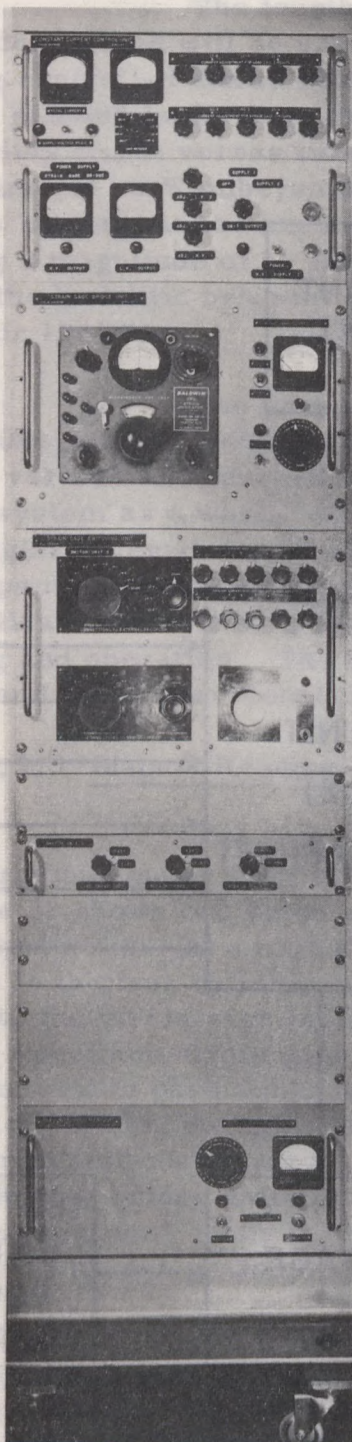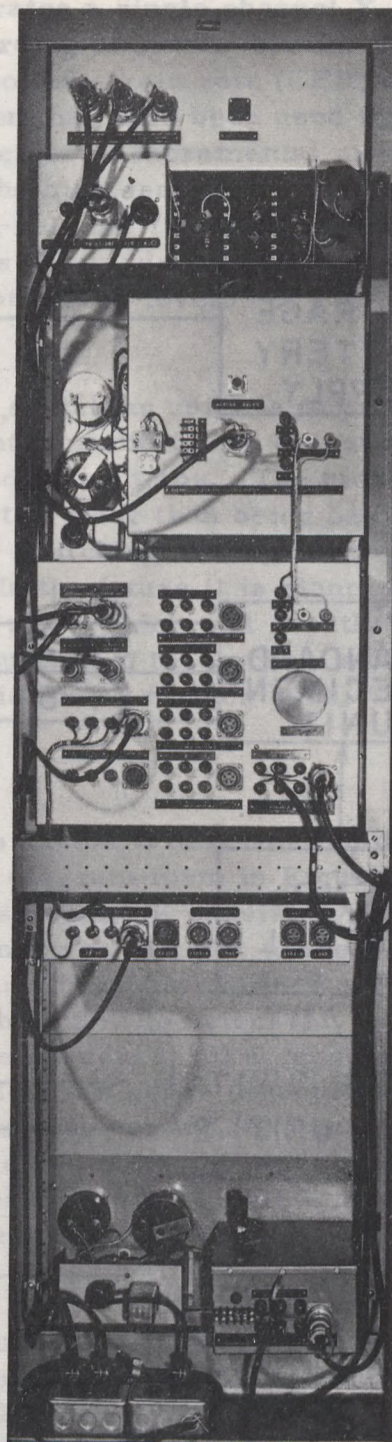
FIGURE 32 - Block Diagram of Manual Readout System.

A.   Front View of System.   B.   Rear View of System.

FIGURE 33 - Photographs Showing Two Views of Manual
Readout System.

measurements over long periods of time under the strict temperature and moisture conditions of the test enclosure. However, higher stability is expected under these conditions.

1.5.4 12-Channel "Slow" Y-T Recorder System

This system provides 12 channels for recording load, strain, confining pressure, and temperature over periods of time from a few hours to many days. Figure 34 shows a block diagram of the system. The complete system is mounted in a standard 24 inch wide relay rack. Figure 35 shows two views of the completed system.

(i) Recorder and Recorder Junction Unit

The recorder itself is a Philips Model PR 3210-A/100, 12 point, printing millivolt recorder with a maximum full scale sensitivity of 5 millivolts. At this sensitivity each small scale division on the recorder chart is equivalent to 50 μv and, since the chart may be read to $\pm$ 1/10 of a division, it is possible to estimate the chart reading to $\pm$ 5 μv. A quick-change gear system provides chart speeds of 40, 80, 300 and 600 mm/hr. To allow the recording of very slowly changing variables, the recorder chart-drive and scan-switch motor circuit has been modified to provide an adjustable scan/hold time ratio. A timer in the recorder scan control unit turns this motor on for a period of time during which data is printed out. The motor is then shut off for a period of time (the recorder amplifiers etc. remaining on). In this way, for example the system might be set to print out data for five minutes every four hours, giving an equivalent chart speed of approximately 1 mm/hr on the 40 mm/hr chart speed setting. The recorder scan control unit also contains a highly stable 6 V d-c power supply* that powers the various transducers.

All twelve inputs to the recorder scanning switch are brought out to a recorder junction unit. This unit includes a convenient terminal arrangement to allow individual recorder channels to be connected either to the appropriate transducers or to a common adjustable voltage source; this allows unused channels to be positioned on the recorder chart at a convenient position well away from the active channels. The circuit for the recorder junction unit is given in Figure 36. Wires carrying signals from the various transducers are connected to the unit via the lower set of

---

*Valor Power supply, Model MB 6.3K 0.5, rated at a stability of better than 0.1 per cent.
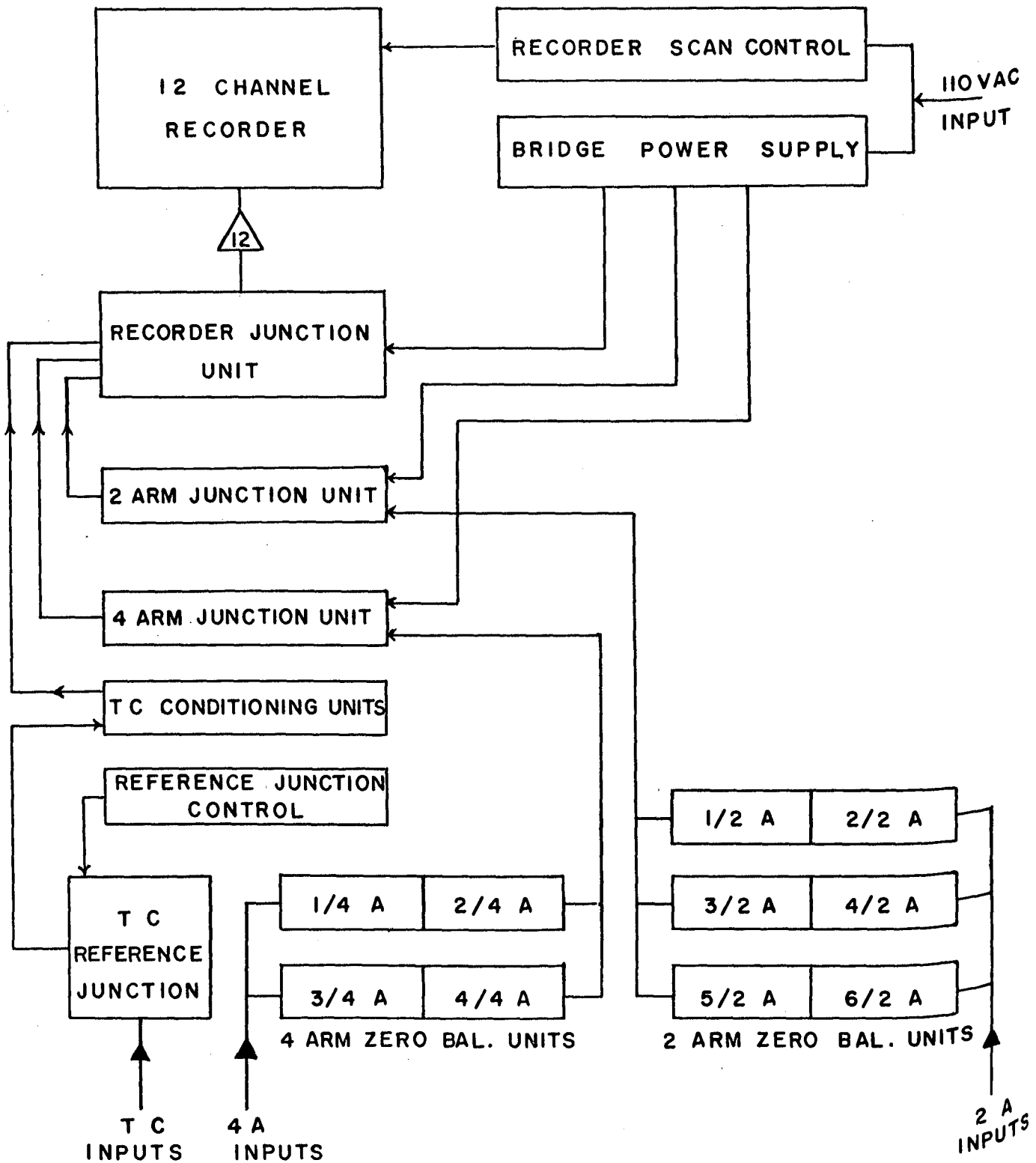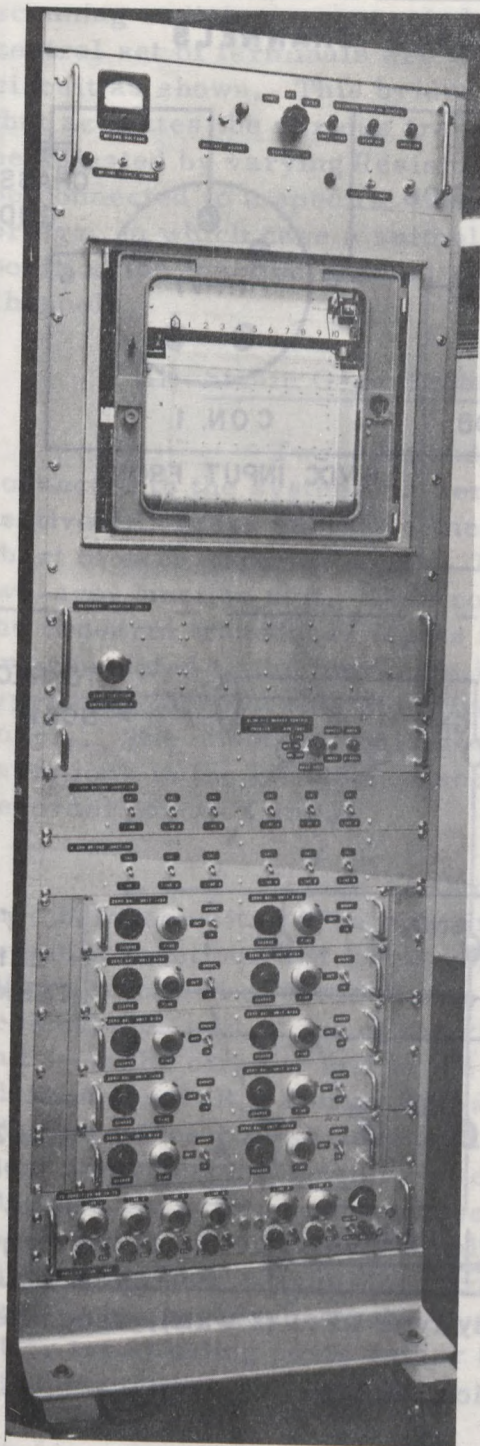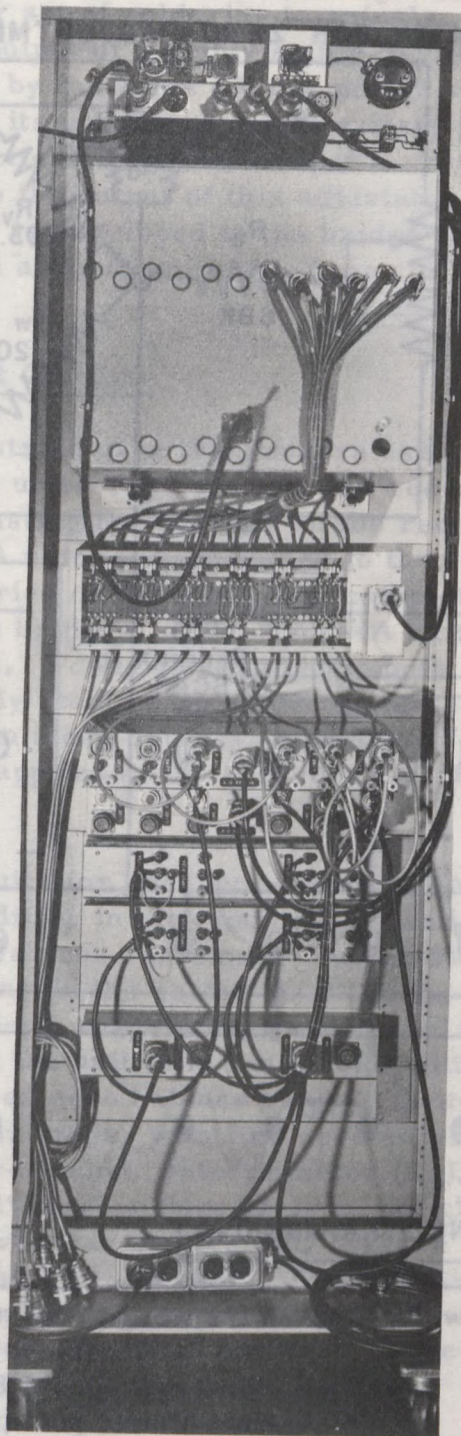
FIGURE 34 - Block Diagram of 12-Channel "Slow"
Y-T Recorder System.

A. Front View of Recorder. B. Rear View of Recorder.

FIGURE 35 - Photographs Showing Two Views of 12-Channel,
"Slow", Y-T Recorder System.

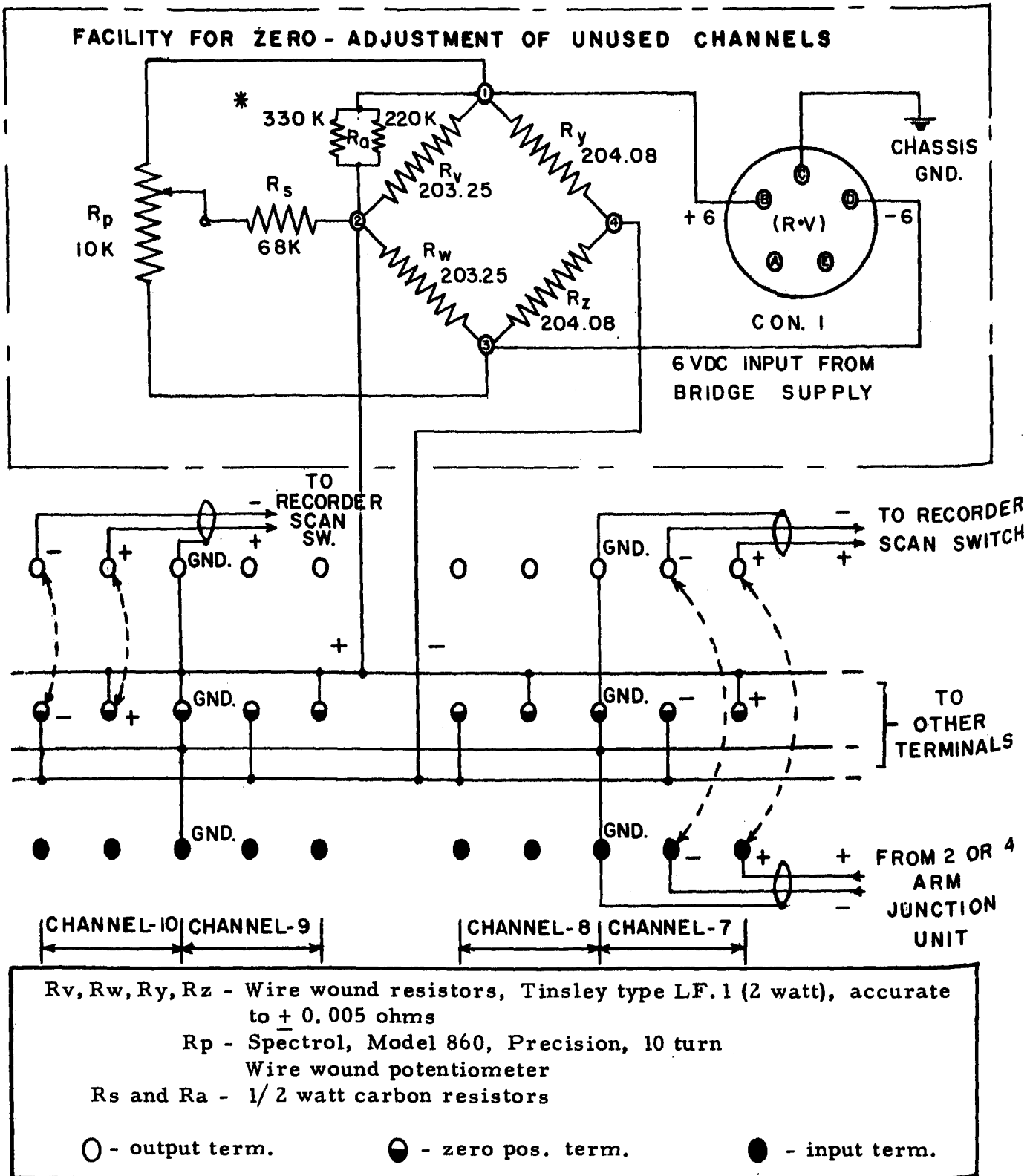FACILITY FOR ZERO - ADJUSTMENT OF UNUSED CHANNELS

FIGURE 36 - Circuit Diagram of Recorder Junction Unit.

soldering terminals. Connections from the various positions on the recorder scanning switch are connected to the upper set of soldering terminals. The central set of terminals are wired to the output of a highly stable bridge circuit as shown. This bridge is powered by the same 6 V d-c power supply that activates the various transducers and its unbalance output voltage may be adjusted by varying Resistor R_p. A particular recorder input may either be connected to a specific transducer or to the output of this adjustable bridge, in which case a suitable unbalance is developed in the bridge to position the inactive channel print-out well away from those of the active channels.

(ii) Strain Gage Transducer Input Circuits

Two-arm and four-arm strain gage transducers are connected to the system via zero balancing units Type-2A and -4A respectively. These provide a means for adjusting the position on the recorder chart of each separate input. The Type-2A units are connected to the two-arm junction unit. This contains a series of resistors that complete the two-arm transducer inputs forming full bridges. The Type-4A units are connected to the four-arm junction unit. Power is supplied to both types of bridges at this point from the highly stable 6 V d-c bridge power supply. The unbalance voltages produced in these bridges, as a result of variations in the transducer sections, are applied to the recorder via the recorder junction unit.

Figure 37 shows the circuits for the Type-2A and -4A zero balance units. The two circuits only differ in the type of input and output connections and in the values of the various resistors. Switch SW-1 allows selection of three modes of operation: in the centre-position the zero balance unit is out of the circuit, in the down-position the zero balance unit is in the circuit, and in the up-position the unit is in the circuit with an addition shunt (R_s) that provides an increased zero balance range. Switch SW-2 provides coarse zero adjustment in six steps, with fine zero adjustment being accomplished by a ten-turn, wire wound, potentiometer (R_p). All fixed resistors used in these units are 1% carbon deposit-type, which have been found extremely stable in this particular application. Figure 38 shows a number of views of a completed dual Type-4A unit. This unit is similar in appearance to the Type-2A unit with the exception that in the latter type binding posts rather than AN-type connectors are used on the input and output.
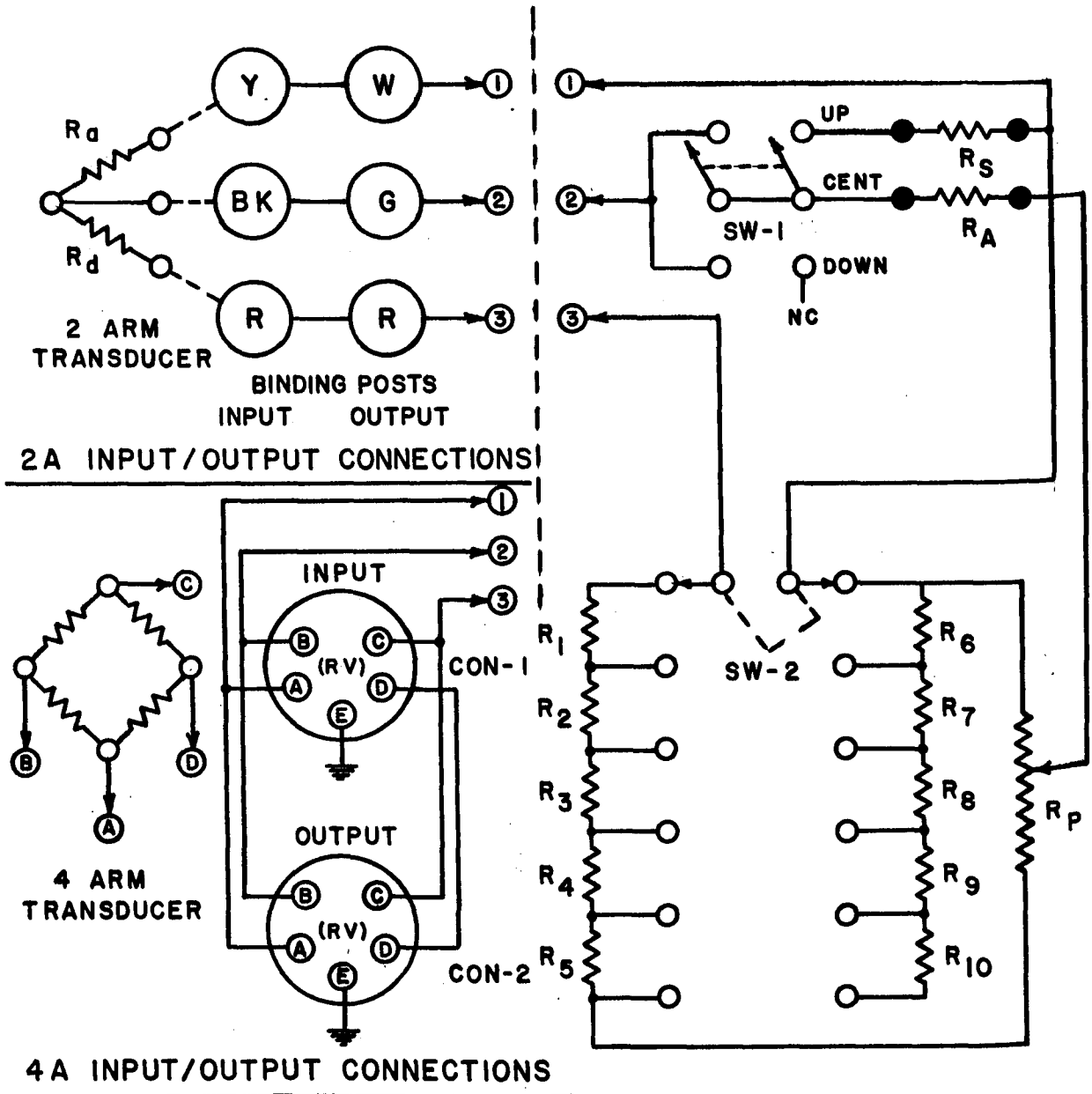
Resistors	Type	2-ARM*	4-ARM*
R_1, R_{10} R_s, R_d	1/4 Watt, precision carbon deposit resistors, 1% rating.	9760	4750
R_p	Spectrol Model 860 10-turn potentiometer	10K	5K
* Resistance values in ohms.			

FIGURE 37 - Circuit Diagram of 2-Arm and 4-Arm Zero Balance Units.
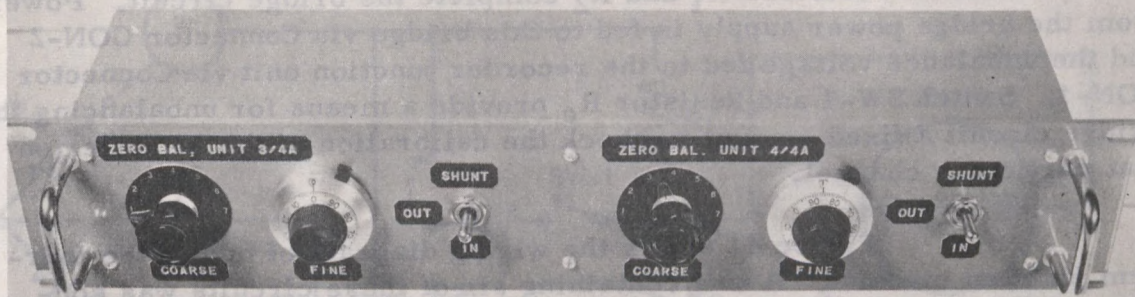
A. Front View of 4-Arm Zero Balance Unit.
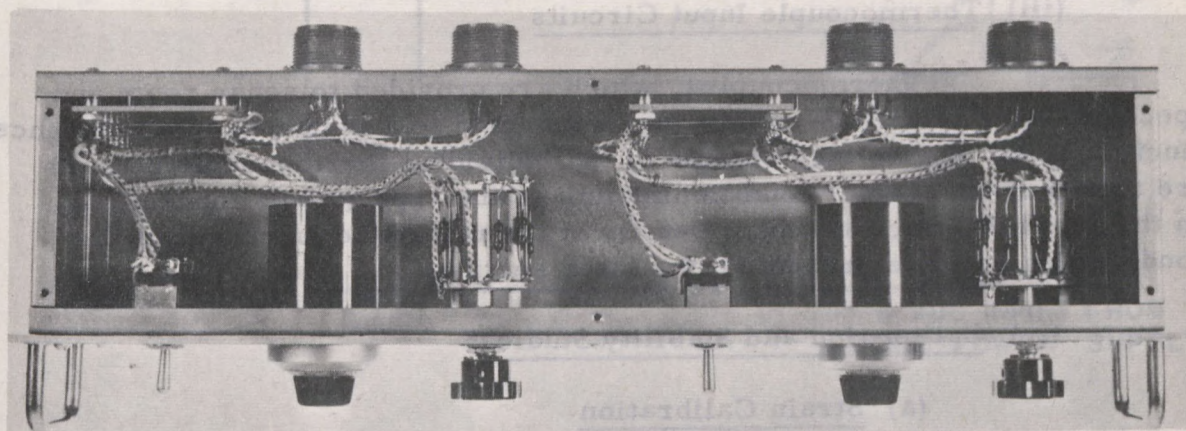
B. Bottom View of 4-Arm Zero Balance Unit.

FIGURE 38 - Photographs Showing Two Views of 4-Arm
Zero Balance Unit.

Figure 39 shows the wiring diagram of one of the two-arm junction circuits. A unit containing six of the circuits was constructed as shown in Figure 40. In these circuits the two external resistors R_a and R_d shown are respectively one of the strain gages attached to the test specimen and a similar unstressed dummy gage located beside the loading frame. The two internal resistors R_1 and R_2 complete the bridge circuit. Power from the bridge power supply is fed to this bridge via Connector CON-2 and the unbalance voltage fed to the recorder junction unit via Connector CON-1. Switch SW-1 and Resistor R_c provide a means for unbalancing the bridge circuit a fixed amount to check the calibration of the recorder on that particular channel.

Figure 41 shows the wiring diagram of one of the four-arm junction circuits. A unit containing six of these circuits was constructed and Figure 42 shows two views of this completed unit. In these units the complete bridge circuit is outside the unit and is connected to it via connector CON-3. The function of the other connectors and SW-1 are the same as for the two-arm units.

(iii) Thermocouple Input Circuits

Thermocouples, which are provided to sense room and specimen temperature variation, are connected to a thermocouple reference junction unit. The voltage outputs of the individual thermocouple circuits are then fed via a signal conditioning unit to the appropriate connections on the recorder junction unit. Details of the reference junction and the conditioning unit are presented in a later section.

(iv) Calibration and Stability Studies*

(a) Strain Calibration

A highly stable two-arm bridge unit was constructed for strain calibration of the system. This bridge consisted of two 120 ohm strain gages attached to a steel block with a precision low resistance slide wire connected in series with one of the gages. The bridge itself was calibrated initially against a Baldwin portable strain indicator (Type-N) and the slide wire calibrated in terms of strain. This unit was then attached to one of the 2-arm inputs of the recorder system and the slide wire varied over its complete range (a simulated strain of $0-700\,\mu s$); the position of the recorder pen carriage was noted for a range of simulated strains. A plot of pen

---

* Calibration and stability studies (Test 64-1) were carried out under conditions of normal room temperature fluctuation.

INPUT
TERMINALS
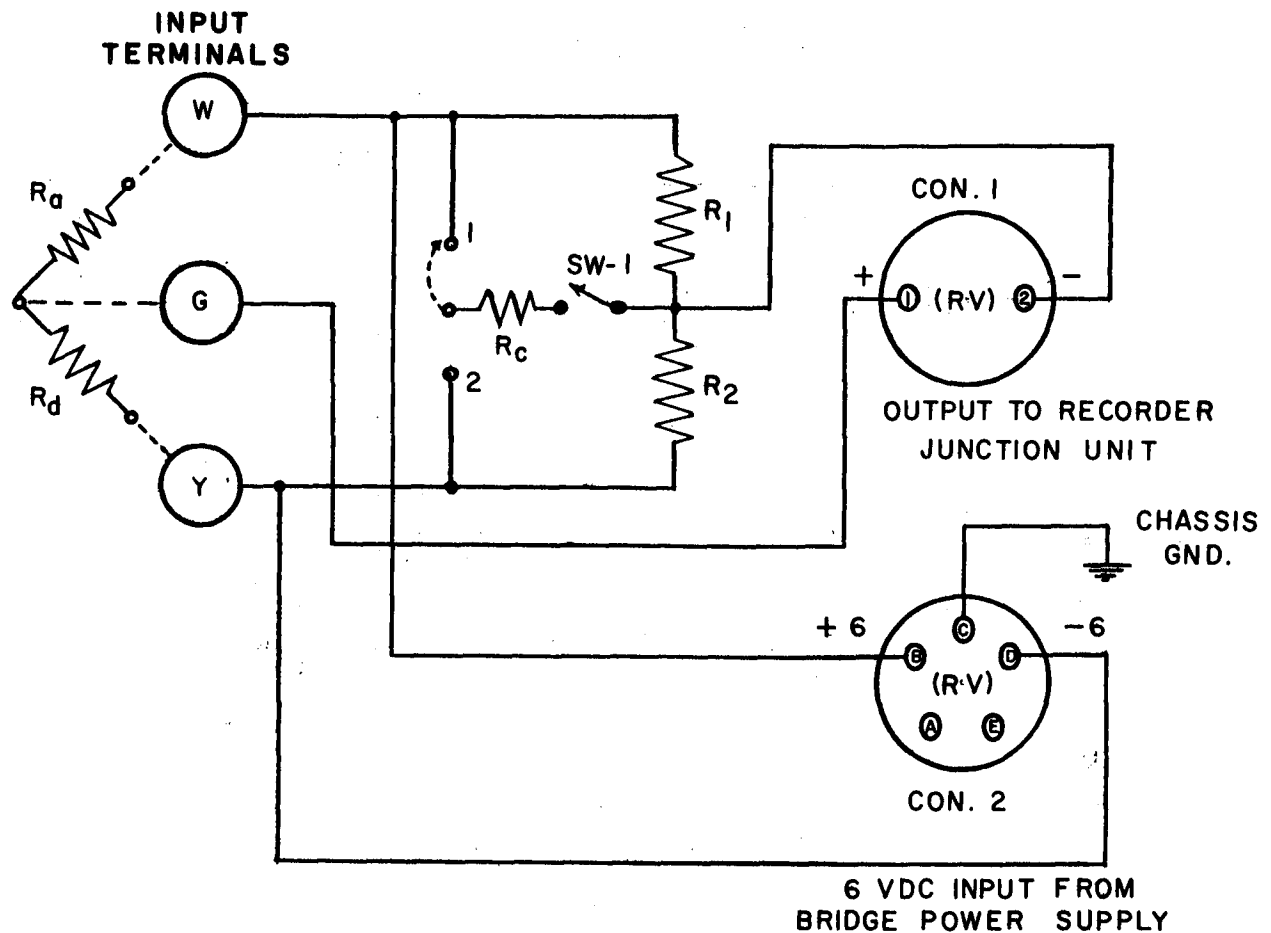
R_1 and R_2 - Wire wound resistors, Tinsley Type LF.1(2 watt) ≈200 ohms, matched
to ± 0.005 ohms.
R_a and R_d - External strain gages (≈ 120 ohms),
direct or via zero balancing units M/2A.
R_c - Calibration check resistor, 470K ohms (1/2 watt carbon type)
gives approximately 20 scale divisions
(1 MV) zero shift on 5 MV f.s. sensitivity

FIGURE 39 - Circuit Diagram of 2-Arm Junction Unit.
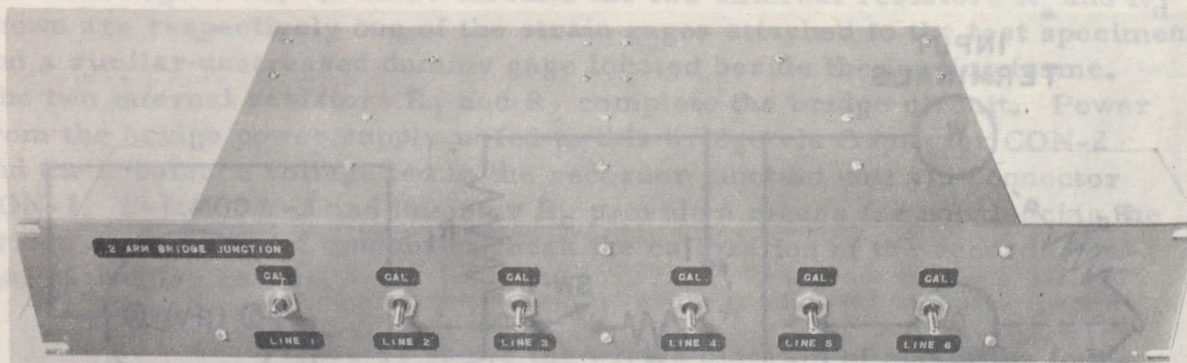
A.   Front View of 2-Arm Junction Unit.
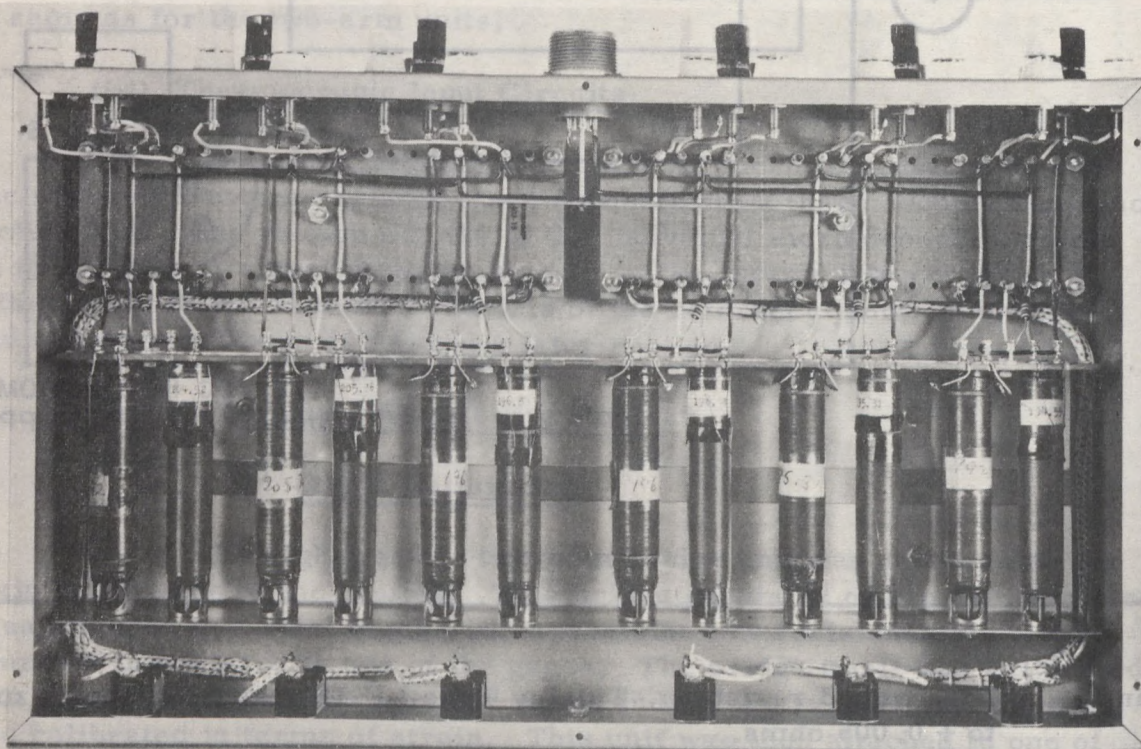
B.   Bottom View of 2-Arm Junction Unit (large resistors
form two arms of the completed bridge).

FIGURE   40 - Photographs Showing Two Views of 2-Arm Junction
Unit Containing Six Junction Circuits.

CON. 3

(OUT)   (IN)

(IN)   (OUT)

(R·V)

INPUT
CONNECTOR

EXTERNAL 4-ARM BRIDGE (≈ 120 Ω)
DIRECTLY, OR VIA ZERO BALANCING UNITS

(IN)

(OUT)   (OUT)

(IN)

(R·V)

NC

SW-1

R_C

CON. 1

+   −

(R·V)

OUTPUT TO RECORDER
JUNCTION UNIT

CHASSIS
GND.

+6   −6

(R·V)

CON. 2

6 VDC INPUT FROM
BRIDGE POWER SUPPLY

R_C - Calibration check resistor, 220K ohms (1/2 watt carbon type
gives approximately 20 scale divisions (1 MV) zero shift on
5 MV f.s. sensitivity.

FIGURE 41 - Circuit Diagram of 4-Arm Junction Unit.
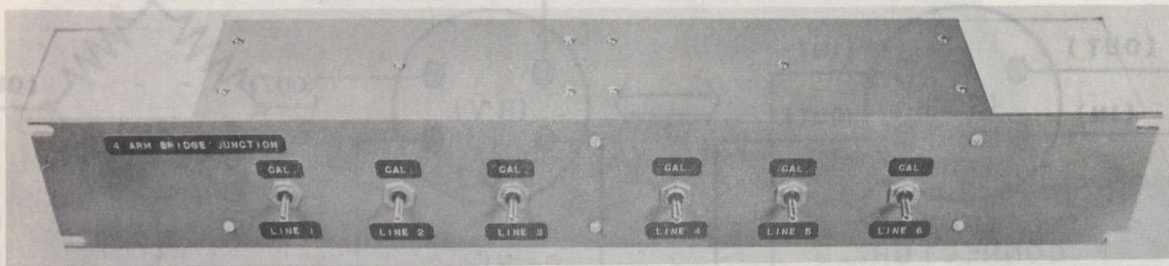
A. Front View of 4-Arm Junction Unit.

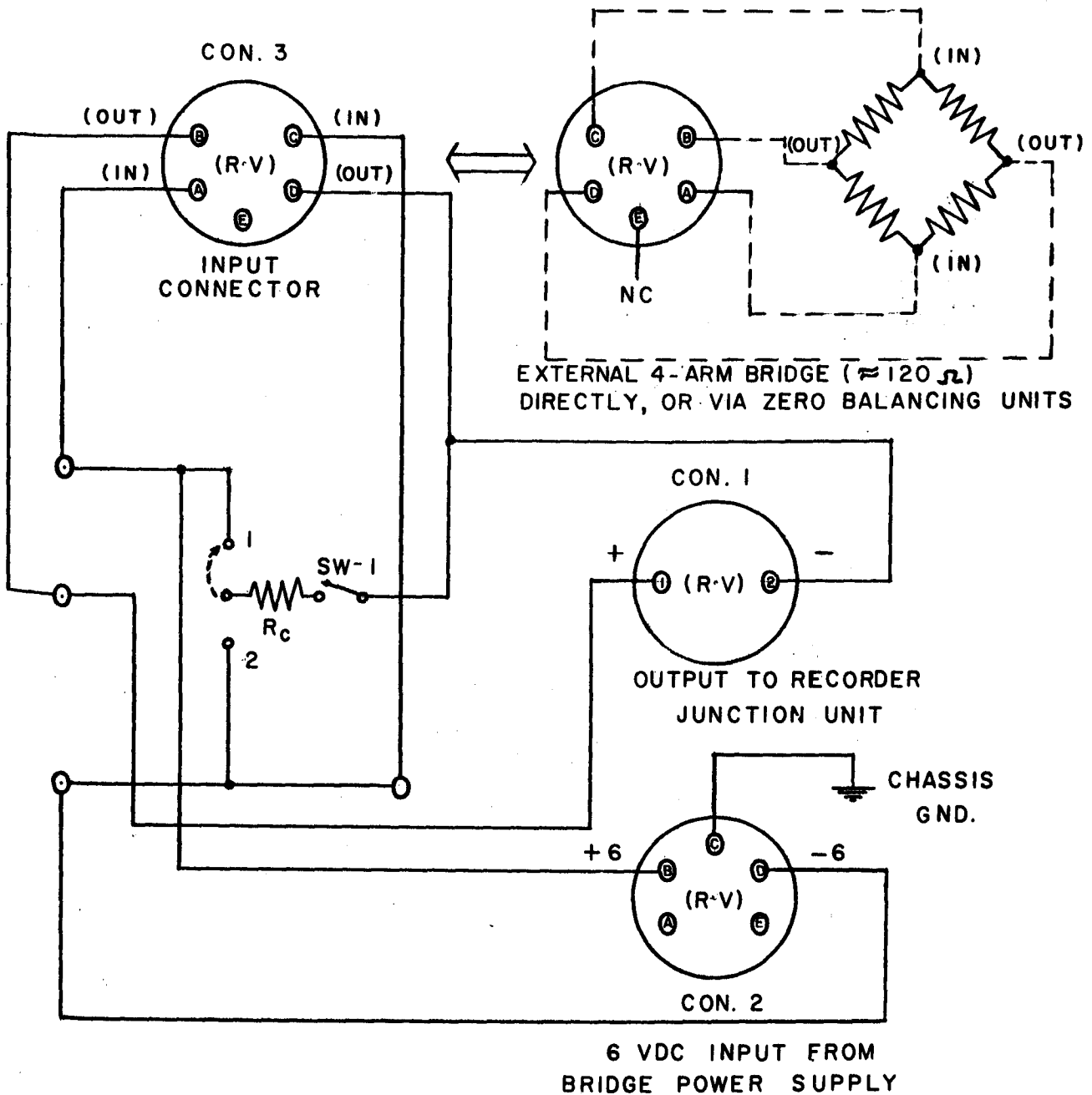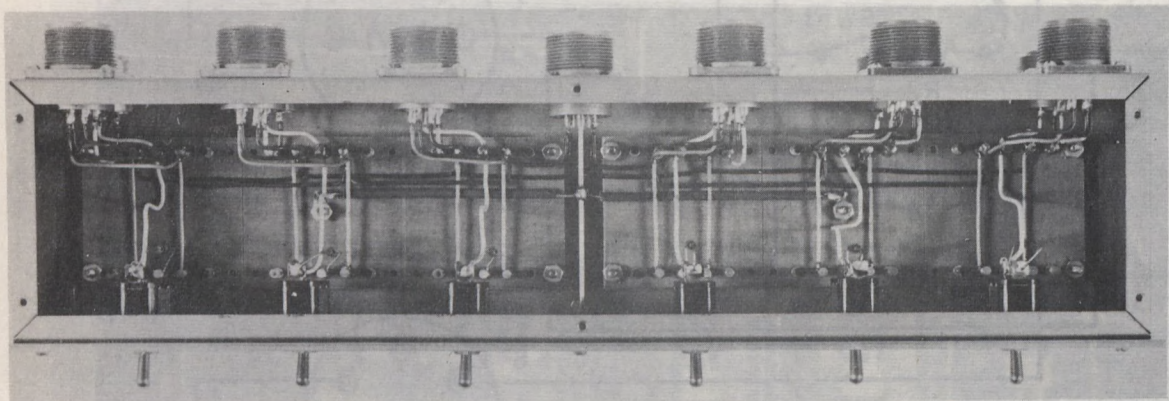B. Bottom View of 4-Arm Junction Unit.

FIGURE 42 - Photographs Showing Two Views of 4-Arm Junction Unit.

carriage displacement against simulated strain was found to be linear. The strain sensitivity of the system was determined from this data to be $K_e(v)$ = 323 µs/MV or $K_e(d)$ = 16.1 µs/ssd*. A series of later checks using a "strain calibrator" developed for this purpose indicated the same sensitivity. The strain sensitivity of the system was also determined at various degrees of zero unbalance in the external bridge (necessitating various degrees of zero adjustment in the zero balance units). In all cases the same value of sensitivity was found. It was estimated that the error in the strain sensitivity factors was less than $\pm$ 2%.

(b) Load Calibration

Since no simulation method for load calibration was available, it was decided to calibrate the recorder directly against a 20K load cell under actual load. The cell was connected into one of the 4-arm inputs of the recorder system and the load on the cell varied over the range 0-6630 lb. The recorder pen carriage position was noted for various values of applied load and a plot of this data was found to be linear. The load sensitivity of the system was determined from this data and from a direct calculation based on the manufacturers quoted sensitivity for the load cell and was found to be $K_L(v)$ = 1633 lb/MV or $K_L(d)$ = 81.6 lb/ssd. The experimental error in the load sensitivity factors was estimated to be less than $\pm$ 2%.

(c) Effect of Line Voltage Variations

The effect of line voltage variations on the zero point and on the sensitivity of the recorder system was briefly investigated (Test 64-1). For this purpose a Variac was placed in series with the 110 V a-c power supplied to the recorder system. A stable 2-arm external bridge was connected to one of the 2-arm inputs and the performance of the system observed for various levels of line voltage. For line voltages in the range 105-115 volts, any zero drifts or changes in sensitivity were within the reading error of the recorder itself. The overall system appeared, therefore, to be completely independent of the line voltage in this range.

(d) Time-Stability

The stability of the overall system over a period of time was investigated for both 2-arm and 4-arm inputs. In a 48 hour test (64-1), during which the room temperature fluctuated over the range 24.5 - 30°C, no long term drift was noted for either type of input. Random fluctuations in the zero point, about a relatively constant mean, were observed. These

---

* Note that "ssd" is the abbreviation used for small scale division, which in this case represents 0.05 MV.

were approximately equivalent to ± 10 μs and ± 40 lb for the strain and load channels respectively. A later test (64-7) conducted under temperature controlled conditions of 23 ± 0.2°C also indicated no long term drift. Under these conditions the random fluctuations in the strain and load channels were reduced to the equivalent of less than ± 6 μs and ± 8.5 lb respectively.

(e) General

Table 9 lists the general characteristics of this measurement system. It should be noted that in the stability experiments what is actually being determined is the overall stability of the measurement system and the external transducers. As a result, the stability of the measurement system may be actually somewhat higher than that quoted.

TABLE 9

Characteristics of 12-Channel
"Slow" Y-T Recorder System

Chart Speed (direct)	- - - - - - - - -	40-600 mm/hr
Basic Sensitivity	- - - - - - - - -	5 MV full scale
Chart Readability	- - - - - - - - -	± 0.1 ssd (± 5 μv)
Strain Sensitivity	- - - - - - - -	$(K_e(v) = 323$ μs/MV
		$(K_e(d) = 16.1$ μs/ssd
Load Sensitivity	- - - - - - - - -	$(K_L(v) = 1633$ lb/MV
(20K load cell, 6 V d-c		$(K_L(d) = 81.6$ lb/ssd
excitation)		
Line Voltage Effect	- - - - - - - - -	Nil
(105-115 volts)		
Long Term Drift	- - - - - - - - -	Nil
(48 hour test)		
Zero Fluctuation	- - - - - - - -	$\{ \Delta e(d) = \pm 6$ μs
(Temp 23 ± 0.2°C,		$\} \Delta L(d) = \pm 8.5$ lb
48 hour test)		

1.5.5 2-Channel "Fast" Y-T Recorder System

This system incorporates a Sanborn Model 60-1300 dual pen recorder equipped with two strain gage amplifiers* (Model 64-500B), two individual four-arm zero balancing units (which have been described in

*Further details on the operation of the recorder and the strain gage amplifiers are given in the following Sanborn manuals: Instruction Manual - Sanborn Twin-Viso, recorder Unit, Model 60 and Instruction Manual - Sanborn Strain Gage Amplifier, Model 64-500B.

the previous section), and a marker pen control (to allow the initiation of important operations to be indicated on the recorder chart by the action of a third recorder pen called the marker pen). This system provides facilities for plotting of axial strain and axial load versus time during the incremental loading stages of creep experiments. The behavior of the material during the actual loading period and the transient period that follows it may be investigated in detail with this arrangement. Figure 43 illustrates a block diagram of this system and a photograph of the completed system is shown in Figure 44.

The sensitivity of the recording system was measured in a manner similar to that discussed for the 12-channel system. At full gain setting of the strain gage amplifiers the strain sensitivity was found to be $K_e(d) = 3.1 \mu s/ssd$ and the load sensitivity (using a 20K load cell) found to be $K_L(d) = 25.4$ lb/ssd, one small scale division (ssd) on the chart paper being 1.0 mm. It was found that, if both channels were in use at the same time, the noise level on both channels increased necessitating operation at lower sensitivities. The system was found to exhibit some long term zero drift and variation in sensitivity even after a relatively long warm up period. The magnitudes of these variations were determined using the internal zero check and sensitivity check switches on the amplifiers, and it was found that over short periods of time (up to 1 hour) these effects either were not serious or could be easily corrected mathematically. Table 10 lists the general characteristics of this measurement system.

TABLE 10

Characteristics of 2-Channel
"Fast" Y-T Recorder System

Chart Speed	---------	0.5 - 100 mm/sec
Chart Readability	---------	± 0.1 ssd
Strain Sensitivity (Maximum)	---------	$K_e(d) = 3.1 \mu s/ssd$
Load Sensitivity (Maximum, 20K load cell)	---------	$K_L(d) = 25.4$ lb/ssd
Response Time (Full scale deflection)	---------	15 milliseconds
Marker Pulse Rate	---------	1 per second

FROM
AXIAL STRAIN
TRANSDUCER

FROM
AXIAL LOAD
TRANSDUCER

TWO - ARM
BRIDGE UNIT
(LOCATED IN SW-U3)

ZERO
BALANCE
UNIT
(4 A)

ZERO
BALANCE
UNIT
(4 A)

①
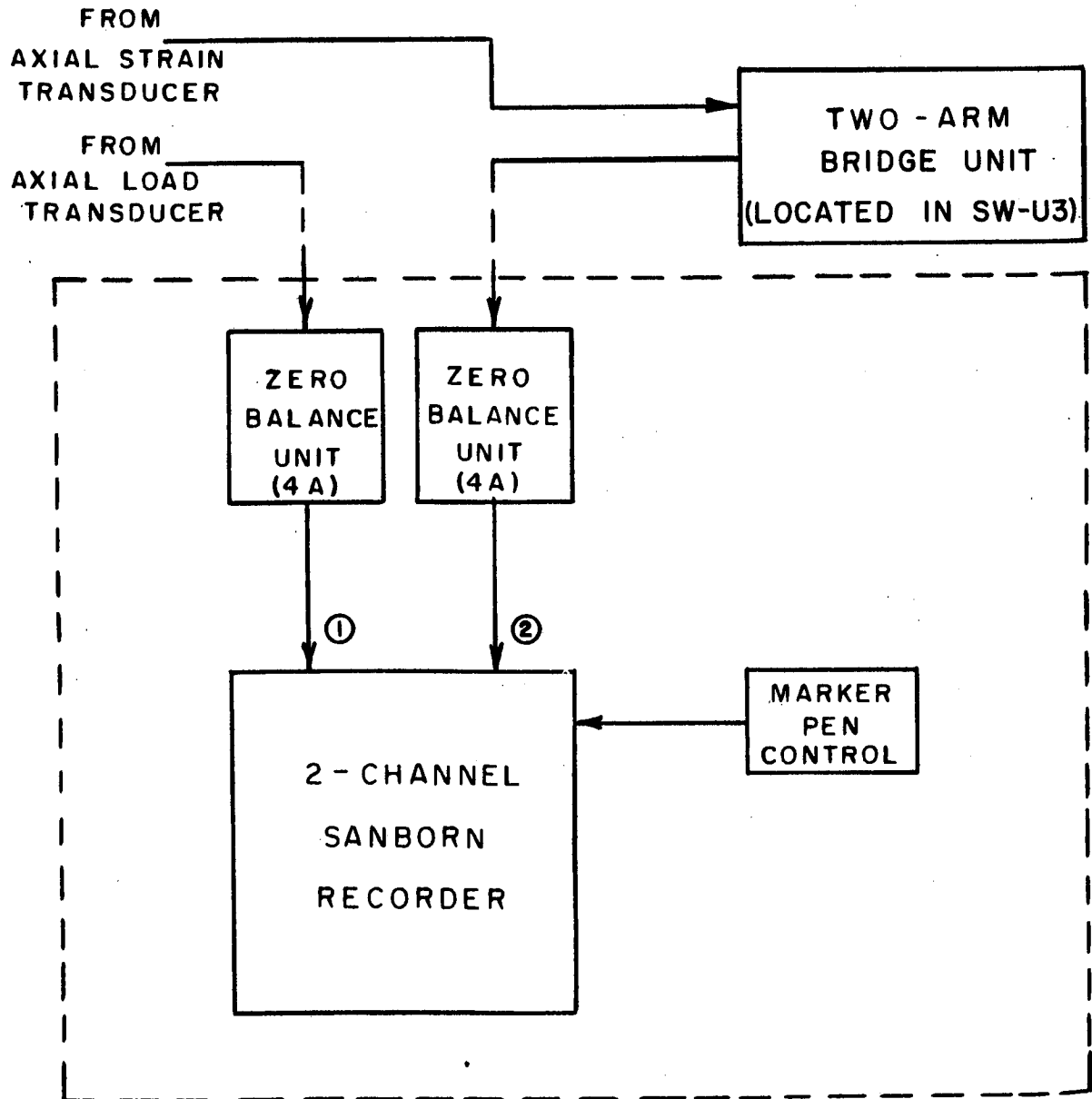
②

2 - CHANNEL

SANBORN

RECORDER

MARKER
PEN
CONTROL

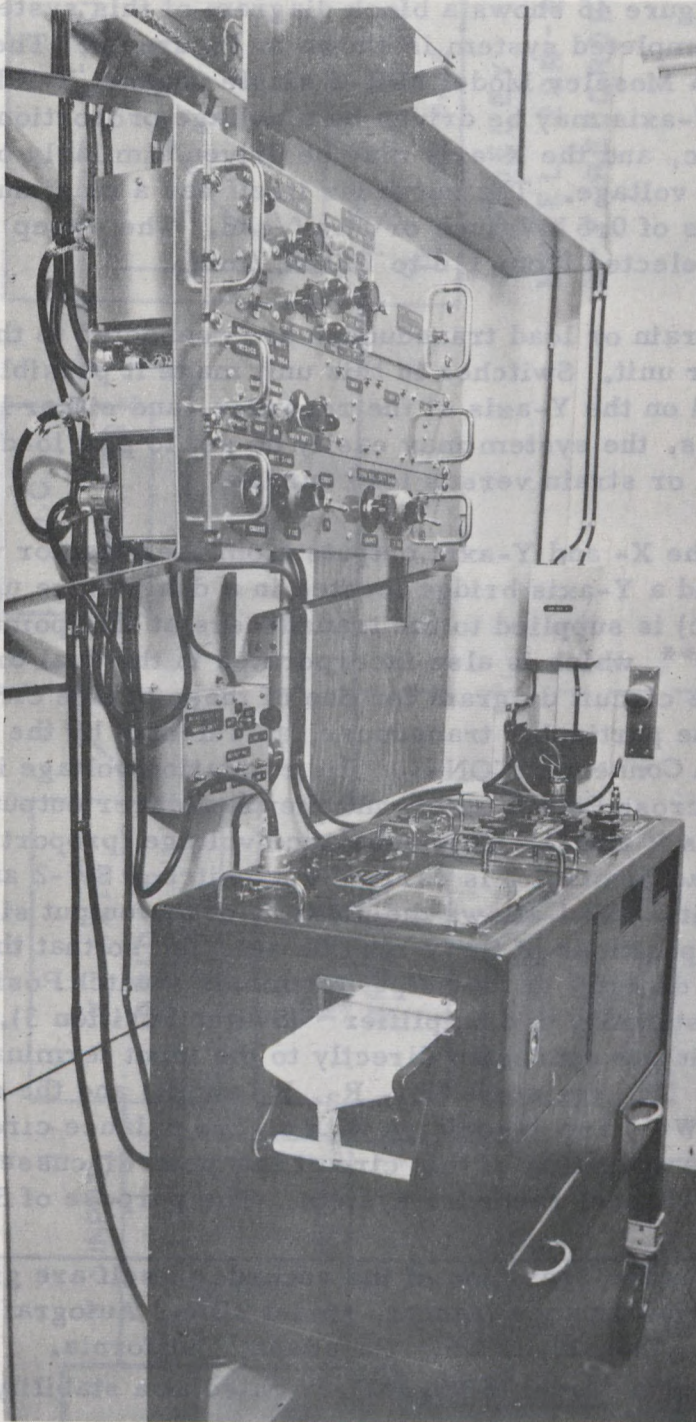FIGURE 43 - Block Diagram of 2-Channel "Fast"
Y-T Recorder System.

FIGURE 44 - Photograph Showing Two-Channel "Fast"
Y-T Recorder System.

1.5.6 Single Channel Y-XT Recorder System

Figure 45 shows a block diagram of this system and a photograph of the completed system is shown in Figure 46. The recorder section consists of a Moseley Model 2DR-2 single channel Y-XT recorder*. In this system the Y-axis may be driven by a voltage proportional to strain, stress, pressure etc, and the X-axis may be driven similarly or from an internal time-based voltage. The recorder itself has a maximum sensitivity on the X- and Y-axis of 0.5 MV/inch or 50 µV/ssd. The sweep rate in the Y-T mode may be selected from 1.2 to 120 in./min.

Strain or load transducers are connected to the system via an input selector unit. Switches in this unit make it possible to display either strain or load on the Y-axis of the recorder, and either load or time on the X-axis. Thus, the system may easily be set to plot load versus time, strain versus time, or strain versus load curves.

The X- and Y-axis outputs from the selector unit are fed directly to an X- and a Y-axis bridge located in a dual bridge unit. Excitation voltage (6 V d-c) is supplied to the transducers at this point by a highly stable power supply**, which is also incorporated in the dual bridge unit. Figure 47 shows the circuit diagram for one of these bridge circuits. The connections from the particular transducer, as selected by the selector unit, enter the bridge via Connector CON-3. The excitation voltage is applied to the transducer across Pins A and C and the transducer output voltage is detected across Pins B and D. This unbalance voltage (proportional to the magnitude of the load or strain) is carried via Switches SW-2 and SW-1 to the output of the unit. SW-1 allows the polarity of the output signal to be selected. Various positions of SW-2 may be selected so that the unbalance voltage either goes directly to the output terminals (Switch Position 4) or indirectly via a high stability d-c amplifier***(Switch Position 3). The output terminals of the unit are connected directly to the input terminals of the Moseley recorder. The resistors (R_1, R_2, R_s and R) and the switches (SW-4, SW-5 and SW-6) are associated with a zero balance circuit contained in each bridge. The operation of this circuit has been discussed earlier when considering the 12-channel recorder system. The purpose of SW-3 and R_c

---

* Further details on the operation of the recorder itself are given in "Operating and Maintenance Manual, Model 2DR-2 Autograf X-Y Recorder", F.L. Moseley & Co., Pasadena, California.

** Valor power supply, Model MB 6.3KO.5, rated at a stability of better than 0.1 per cent.

*** A Keithley Model 150AR d-c amplifier has been utilized to date for this purpose. This unit provides a number of calibrated gains ranging from 10 to 10^6, and is capable of extremely low drift, low noise operation.

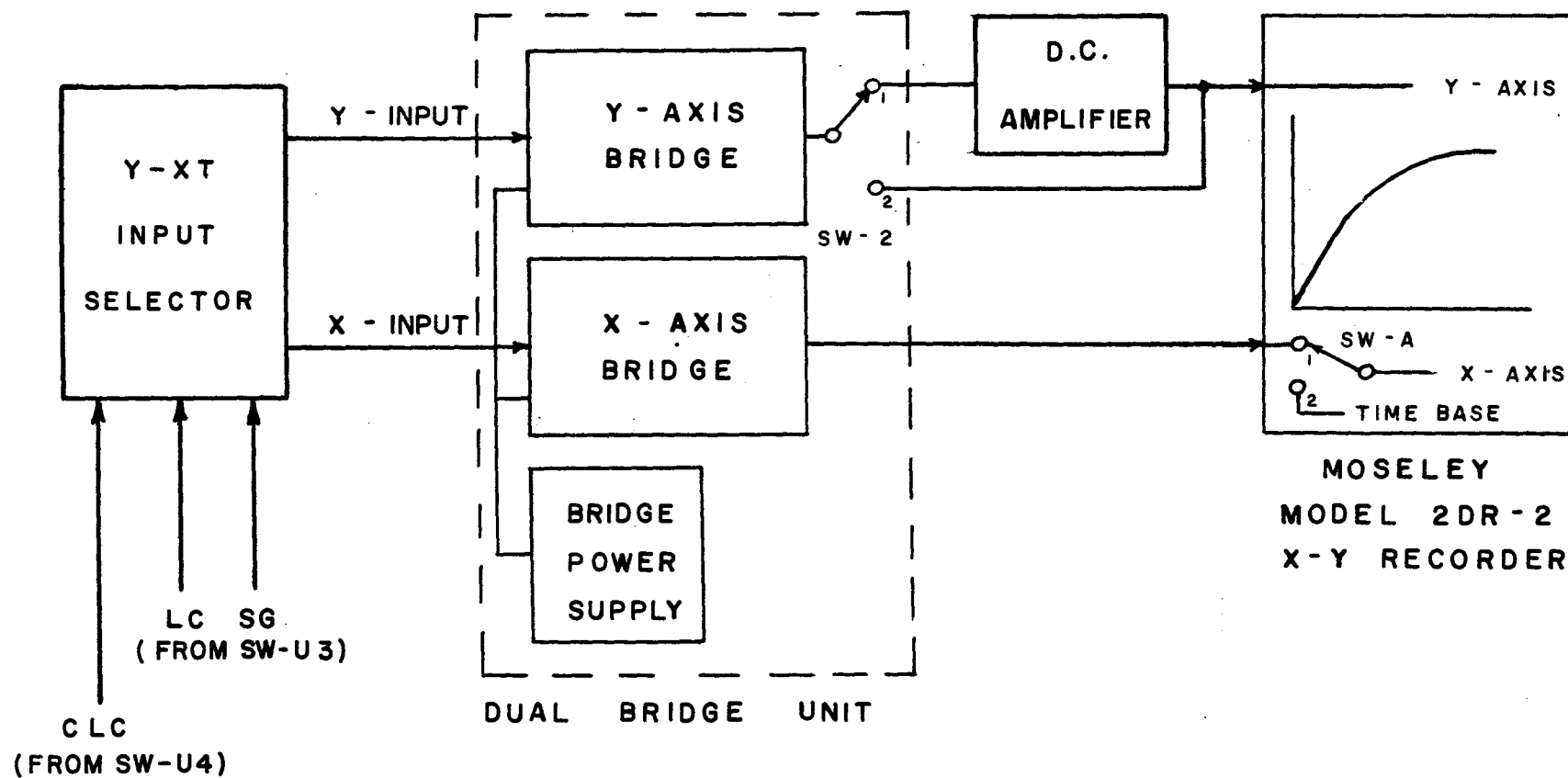FIGURE 45 - Block Diagram of Single Channel Y-XT Recorder System.
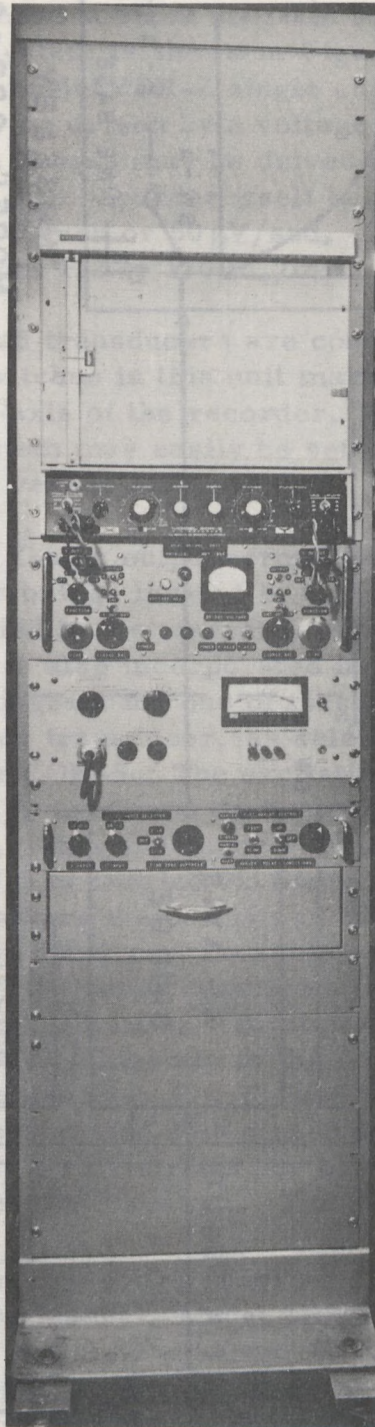
FIGURE   46 – Photograph Showing Front View of Completed
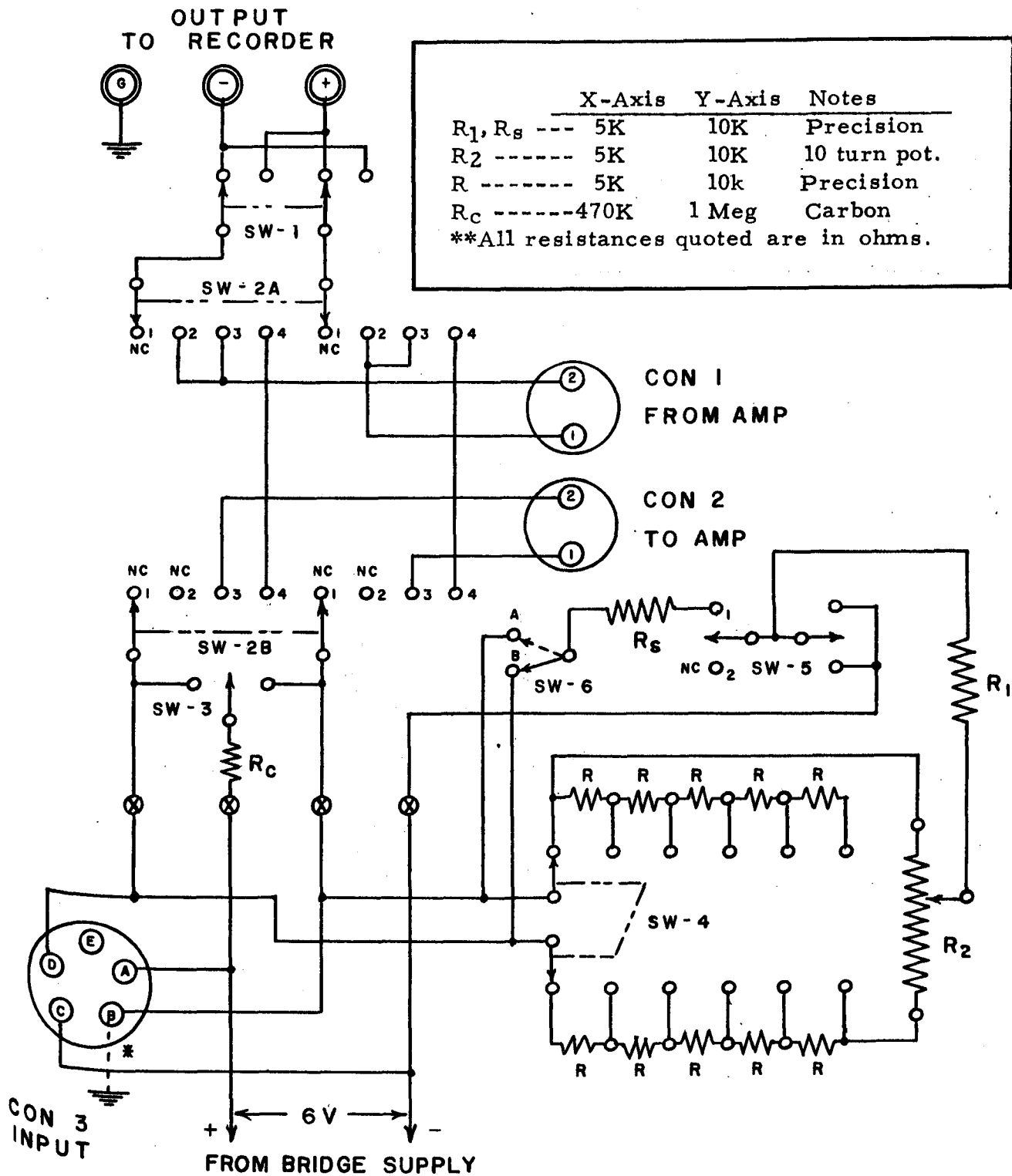Y-XT Recorder System.

FIGURE 47 - Circuit Diagram of Dual Bridge Unit.

is to provide an available fixed bridge unbalance to allow a periodic check
to be made on the overall sensitivity of the system. Two views of the dual
bridge unit and the selector unit are shown in Figure 48. To date this
recorder system has been utilized mainly for recording of very low level
strains (2-100 μs) associated with creep experiments on Wombeyan marble.
For these experiments the Y-axis of the recorder has been used on its
50 MV/inch range and the d-c amplifier has been operated at a gain of 1000.
Under these conditions the relationship of recorder deflection to simulated
input strain was found to be linear and the strain sensitivity of the system
was found to be $K_e(d) = 1.65$ μs/ssd. This appears to be the optimum
combination of recorder and amplifier settings for low noise operation.
Table 11 lists the general characteristics of this measurement system.

TABLE 11

Characteristics of Y-XT Recorder System

| Time Base	----------	1.2 - 120 in./min
Chart Readability	----------	$\pm$ 0.1 ssd
Strain Sensitivity	----------	$K_e(d) = 1.65$ μs/ssd
Response Time (full scale deflection)	----------	0.5 seconds

1.5.7 Development of Marker System

During some stages of certain deformation experiments
strain and load data are being recorded on all three recording systems.
In order to properly correlate these recordings with respect to time, it
was found necessary to develop a system that would simultaneously put
marker points on all three recorder charts at fixed intervals of time through-
out the deformation experiment. Figure 49 shows a block diagram of the
system developed for this purpose. It consists of a master marker unit and
a remote marker unit located at each of the three recorders. The master
marker unit consists of a set of three timer units each consisting of two
small microswitches operated by a double-deck cam (one deck having 6
detents the other having 1 detent) driven by a small synchronous motor.
The motor in each timer unit operates at a different speed and the speeds
of the three motors were selected so that the unit would provide a wide
range of pulse rates.

When the motor in a specific timer is activated, it causes
the cam arrangement to rotate switching the associated microswitch on and
off at a rate dependent on the motor speed and the number of detents in the
timing cam. The microswitch itself activates a relay in the master marker
unit, which in turn operates a relay in each of the three remote marker units
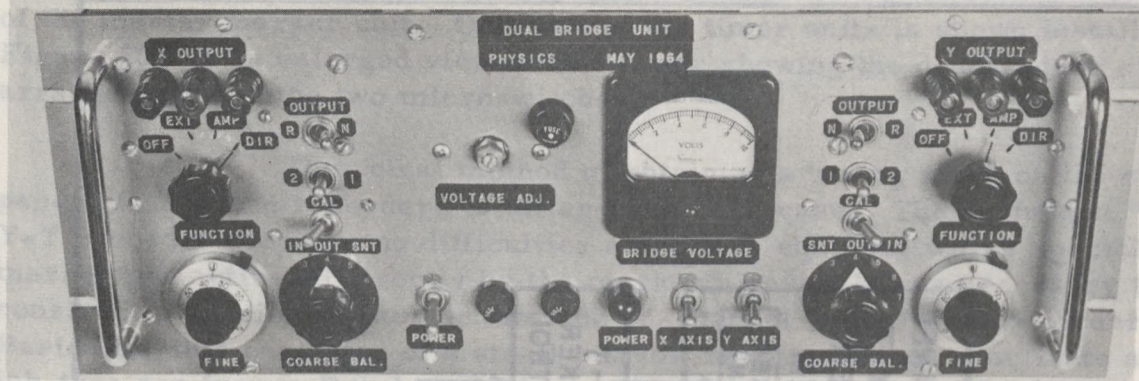
A. Front View of Dual Bridge Unit.
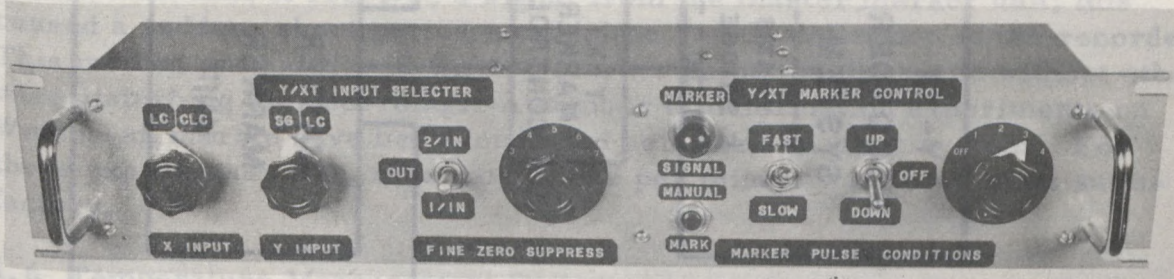
B. Front View of Selecter/Marker Unit.

Figure 48 - Photographs Showing a View of the Dual Bridge
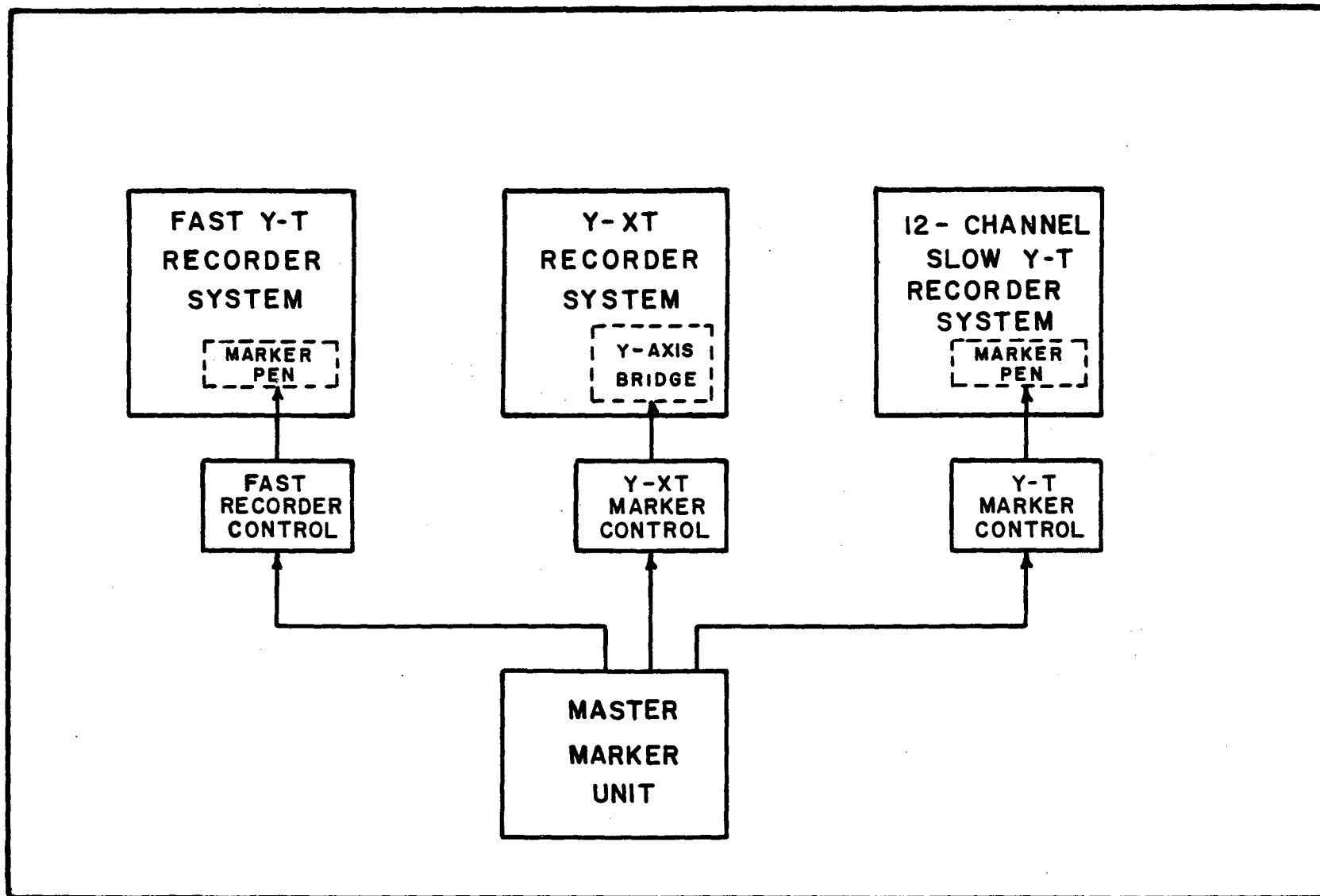and the Selecter/Marker Unit.

FIGURE 49 - Block Diagram of Marker System.

that are located at the respective recorders. Figure 50 shows three views of the master marker unit. Only one of the timer units is shown installed. Figure 50C is an enlarged view of this timer showing the double-deck cam arrangement and the two microswitches.

The actual method of obtaining a timing mark on the chart paper of the three recorders is different in each case. The 2-channel "fast" Y-T recorder presents no difficulties since it is equipped with a special marker pen activated directly by the marker signal. It was necessary to construct a special marker pen for the 12-channel "slow" Y-T recorder. Basically, this consisted of a small six volt relay modified to activate an ink-type pen from a Brush recorder. This relay and the attached pen were mounted at the top corner of the recorder frame so that the pen rested on the chart paper near its extreme right edge. The pen relay is connected to the remote marker unit associated with this recorder and is activated each time the unit receives a signal from the master unit. The method of obtaining a timing mark on the Y-XT recorder chart was more involved since in this case the paper was fixed and the time axis itself moved. The method finally decided on involved introducing a small, short period unbalance in the bridge circuit associated with the Y-axis signal to the recorder. A high-value resistance was connected in series with the contacts of a normally open relay across one arm of the Y-axis bridge circuit. This relay was triggered closed each time it received a signal from the master marker unit; this caused a sudden, short period jump in the Y-axis deflection of the recorder. This method produced well defined marker points on the curve without other- wise disturbing the recording. A number of deformation experiments on Wombeyan marble have been conducted using this marker system. For these experiments a marker rate of one per minute was found most satis- factory.

1.6 Temperature Measurement System

1.6.1 General

Since the temperature control system was designed to maintain the temperature of the test enclosure within $\pm 1/10°C$, it was considered desirable to develop a temperature measurement system capable of monitoring temperatures at various locations within the enclosure to at least $\pm 1/20°C$. Since it was particularly important to be capable of sensing any long term drift of the control temperature, an extremely stable system was required. With this stability requirement in mind, it was decided to employ thermocouple-type temperature transducers. Lion (32) and Cermi and Foster (5) discuss thermocouples and the design of thermocouple signal
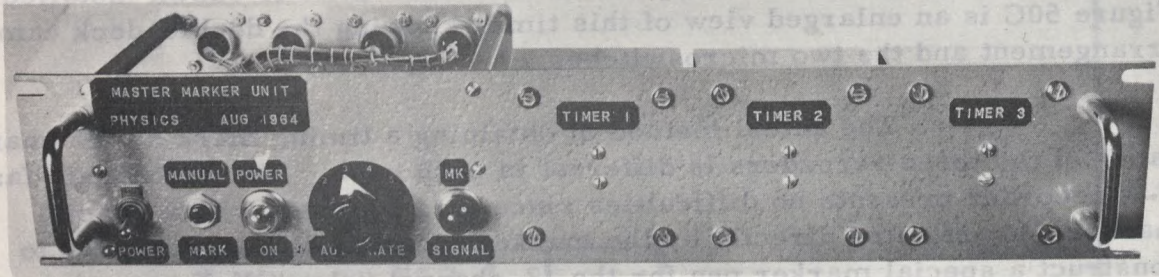
A. Front View of Marker Unit.
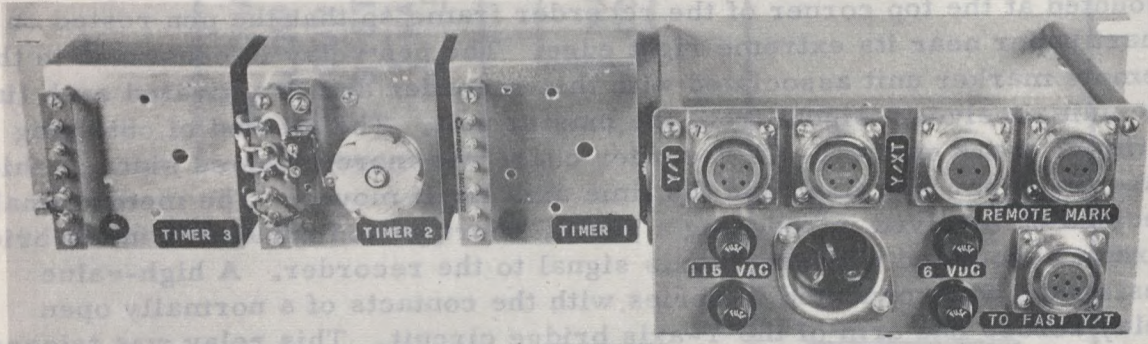
B. Rear View of Marker Unit.

C. Enlarged View of Timer.

FIGURE 50 - Photographs Showing Master Marker Unit.

conditioning circuits in detail. Considering the temperature range involved (15-40°C), copper-constantan thermocouples were judged to be the most satisfactory. These were manufactured by the writer from standard thermocouple wire*.
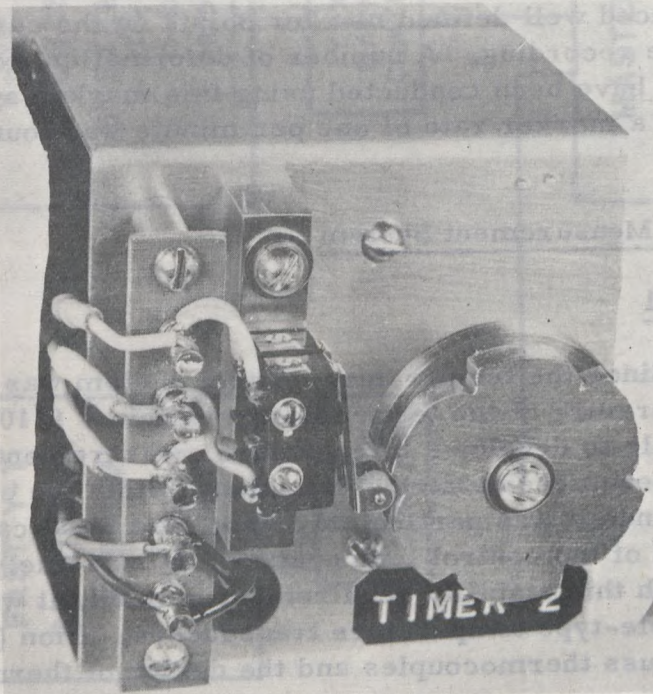
Figure 51 shows a floor plan of the test enclosure, which includes the locations of the various parts of the temperature measurement system. The locations of three thermostats (TH_1, TH_2 and TH_3) associated with the temperature control system are also indicated. Four permanent thermocouples (T-1, T-2, T-3 and T-4) were installed for the measurement of control temperature (T_c), duct discharge temperature (T_D), hall temperature (T_0), and inner room temperature (T_{in}). Thermocouple connectors were installed at the locations marked 5 and 6 for possible use in temperature stabilization of various parts of the control and measurement system. A set of four similar connectors marked 7 to 10 was installed between loading frame Bases 1 and 2 for measurement of the specimen temperature.

Figure 52 shows a block diagram of the temperature measurement system. It consists of a thermocouple patch panel, a reference junction unit, and a signal conditioning unit. Connections from each of the various thermocouple locations are connected via thermocouple lead wire** to a dual female TC connector+ on the patch panel (marked T-1 to T-10). The thermocouple reference unit located near the patch panel contains a set of six refernce junctions that are held at a fixed temperature. Patch cables connected to the junction unit allow various thermocouples to be connected into the reference unit. The outputs from the reference junction unit are connected to a signal conditioning unit located in the 12-channel recorder system rack and the outputs from the conditioning unit are fed directly to the recorder for display. In cases where greater sensitivity is desired, a high stability d-c amplifier***may be inserted in the circuit between the conditioning unit and the recorder.

---

* Type GG-18-DT, copper-constantan thermocouple wire, 18 gauge B & S, solid, fibre glass insulated, manufactured by the Thermo Electric Company, Inc.
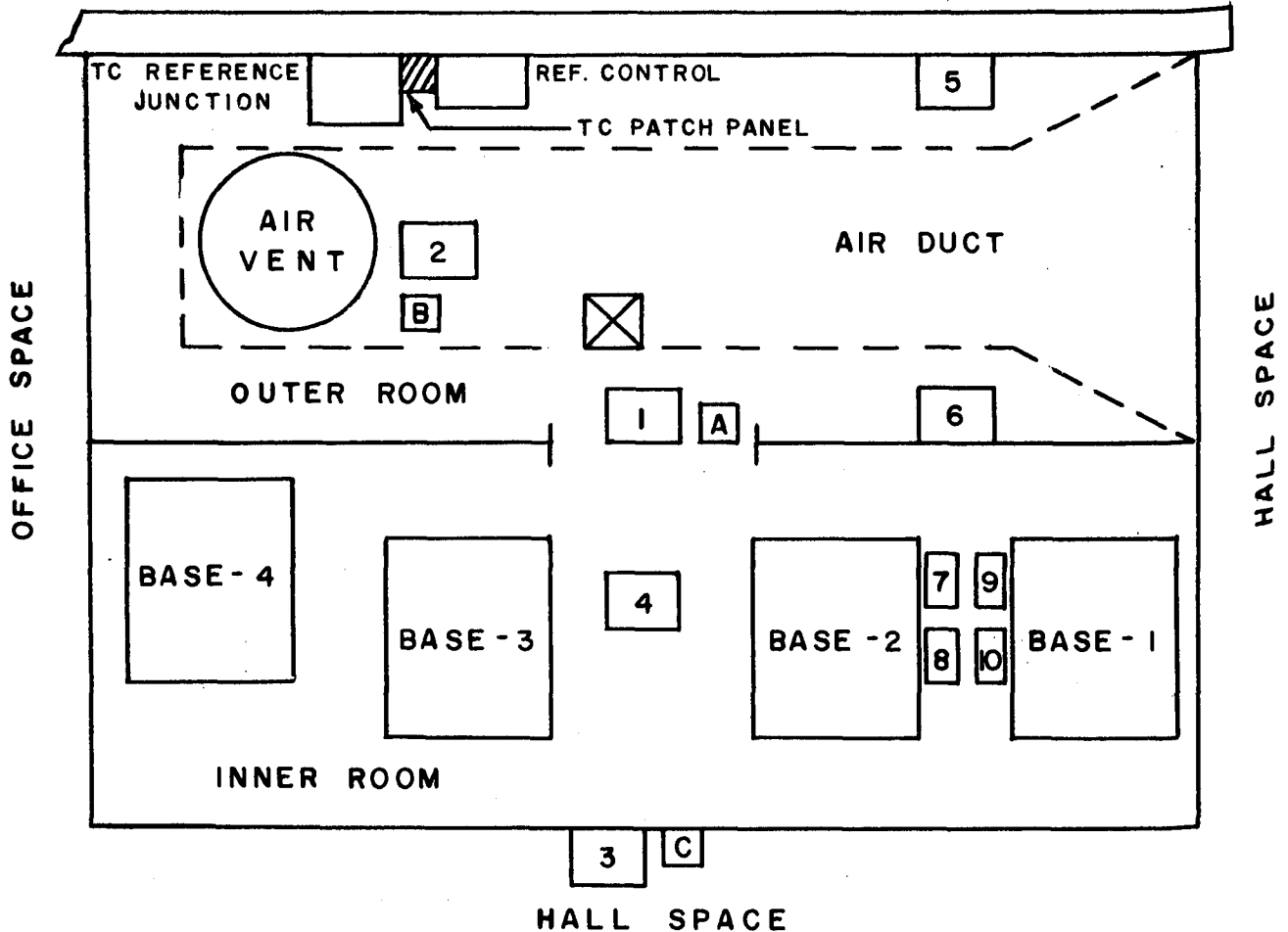
** Type GGF-18-D, copper-constantan thermocouple lead wire, 18 gauge B & S, stranded, fibre glass insulated, manufactured by the Thermo Electric Company, Inc.

+ TC connectors are made from thermocouple metals. Jack Type-12JB, plug Type-2PSS manufactured by Thermo Electric Company, Inc.

*** Dymec Model 2460A amplifier with plug-in Type 2416A-M2 gain unit.

TC REFERENCE JUNCTION

REF. CONTROL

5

TC PATCH PANEL

AIR VENT

2

B

AIR DUCT

OUTER ROOM

1

A

6

OFFICE SPACE

HALL SPACE

BASE-4

BASE-3

4

BASE-2

7 9

8 10

BASE-1

INNER ROOM

3

C

HALL SPACE

1.	Thermocouple Measuring Control Temperature (T_c).
2.	Thermocouple Measuring Duct Discharge Temperature (T_D)
3.	Thermocouple Measuring Hall Temperature (T_o)
4.	Thermocouple Measuring Inner Room Temperature (T_{in})
5,6	Spare Thermocouple Connections.
7-10	Specimen Thermocouple Connections.
A	Room Thermostat (TH_1)
B	Duct Discharge Thermostat (TH_2)
C	Hall Thermostat (TH_3).

FIGURE 51 - Location of Temperature Monitoring Facilities in Test Enclosure.
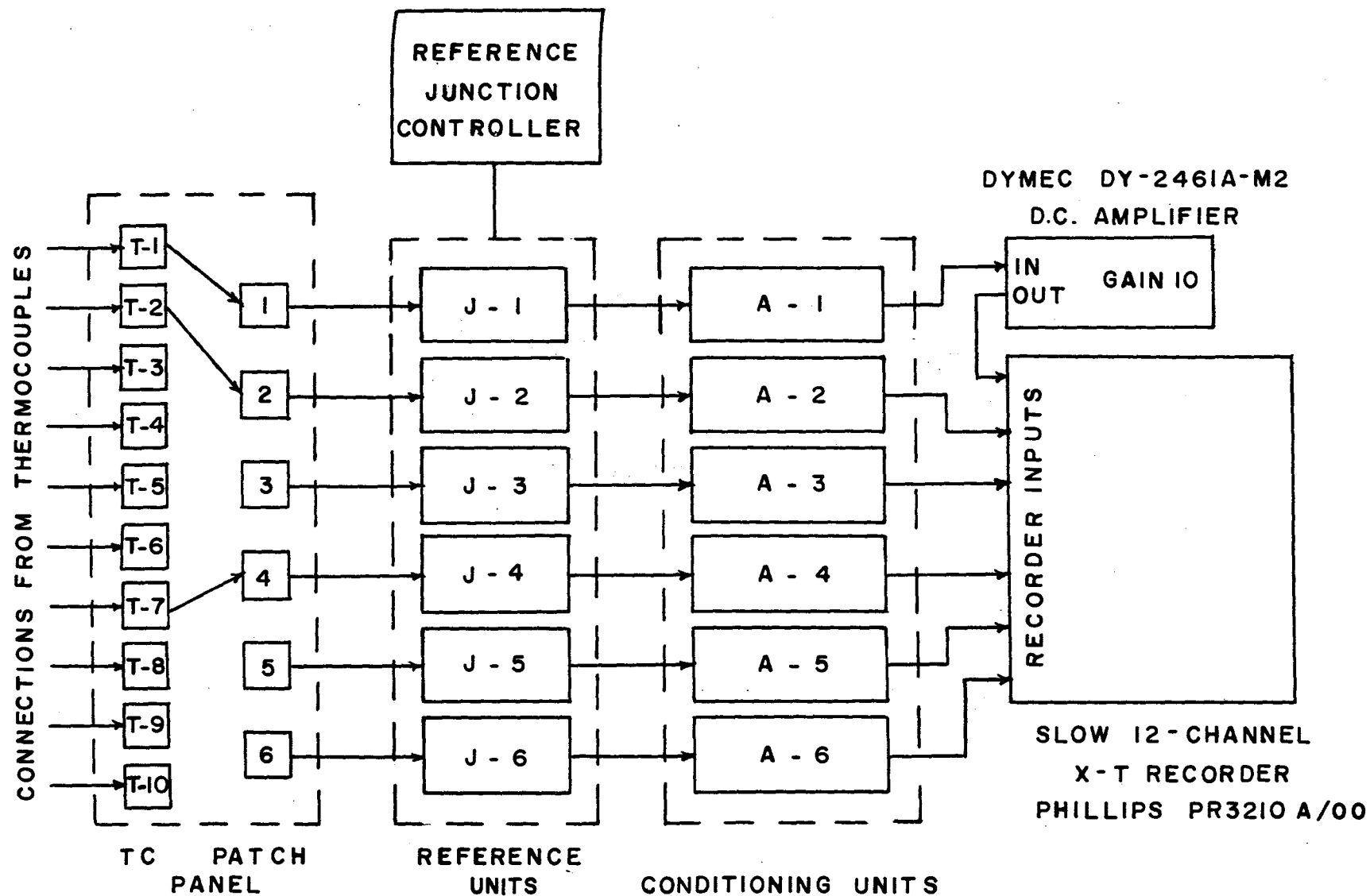
FIGURE 52 - Block Diagram of Temperature Measurement System.

Figure 53 shows a simplified circuit of the thermocouple measurement system indicating the relationship of the various sections. The voltage (V_o) observed by the recorder is given by

$$V_o = V_m - V_j \overset{+}{-} V_{zb} \overset{+}{-} V_c \qquad \text{(Eq. 1)}$$

where V_m is the thermal emf produced at the measuring thermocouple, V_j is the thermal emf produced in the junction thermocouple (dependent on junction temperature), V_{zb} is the emf induced in the conditioning circuit in order to position the recorder pen to a convenient location and V_c is the small emf induced in the conditioning circuit for purpose of determining the overall sensitivity of the measurement system. It is important to note that, if a stability of $\pm 1/20°C$ is required in temperature measurement, then an equivalent stability is required in the junction unit, the conditioning circuits, and in the d-c amplifier if it is employed.
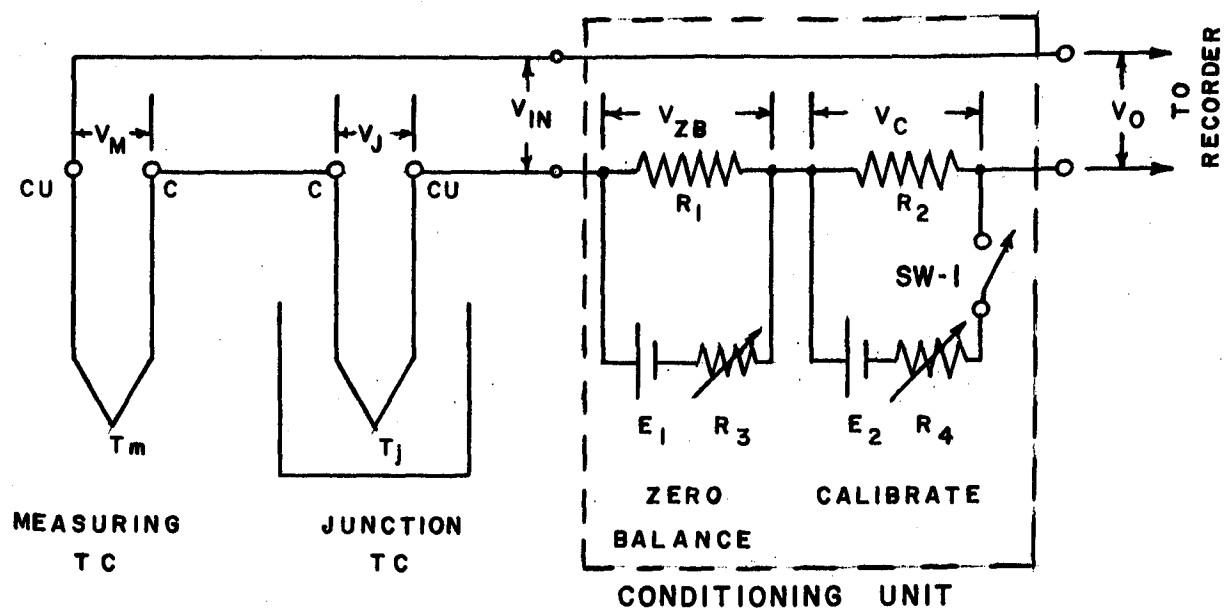
1.6.2 Reference Junction Unit

Figure 54 shows a cross-section of the reference junction unit. Basically it consists of a bundle of six copper-constantan thermocouples immersed in a vessel of oil which is held at a fixed temperature. This temperature is maintained constant to $\pm 0.05°C$, at a value of approximately $42°C$, by a heater immersed in the oil and controlled by a high sensitivity mercury-type thermoregulator*. A motor-driven stirrer operated continuously to prevent the development of thermal gradients in the oil bath. The circuit of the junction temperature control system is shown in Figure 55. The control thermoregulator is connected to terminals (4) and (5), and the heater to terminals (F) and (G) as shown. If the junction temperature is below the control point, Relay RL-1 is in the position shown (high current) and power to the heater is controlled by Variac VAR-2. Once the control point is reached, the thermoregulator effectively provides a short circuit across (4) and (5), which switches RL-1 into its other position (low current). Power to the heater is now supplied from another source and its magnitude is controlled by the setting of Resistor R_s. The system thus provides two heating rates, one (low current) to maintain the junction temperature just below the control point and the other (high current) to add sufficient heat, when required, to maintain the temperature at the control point.

A second thermoregulator unit, connected across terminals (1) and (2), is also immersed in the oil bath and is set a few degrees above the control point. This unit and the associated circuit (Relay RL-3 etc.) provide overheat protection for the junction unit. If the control temperature is exceeded, due to some circuit malfunction, this circuit shuts off all power to the heaters until the trouble is corrected. The stirrer motor is

---

* Type 4-200, Metastatic Mercury thermoregulator, manufactured by American Instrument Co. Inc.

A. ELECTRICAL CIRCUIT

$$V_O = V_M - V_J \pm V_{ZB} \pm V_C$$
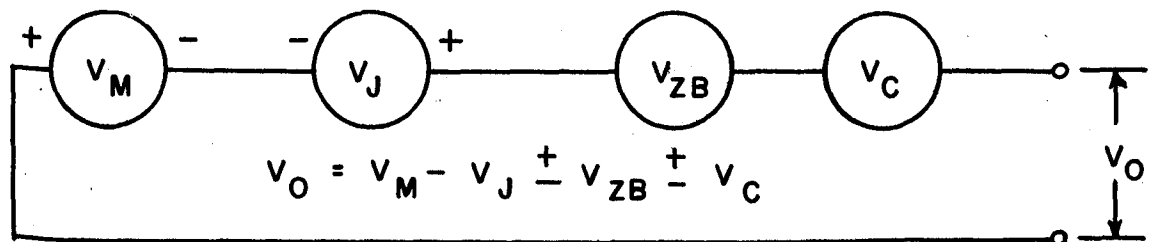
B. EQUIVALENT CIRCUIT

FIGURE 53 - Simplified Circuit Of Temperature Measurement System.

STIRRER
MOTOR

THERMOREGULATOR
(2, ONLY 1 SHOWN)

DIAL THERMOMETER

BAKELITE COVER

CONNECTIONS
TO
CONTROLLER

JUNCTION OUTPUTS
TO CONDITIONING
UNITS

JUNCTION INPUTS
FROM PATCH PANEL

STIRRER

HEATER

OUTER CASE

INNER
VESSEL

GLASS WOOL
INSULATION

THERMOCOUPLE
BUNDLE

30 SAE OIL
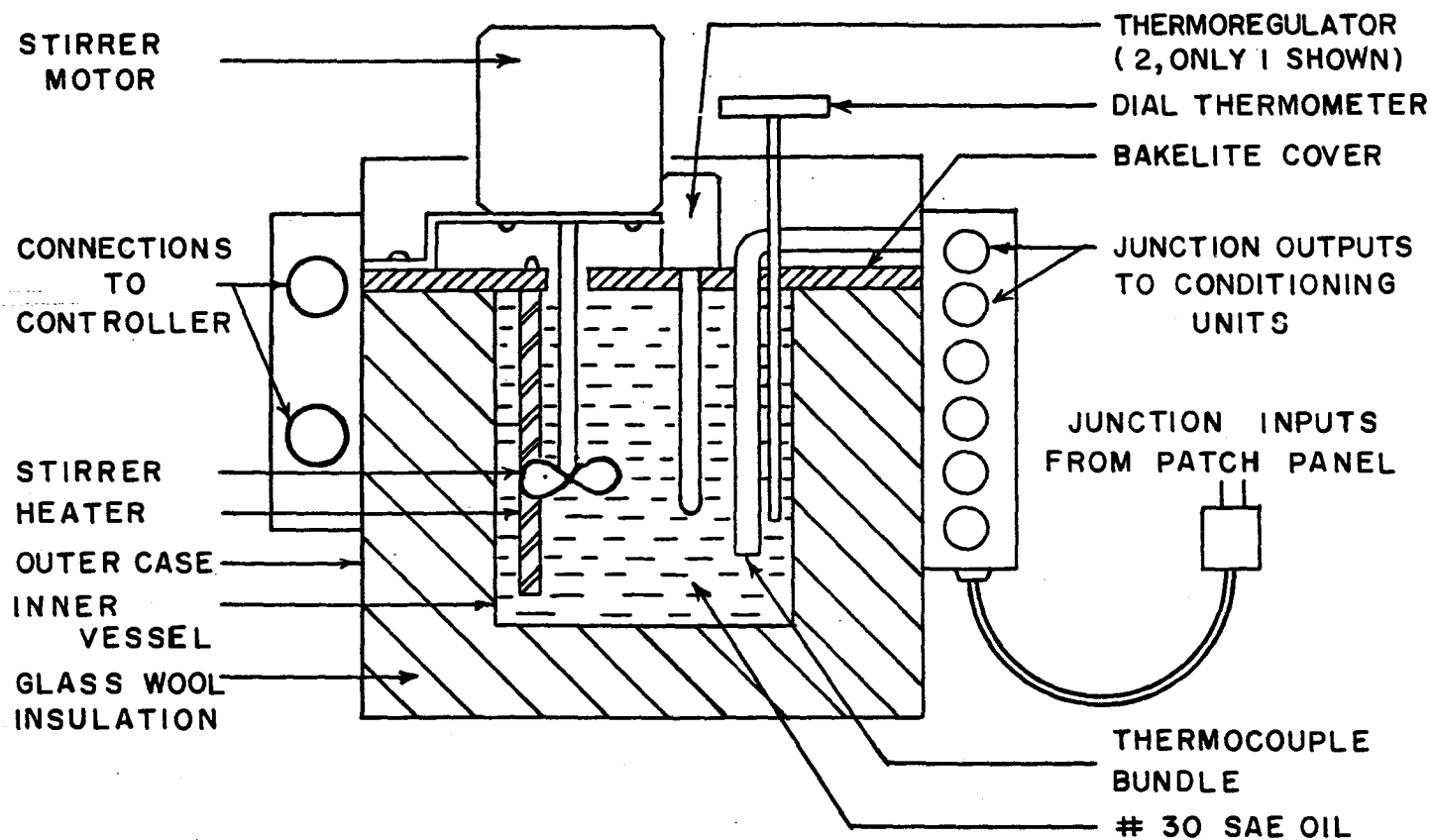
FIGURE 54 - Construction Details of Reference Junction Unit.

RL-2

TO OVERHEAT THERM. REG.

1N2070

NC

2A

110 VAC IN

SW-1

2A

CON-1

① ⑤
② ⑥ ④
(RV)
③

CON-2

Ⓐ Ⓕ
Ⓑ Ⓖ Ⓔ
Ⓒ Ⓓ

TO JUNCTION

ON (CL)

OVERHEAT (R)

RL-3

SW-3

1N2070

C_1 C_2

SW-4

167 K

VAR-1

TO STIRRER

Ⓐ
Ⓑ

SW-2

(Y)

CONTROL THERM. REG.

④ SW-5 SW-6 ⑤

1K

C_3

1N2070

125 (10W)

R_S

0.5A

0 - 0.1A

RL-1

TO HEATER

Ⓕ
Ⓖ

167 K

VAR-2

1A

0 - 1.5 A

167-N

C_1, C_2 and C_3 ----20µfd, 50v.
RL-1 ---Sigma 4IJO/500s-SIL.
RL-2 ---Potter-Brumfield KRP11A.
RL-3 ---Sigma 80030.
All transformers are Hammond Co.
Sw-3 : pos 1-normal, pos 2-reset
SW-4 : overheat shut-off check
SW-5 : high-current check
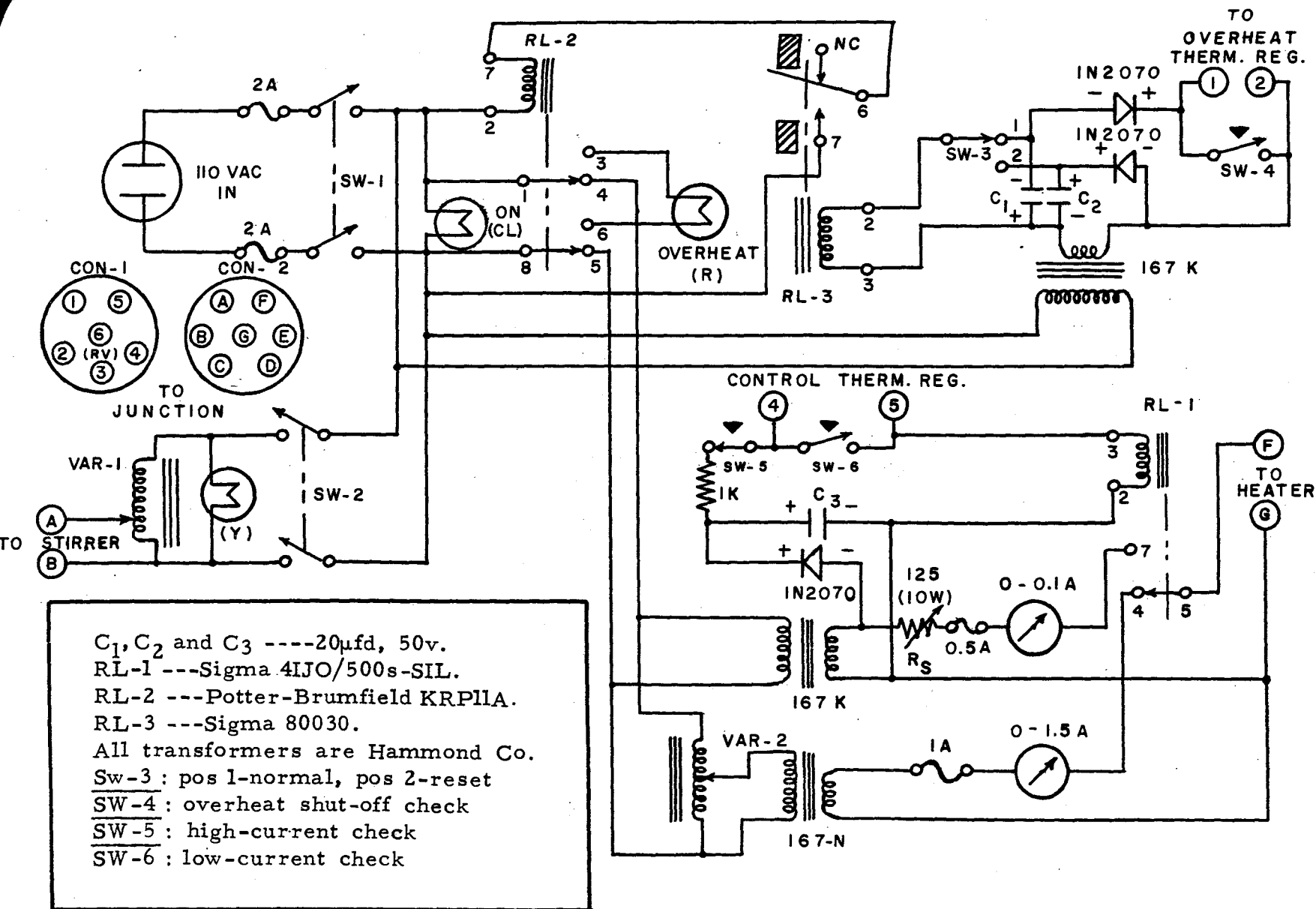SW-6 : low-current check

FIGURE 55 - Circuit Diagram for Reference Junction Controller.

connected to the controller at Terminals (A) and (B) and its speed is controlled by Variac VAR-1. Figure 56 shows a top view of the reference junction unit, and Figure 57 shows a front view of the junction controller unit. An extensive series of experiments (Test 63-2) was conducted to determine the long term temperature stability of the junction unit. Over a typical ten day period the maximum fluctuation of junction temperature was $\pm$ 0.05°C and no long term drift of the control point was observed.

1.6.3 Signal Conditioning Unit

The conditioning unit contains six separate conditioning circuits. The purposes of these circuits are first to provide a zero adjustment for the thermocouple recording channels and secondly to provide a method for checking the overall sensitivity of the thermocouple recording system. Zero balancing is provided by the addition or subtraction of a fixed (but adjustable) d-c voltage to the output of the TC junction unit (V_{in}). Figure 53A outlines how both the zero balance (V_{zb}) and calibrate voltages (V_c) are developed. The circuit designed for this purpose is shown in Figure 58. The signal (V_{in}) from the junction unit enters the conditioning circuit via Connector CON-1 and the modified signal leaves the unit via Connector CON-2.

The zero balance voltage (V_{zb}) is developed by passing a current through R_1. This current is developed by a 1.36 volt mercury cell and is adjusted to the correct value by an associated resistance network. Switch SW-1 allows the polarity of the zero adjustment voltage to be selected and provides a coarse zero adjustment. A 10-turn wire-wound potentiometer (R_5) serves as a fine zero adjustment control. Switch SW-2 allows a small calibration voltage to be introduced across R_2. This voltage is developed by a 1.36 volt mercury cell in the calibration circuit. The magnitude of the calibration voltage is selected by Switch SW-4, which places either a 10K or a 100K ohm resistor in series with the mercury cell.

The conditioning unit contains six zero-adjusting circuits similar to that shown in Section A of Figure 58. The calibration and voltage check circuits shown are common to all six zero adjusting circuits. Figure 59 shows two views of one section of the conditioning unit, which contains four of the zero-adjusting circuits. It was estimated that at least thirty days of continuous operation could be expected for each mercury cell in the zero adjustment circuits.

The behavior of the conditioning unit was studied over a period of five days. Table 12 lists a number of the important characteristics obtained from these experiments.
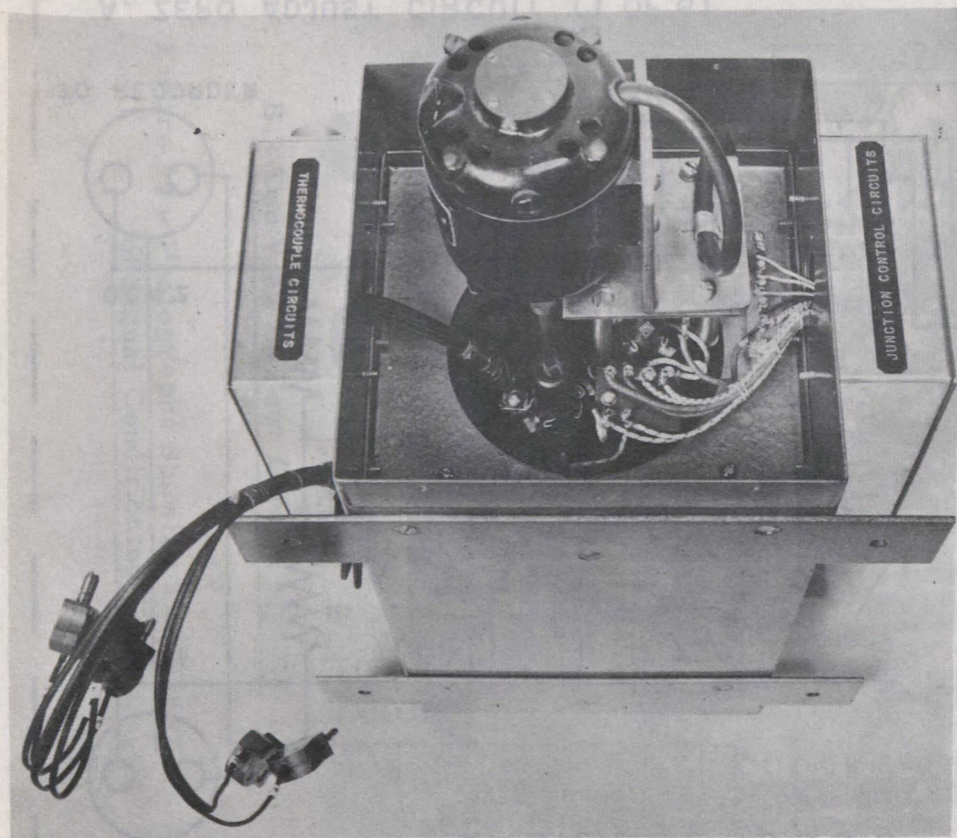
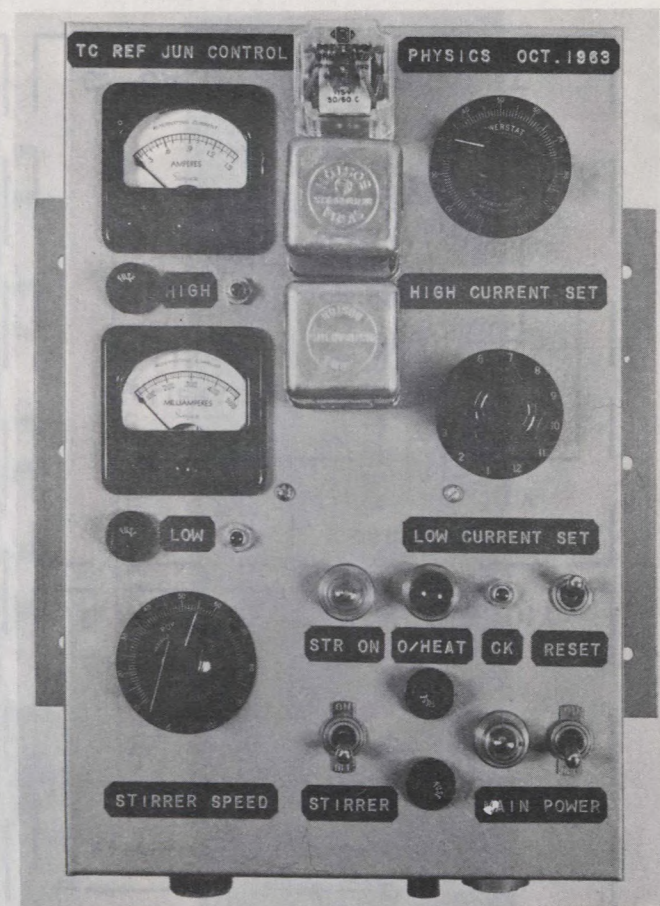FIGURE 56 - Photograph Showing Top View of Reference Junction Unit.

FIGURE 57 - Photograph Showing Front View of Reference Junction Control Unit.
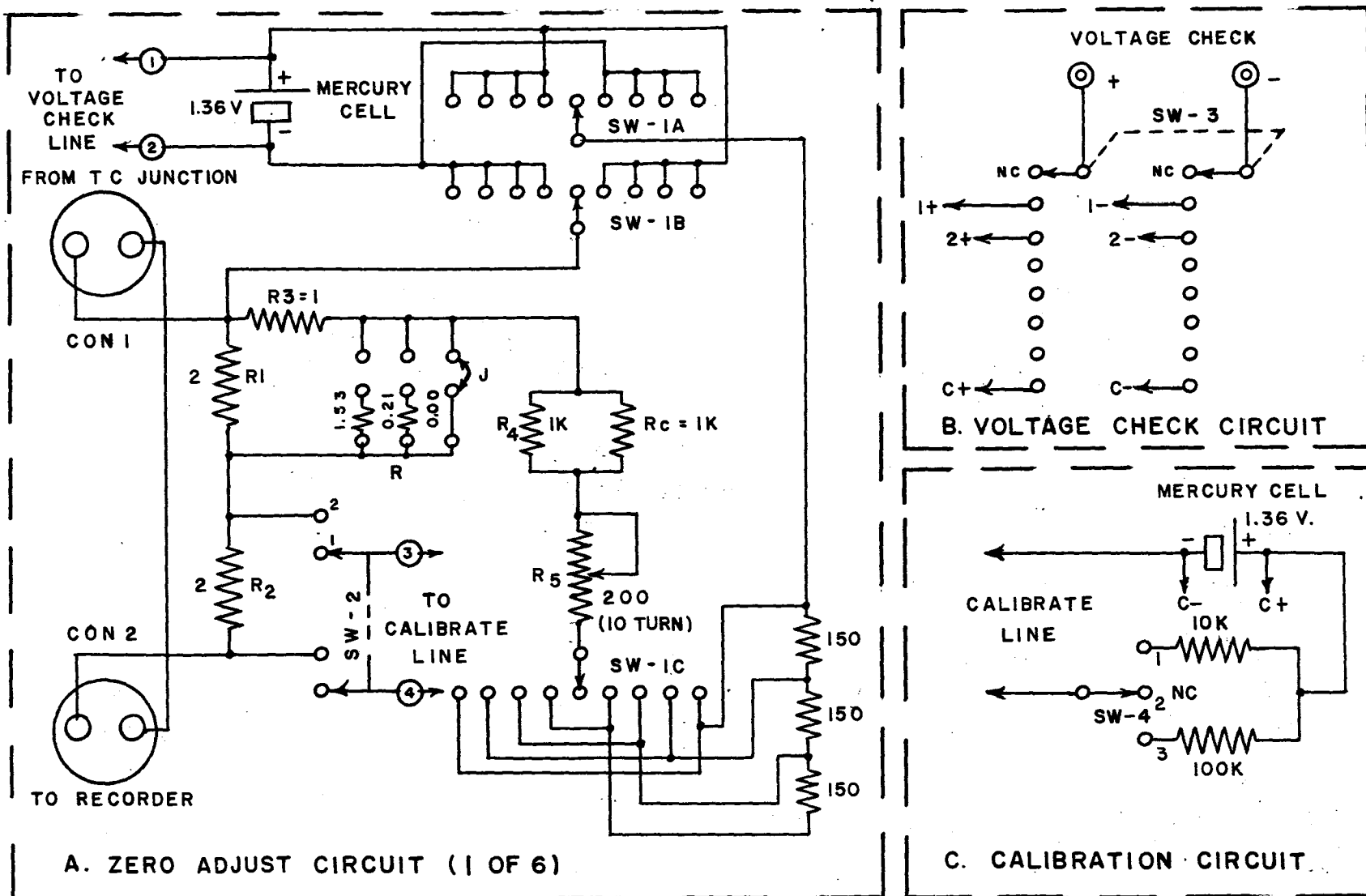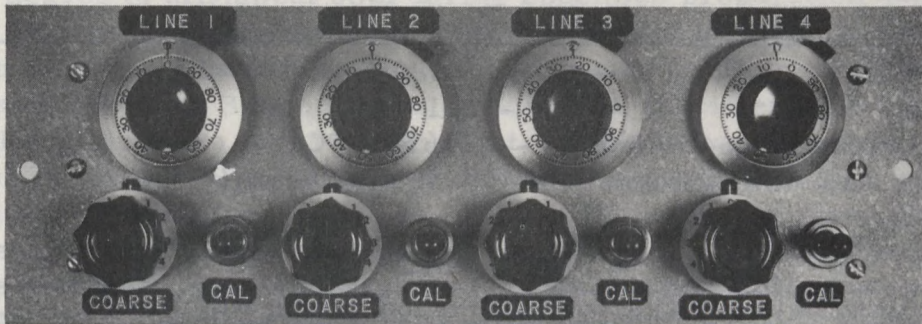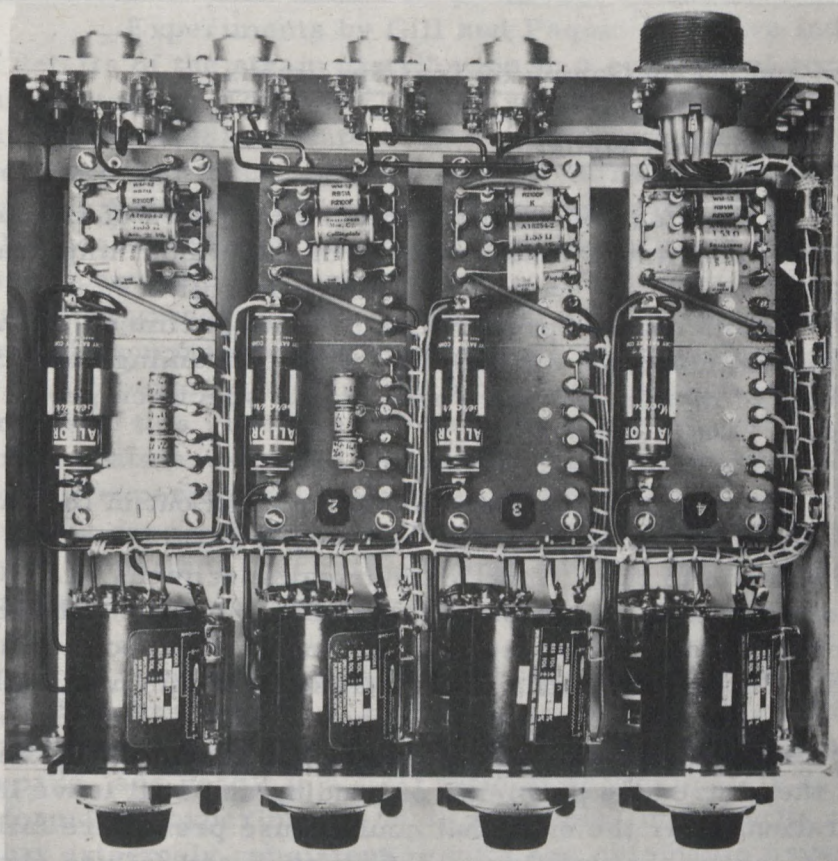
FIGURE 58 - Circuit Diagram for Thermocouple Signal Conditioning Unit.

A. Front View of Four Circuit Module.

B. Top View of Four Circuit Module.

Figure 59 - Photographs Showing Two Views
of Signal Conditioning Unit.

TABLE 12

Characteristics of Thermocouple Signal Conditioning Unit

Stability*	-------	$\pm$ 1.0 μv
Drift*	-------	Nil
Temperature coefficient	----	0.65 μv/°C
Zero Adjustment Range	----	$\pm$ 400 to 900 μv ($\pm$ 10-22°C)[+]
Calibration Signal	-------	Low - 34 μv ($\approx$ 0.81°C)[+]
		High - 340 μv ($\approx$ 8.1°C)[+]

* Determined over a three day test period during which the ambient temperature varied from 21 to 27°C.

[+] Equivalent temperature based on the use of a copper-constantan thermocouple which has a sensitivity of 42 μv/°C.

1.7 Preparation and Strain Gaging of Test Specimens

1.7.1 Test Specimen Geometry

In the study of the mechanical properties of solids the geometry of the test specimens themselves is of the utmost importance. This is particularly true in the case of quasi-brittle solids such as geologic materials. Furthermore, preparation of test specimens from such materials is considerably more difficult and time consuming than for more ductile solids such as metals and, as a result, the specimen geometry selected must be at best a compromise.

The majority of experiments carried out in the past have utilized solid cylindrical test specimens with a L/D ratio (length to diameter ratio) ranging from one to two. Short cylindrical specimens, L/D < 2, are unsatisfactory due to a distortion of the stress field along the axis of the specimen caused by forces acting at the interface of the specimen and the loading plattens. These distortions in the stress field diminish with distance from the end of the specimen and become small at distances equivalent to the specimen diameter. Long narrow specimens overcome the end-effect, but they introduce problems of bending and still leave large stress concentrations near the ends that could cause premature failure at these points. To ensure that maximum deformation and failure occur in the centre region of the test specimen, a reduced diameter section may be machined in this region. However, this specimen shape, like the previous shape, is susceptible to bending and as well will have stress concentrations in regions where the section diameter is abruptly changed. However, these stress concentrations may be greatly reduced by gradually necking down from the end of the specimen to the reduced centre section. In other words,

a fillet of large radius of curvature is provided between the end section and the reduced central section. For this geometry the possibility of bending remains, but it may be greatly reduced or eliminated by very careful finishing of the specimen end-surfaces and by the maintenance of a high degree of alignment both during specimen preparation and during the actual deformation experiments. The techniques involved in the design of such specimens have been described recently by Peterson (37). Based on these techniques Brace (3) has developed a specimen with a reduced central section and a large radius fillet, which he has used with great success for both compression and extension experiments on a wide range of sedimentary and igneous rocks. The undesirable features of this specimen design are the time and special machines required for their preparation, and the fact that relatively large pieces of test material are required. As a result, it was decided initially to utilize cylindrical specimens and to consider the use of filleted specimens only in the event that more refined experiments were required.

Experiments by Gill and Paquin (11) have indicated a number of details of the strain distribution in a cylindrical rock specimen under uniaxial stress. Their work along with a complementary photo-elastic study by Udd (48) indicates that a cylindrical specimen with an L/D ratio between two and three should provide a satisfactory compromise between bending and end-effects. Recently, experiments have been con-ducted by Larocque (29) on a number of sedimentary and igneous rocks, under uniaxial compression, using cylindrical specimens with L/D = 1.71. The finer grained groups of igneous rocks studied gave extremely consistent results for both compressive strength and elastic modulus, standard devia-tions of 0.4 - 7.5 per cent and 4.5 - 8.5 per cent respectively being obtained. Since the rocks in this group were inherently macroscopically homogeneous, the standard deviations obtained were mainly representative of the repro-ducibility of the experimental technique including any effects of specimen geometry. This does not preclude the fact that specimen dimensions them-selves may be important, but rather points out that for this particular L/D ratio experimental results are reproducible.

It was finally decided to utilize cylindrical test specimens nominally 1.75 inches long by 0.75 inch in diameter. These dimensions allow the most economical use of the available test material, are relatively easy to prepare, and result in a L/D ratio of approximately 2.33. Sub-sequent deformation experiments on an isotropic, high-purity marble have indicated that extremely consistent results are obtainable using this geo-metry.

1.7.2 Test Specimen Preparation

A great number of deformation experiments on geologic materials and most routine testing of these materials for engineering purposes have employed test specimens prepared directly from existing diamond drill core by simply cutting sections to length with a diamond saw and either lapping or grinding the ends plane-parallel (no attempt being made to first improve the quality of the circumferential surfaces). This procedure, which has been outlined by the writer (19) and by other workers (9, 34), results in specimens with ends plane-parallel to an accuracy of 0.005-0.00001 inch depending on the method. However, in most cases, and particularly where the core was drilled in the field, the specimen axis will have a small but finite radius of curvature and will not be normal to the ends of the specimen. Such specimens when loaded in compression will strain non-uniformly and will fail prematurely due to an induced bending moment. Such specimens may be sufficiently accurate for use in the determination of rough engineering parameters, but they are completely unsatisfactory for refined experiments.

In order to obtain reliable, reproducible data it is felt that the following conditions are required: the axis of the test specimen must be straight and normal to the end surfaces, the end surfaces must be plane-parallel to at least ± 0.0005 inch (over a specimen length of 1.7500 inches), the specimen cross-section must be circular to 0.001 inch at any position along the axis, and the diameter (0.750 inch) must be constant to at least ± 0.001 inch over the length of the specimen. Cylindrical specimens of this quality have been prepared by Robertson (41) using a centerless and a surface grinder and more recently at the Mines Branch using a lathe with an attached tool post grinder.

The procedure used to prepare test specimens for the current research is as follows:

(i) Sections of EX-diameter diamond drill core (nominally 0.85 inch in diameter and approximately six inches in length, free of obvious fractures or planes of weakness) are selected from the available field core (or from core drilled from block samples of the test material in the laboratory using a thin walled diamond coring drill).

(ii) The rough ends of the core are cut off with a diamond saw using "Almag" oil lubrication*.

(iii) The core is gently clamped in the lathe chuck with about 0.5 inch of core exposed.

(iv) The exposed end of the core is ground perpendicular to the axis of the lathe using a three inch tool post grinder**, with the plane of the grinding wheel oriented 15°-30° to the plane end of the core. The rotary speed of the grinder under no-load conditions is approximately 8000 RPM. Experience has shown that for this particular operation a chuck speed of 300 RPM and a cross feed of 0.0022 in./rev gives satisfactory results.

(v) Without disturbing the core, a 0.25 inch diameter hole, 0.25-0.40 inch deep is drilled into the ground-end of the core. In this operation the drill***is held fixed in the tail stock and the core is turned at a chuck speed of 300 RPM. With the softer materials it is important to use a very slow rate of drill feed, and to back the drill off after every few thousands of an inch penetration.

(vi) The core is then removed from the chuck and its other end prepared in a similar manner following steps (iii)-(v).

---

* Almag oil is manufactured in Canada by the Texaco Oil Company. Cleaning the specimen with perchlorethylene after preparation removes all visible traces of the oil. Experience has shown that its use in specimen preparation does not appear to affect the properties of the test material.

** Two types of carborundum grinding wheels are used depending on the hardness of the materials being prepared. For soft rocks, such as marble, a fine wheel, Type-C220K5V6C, 3 x 3/8 x 14 mm has been found satisfactory. For the harder rocks, such as granite, a coarser wheel, Type-C150K5V6C, 3 x 3/8 x 14 mm is employed. These wheels are manufactured in Canada by the Canadian Carborundum Company Ltd., Niagara Falls, Ontario.

*** For the softer materials, such as marble, an ordinary high speed steel drill was used. For the harder materials, such as granite, a small diamond coring drill was employed with either oil or air coolant.

(vii) The core is mounted axially between the chuck and tailstock of the lathe, being supported at each end by a brass jig the diameter of which is a few thousands less than that of the required finished specimen. A short 0.25 inch diameter concentric projection on these jigs fit into the end holes previously drilled in the core to insure accurate alignment of the core axis.

(viii) Initially, a series of rough cuts is made to bring the core diameter down to approximately the required dimensions. For this series of cuts a chuck speed of 300 RPM, a carriage travel rate of 0.0043 in./rev and a depth of cut of approximately 0.004 inch are used. The diameter of the core is checked at a number of points along its axis after each traverse. If the core develops high spots or a taper, the traversing procedure is modified until these effects are removed.

(ix) When the core diameter is reduced to within 0.010 inch of the required finished diameter, the grinding wheel is re-dressed using a diamond tipped tool and a series of finishing cuts is made with a chuck speed of 167 RPM, a carriage travel rate of 0.0021 in./rev and a depth of cut of approximately 0.001 inch. The final few thousands are removed using a depth of cut of 0.0005 inch or less.

(x) The core is removed from the lathe, wrapped in a piece of plastic sheet to protect the finished surface, and cut into lengths about 0.125 inch longer than the required specimen length, using a diamond saw with Almag lubrication. Identification such as specimen number, orientation etc. must be marked on the core at this time.

(xi) The short lengths of core are then wrapped in a single layer of plastic sheeting and gently positioned in the lathe chuck. The ends of the core are finished using the same grinding arrangement as outlined in (iv), first using a series of rough cuts with a chuck speed of 300 RPM, a cross feed of 0.0022 in./rev and a depth of cut of approximately 0.004 inch. Finally a series of finishing cuts are made with a chuck speed of 167 RPM, a cross feed of 0.0011 in./rev and a depth of cut of 0.0005 inch. One end of the specimen is first ground to the desired surface finish, the specimen is reversed in the chuck, and the other end ground to give the desired specimen length and surface finish.

(xii) The finished specimen is removed from the lathe, its dimensions at a number of locations checked, using a micrometer, to an accuracy of 0.0001 inch, and its weight measured to an accuracy of 0.0005 grams. A set of six to eight specimens is usually prepared at one time. Total preparation time for such a set ranges from 30-40 hours.

Figure 60A shows a number of lengths of Wombeyan marble core as received. Figure 60B shows a number of completed test specimens prepared from this core using the procedures just outlined.
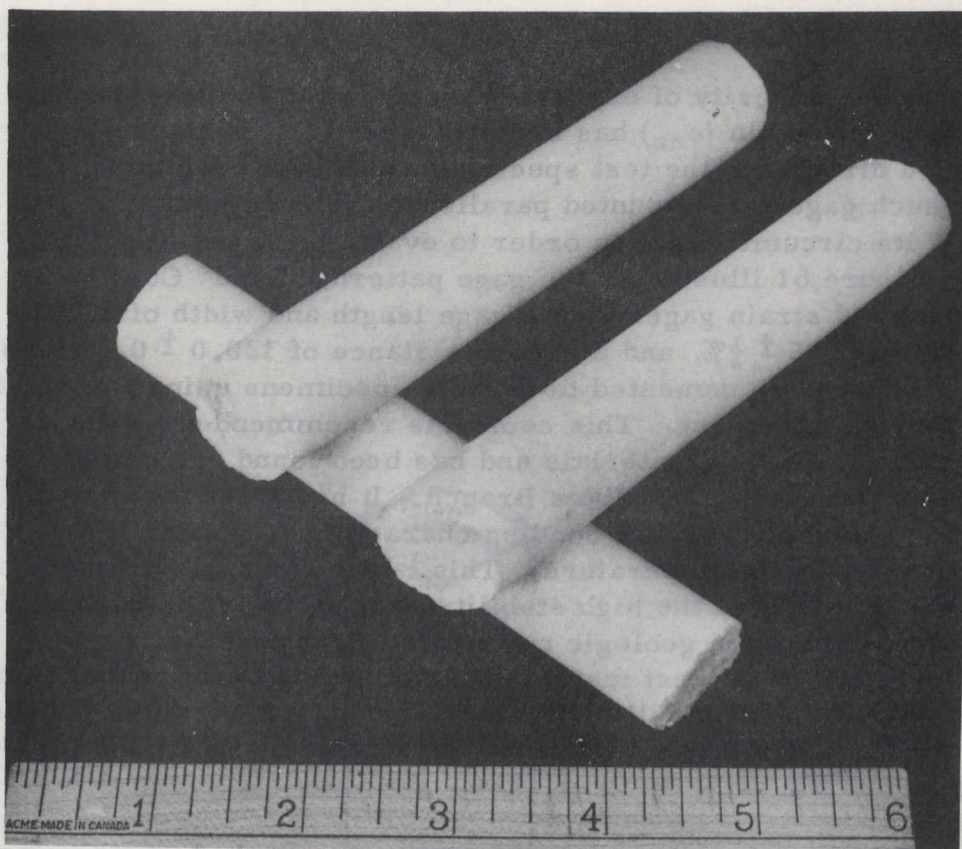
A. Cores of Material as Received.
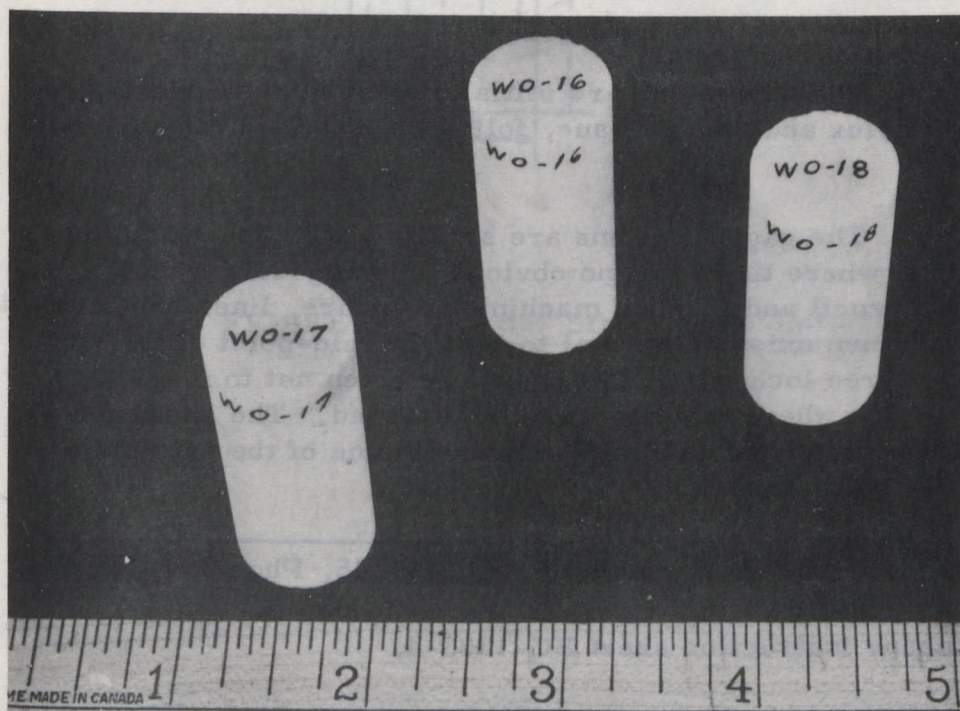
B. Prepared Test Specimens Ready for Strain Gaging.

FIGURE 60 - Wombeyan Marble as Received and after Preparation.

1.7.3 Strain Gaging of Test Specimens

In the majority of experiments conducted to date, only the longitudinal or axial strain (e_{zz}) has been measured. Resistance-type strain gages bonded directly to the test specimen are utilized for this purpose. Three such gages are mounted parallel to the specimen axis 120° apart around its circumference in order to evaluate the uniformity of the axial strain. Figure 61 illustrates the gage pattern. Budd[*] C6-131 foil-type, epoxy-backed strain gages with a gage length and width of 0.187 inch, a gage factor of 2.05 $\pm$ $\frac{1}{2}$%, and a gage resistance of 120.0 $\pm$ 0.2 ohms were employed. These were cemented to the test specimens using Budd B-3 epoxy-type, high stability cement. This cement is recommended by the manufacturer for use on porous materials and has been found extremely satisfactory for this purpose at the Mines Branch. It has a setting time of about 15 minutes and develops its full bonding characteristics after less than 24 hours curing at room temperature. This latter point is extremely important since the majority of the high stability cements must be cured at higher temperatures, which for geologic materials might result in a modification of the properties of the test materials. According to the manufacturer, after this curing period the bond will exhibit zero creep at a strain of 1000μs and will remain stable under static conditions for strains up to 5% and for temperatures up to 200°F.

The procedure for application of epoxy backed gages using this type of cement has been outlined by the manufacturer[**]; however, the following procedure has been found to be more satisfactory for this particular application:

(i) The specimens are initially cleaned of all visible oil and grease using Perlux and paper tissue, followed by a final cleaning with isopropyl alcohol.

(ii) The gage locations are selected 120° apart and, if possible, in regions where there are no obvious inhomogeneities in the material. Using a pencil and a small machinist's square, lines are marked parallel to the specimen axis and normal to it at the mid-point of the specimen at each of the three locations. Care must be taken not to mark the specimen in the region where the gage is to be attached. The specimen is then placed in a sponge rubber padded V-block with one of the sets of orientation axis facing upwards.

---

[*] Budd Company, Instruments Division, P.O. Box 245, Phoenixville, Pa., U.S.A.

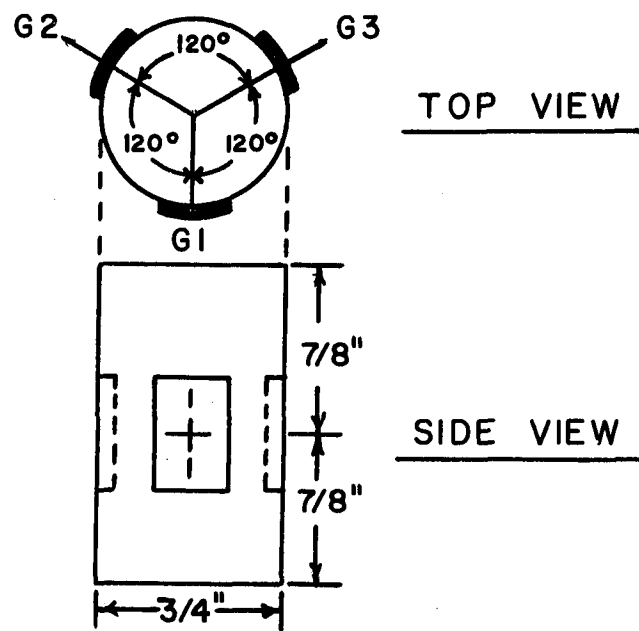[**] See Budd Company instruction sheet BG-1203-4.

FIGURE 61 - Axial Strain Gage Pattern.

(iii) A length of masking tape (3 in. x 3/4 in.) is positioned on a padded block, adhesive side up, and the strain gage pressed, rear side down, on to the tape. Using a fine pair of tweezers, the temporary protective sheet is removed from the gage.

(iv) The gage backing is lightly abraded using a small square (1/8 in. x 1/8 in.) of No. 1 polishing paper held with the tweezers; the gage surface is then cleaned with a cotton swab dipped in isopropyl alcohol.

(v) A small length of the masking tape, with the cleaned gage in place, is cut free and, using a strong light behind the gage, the location of the gage axis is marked on the back of the tape.

(vi) The B-3 cement, which is supplied in a dual compartment plastic envelope, is then prepared by removing the clamp separating the cement and the hardener and kneading the package for about 60 seconds. The package is then opened by cutting one corner, and the contents poured into a watch glass where it is stirred, with a glass rod for about another 60 seconds, at which time it is ready for use.

(vii) A thin even layer of the cement is spread on the exposed gage surface, the gage axis and the orientation axis on the specimen are lined-up as carefully as possible, and the gage is taped in position. A gentle pressure is applied over the surface of the gage to squeeze out excessive cement. The other two gages, which have also been prepared ready for mounting, are then applied following the same procedure.

(viii) Small cellophane pads slightly larger than the gage backing are placed over the gages, and a length of Teflon tape is wrapped firmly around the specimen several times and held in place by masking tape.

(ix) The gage cement is allowed to cure for 24 hours before removing the clamping tape and the gage mounting tape. The gages are then checked visually under a low power magnifier for the quality of the gage bond and the gage orientation. The gages are then coated with waterproofing compound* and allowed to dry.

(x) The specimens are then wrapped in tissue and stored until required. Figure 62A shows a set of specimens with attached gages. The three specimens at the rear of the photograph show the typical arrangement of the gages presently used to measure axial strain (e_{zz}). The specimen in the foreground has an additional set of three gages oriented perpendicular to the specimen axis for the measurement of laterial strain ($e_{\theta\theta}$).

---

*Budd Type GW-1 waterproofing compound has been employed on all gages to date.
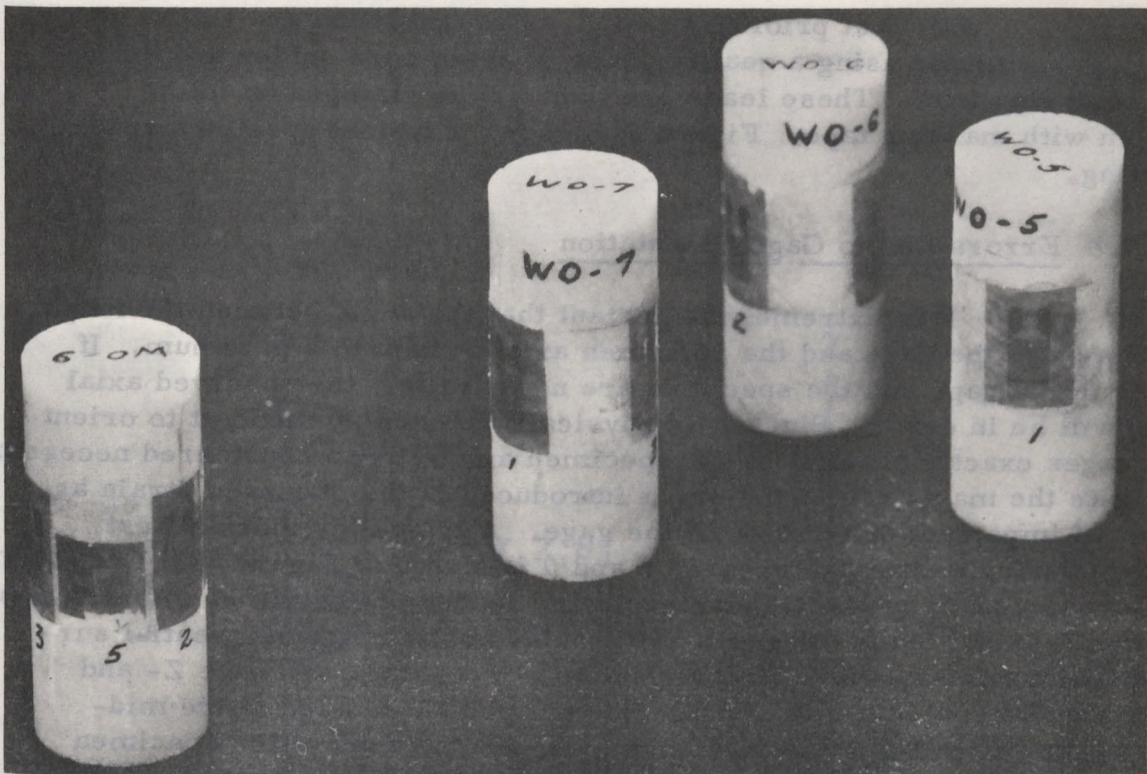
A. Group of Test Specimens with Attached Strain Gages.
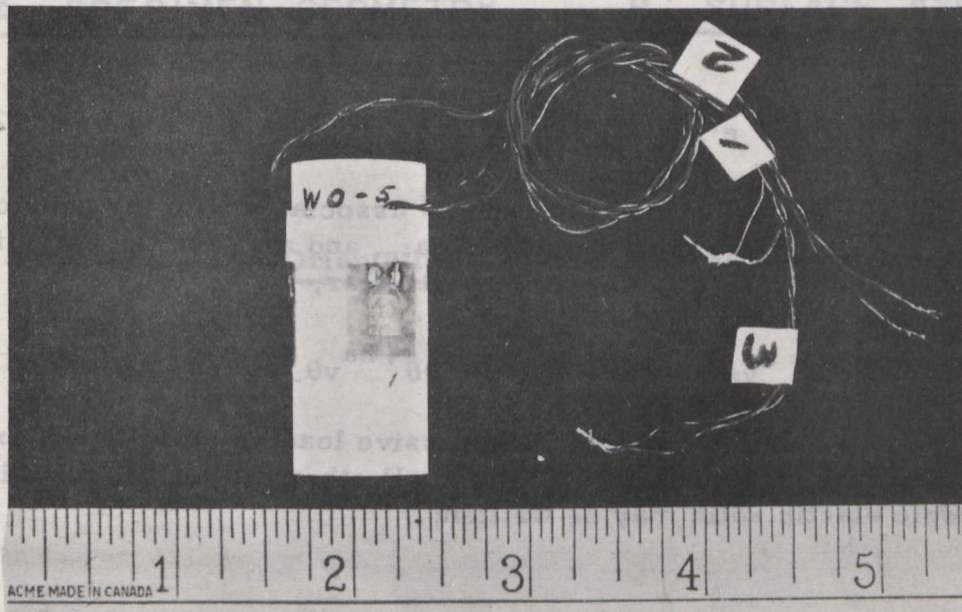
B. Specimen Ready for Testing with Strain Gage Leads Attached.

FIGURE 62 - Photographs Showing a Number of Views
of Gaged Test Specimens.

(xi)   Just prior to testing, extension leads are soldered to the gage terminals using a quality grade of resin core solder and a fine tipped soldering iron.   These leads are then firmly clamped on to the specimen with masking tape.   Figure 62B shows a typical specimen ready for testing.

1.7.4   Errors Due to Gage Orientation

It is extremely important that the angle between the long-itudinal axis of the gage and the specimen axis be kept to a minimum.   If the axes of the gage and the specimen are not parallel, the observed axial strains will be in error.   Since it is physically extremely difficult to orient strain gages exactly parallel to the specimen axis, it was considered necessary to evaluate the magnitude of the error introduced in the observed strain as a result of imperfect orientation of the gage.   A typical cylindrical test specimen having coordinate axes Z, r and θ is shown in Figure 63.   Consider the test material to be elastic, isotropic and loaded uniformly in compression along the Z-axis.   Since the gages are mounted on the circumferential sur-face of the specimen, which is a surface of r = constant, only the Z- and θ-axes need be considered.   Considering the point P located at the mid-point of a line parallel to the specimen axis, let the axes of the specimen at this point be Z and θ, and of the gage be V and β and let the axes of the gage be at an angle α to those of the specimen.   The relationship between strains in these two coordinates systems may be established from elastic theory using indicial notation (see for example Sokolnikoff (44).

Now

$$e'_{ij} = a_{im} \, a_{jn} \, e_{mn} \qquad \text{(Eq. 2)}$$

where e_{mn} and e'_{ij} are the strain components associated with the axes of the specimen and the gage respectively, and a_{im} and a_{jn} are the direction cosines between the two sets of axes.   In particular,

$$e'_{vv} = a_{vz} \, a_{vz} \, e_{zz} + a_{v\theta} \, a_{v\theta} \, e_{\theta\theta} + 2 a_{v\theta} \, a_{vz} \, e_{z\theta} \qquad \text{(Eq. 3)}$$

Assuming uniform compressive loading along the Z-axis of the specimen, the stresses are $\sigma_{zz}{}^*$, and all other $\sigma_{ij} = 0$, Hooke's law for an isotropic elastic solid may be written:

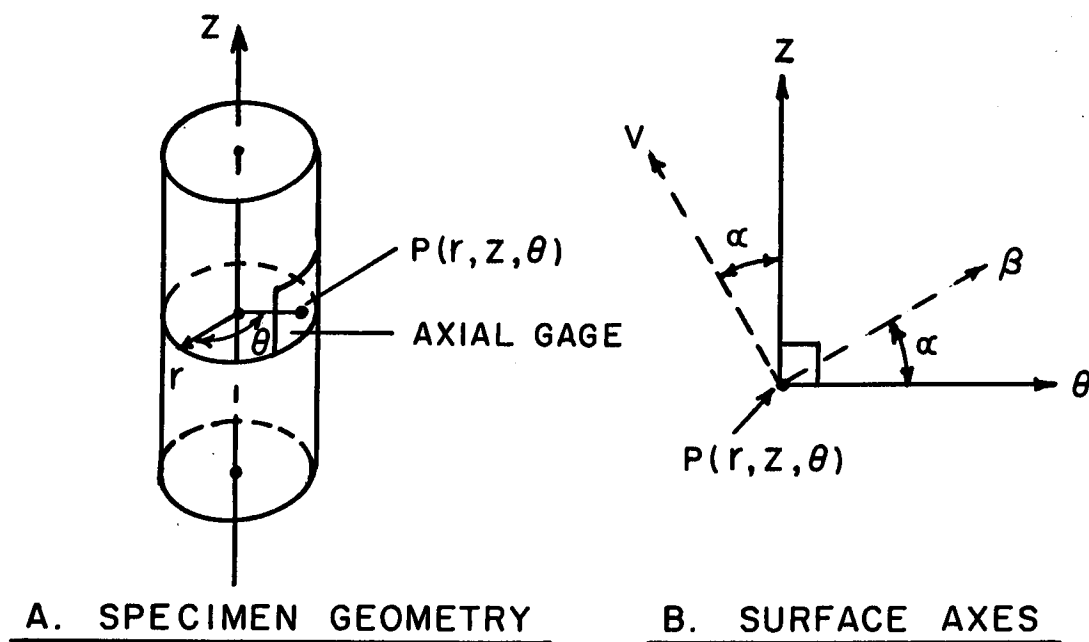* For convenience compressive stresses and strains will be considered positive.

A. SPECIMEN GEOMETRY **B. SURFACE AXES**

FIGURE 63 - Orientation of Gage Axes to Specimen Axes.

$$e_{ij} = \left(\frac{1 + \mu}{E}\right) \sigma_{ij} - \frac{\mu}{E} \Theta \delta_{ij} \qquad \text{(Eq. 4)},$$

where $\Theta = \sigma_{ii} = \sigma_{zz} + \sigma_{rr} + \sigma_{\theta\theta}$, and E and μ are respectively the Young's modulus and Poisson's ratio of the material. Now, using Eq. 4 and the condition that $\sigma_{ij} = 0$ except for $i = j = z$, it may be shown that

$$e_{zz} = \sigma_{zz}/E \qquad \text{(Eq. 5)},$$

$$e_{z\theta} = 0 \qquad \text{(Eq. 6)},$$

$$e_{\theta\theta} = -(\mu/E)\sigma_{zz} \qquad \text{(Eq. 7)}.$$

Substituting for σ_{zz} in Eq. 7 gives

$$e_{\theta\theta} = -\mu e_{zz} \qquad \text{(Eq. 8)}.$$

Substituting Eq. 6 and Eq. 7 into Eq. 3 gives

$$e'_{vv} = (a_{vz})^2 e_{zz} - \mu(a_{v\theta})^2 e_{zz}$$

or

$$e'_{vv} = e_{zz}\left[(a_{vz})^2 - \mu(a_{v\theta})^2\right] \qquad \text{(Eq. 9)}.$$

The direction cosines a_{im}, a_{jn} are the cosines of the angles between two pairs of coordinate axes. These may be obtained from Figure 63 by inspection and are given in Table 13.

TABLE 13

Direction Cosines

AXES	Z	θ
V	(a_{vz}) $\cos \alpha$	$(a_{v\theta})$ $-\sin \alpha$
β	$(a_{\beta z})$ $\sin \alpha$	$(a_{\beta\theta})$ $\cos \alpha$

Substituting these into Eq. 9 gives

$$e'_{vv} = e_{zz} (\cos^2 \alpha - \mu \sin^2 \alpha) \qquad \text{(Eq. 10)},$$

or more conveniently,

$$e_{zz} = \frac{e'_{vv}}{\cos^2 \alpha - \mu \sin^2 \alpha} \qquad \text{(Eq. 11)},$$

where e_{zz} is the true axial strain and e'_{vv} is the apparent (or measured) axial strain. The per cent error (M) due to gage orientation may be written as,

$$M = \left\{ \frac{e_{zz} - e'_{vv}}{e_{zz}} \right\} \times 100\%$$

Substituting for e_{zz} from Eq. 11 gives

$$M = (1 - K) \qquad \text{(Eq. 12)},$$

where

$$K = \cos^2 \alpha - \mu \sin^2 \alpha \qquad \text{(Eq. 13)}.$$

Measurements on a series of gages attached to typical test specimens showed that $0 \leq \alpha \leq 3^\circ$. Table 14 lists the calculated values of M assuming a range of values of μ, and $\alpha = 3^\circ$.

TABLE 14

Effect of Strain Gage Orientation

α	μ	K	M
degrees	---	---	per cent
3	0.25	0.9965	0.35
3	0.50	0.9959	0.41
3	2.0*	0.9918	0.82

*Anomalous values of μ have been reported by Evans and Wood (8) and others for many geologic materials under creep conditions.

Under the worst possible conditions M does not exceed one per cent and hence a correction for gage orientation would not be required under normal conditions.

1.8 Uniform Loading of Test Specimens

1.8.1 Initial Investigations

Deformation of any material under compressive loading presents a number of experimental difficulties. These difficulties are further increased when geologic materials are involved. These materials are usually very weak in tension and, even under moderate confining stress, normally fail as brittle materials. As a result, uniform loading is essential to insure that material does not fail prematurely. Furthermore, if meaningful strain data is to be determined from a finite number of strain gages, it is necessary that the strain distribution throughout the specimen be as uniform as possible. Such a uniform distribution requires first a suitably shaped and accurately prepared test specimen (this requirement has been discussed in detail earlier), and second a method for uniformly loading this specimen.

In previous experiments by the writer an attempt was made to obtain uniform loading by using test specimens with well prepared plane-parallel ends mounted in some form of loading jig or sub-press to maintain specimen alignment during deformation. In these earlier experiments axial strain was measured by two resistance strain gages attached to the specimen and connected in series to give an output equivalent to the average strain. Such a strain measuring arrangement is convenient in some respects, but it provides no indication of whether bending is taking place in the specimen. The three gage arrangement presently utilized provides this additional information and makes it possible to evaluate the uniformity of loading produced by different loading arrangements.

Preliminary experiments on geologic materials indicated that extremely non-uniform loading resulted when the original type of loading jig was employed, in many cases the bending being so large that one and sometimes two of the gages indicated large tensile strains. A review of the literature dealing with geological materials indicated that many workers have recognized the existence of this problem. The majority of those in the geological field (e.g., Griggs (12), Handin (15), Robertson (40), etc.) have incorporated some form of "stress equalizer" and/or a flexible linkage in their loading arrangement. This appears to provide a satisfactory solution, at least for experiments under high confining pressure where the materials are to some extent ductile. Brace (3), however, found this technique unsatisfactory for geological materials under conditions that favoured mainly brittle behavior; he found it necessary to utilize specially shaped specimens that were loaded under forced axial alignment[*]. Such a loading arrangement

---

[*] In Brace's experiments the loading pistons and the enlarged head pieces of the test specimen were very accurately ground and were held concentric by the internal wall of the test vessel.

induces a large frictional force into the loading system, which is undesirable in many types of experiments. Most of those concerned with the testing of geologic materials for engineering purposes have overlooked or ignored the problem, although some consideration has been given to it by Obert et al. (34) and more recently by Grosvenor (14), Paquin (36) and others.

In order to overcome this problem, an experimental program was established to investigate various types of loading arrangements. A ground steel cylinder 0.75 inch in diameter and 1.50 inches in length with three attached axial strain gages (120° apart) replaced the test specimen in the loading jig. The strains at each gage were recorded separately and the average strain, e_a, the maximum deviation between any two gages, Δe, and the per cent deviation $(\Delta e/e_a) \times 100$ were calculated at each stress level. The various jig configurations were tested in one of the loading frames located in the deformation facility described previously. In the majority of cases load was applied to the jig via the loading button on the load cell and a spherical seat attached to the upper surface of the loading jig.

The original type of loading arrangement (20,21) was discarded almost immediately as it was found that the use of small vertical posts to align the upper and lower plattens was unsatisfactory. One modification of this type of jig was made by substituting a ball and socket (using a 0.5 inch diameter ball bearing) for the original fixed lower loading head. Figure 64A illustrates the mechanical arrangement and Figure 65A shows a typical set of experimental curves obtained using this jig[*]. The strain versus stress data for the three individual gages show an increasing divergence with stress, reaching a deviation of 262 μs at 17,500 psi. It is interesting to note, however, that the average strain curve passes through zero at zero load and remains nearly linear with increasing stress. Similar experiments by Grosvenor (14) on rock and by Kerper et al. (28) on brittle cermets[+] have indicated that the use of conventional-type swivel heads may increase rather than decrease non-uniform loading. Grosvenor (14) found it necessary to lock the swivel head after initial contact had been made with the specimen. Kerper et al. (28) found that when using conventional swivel heads considerable bending was induced in the specimen, which was large enough to produce tensile strains in some areas. They found that the most

---

[*] It should be noted that this particular test, denoted as 63-0, was carried out early in 1963 at which time the hydraulic loading ram was hung from the upper platten of the loading press, rather than being threaded into it as was the case for the other experiments.
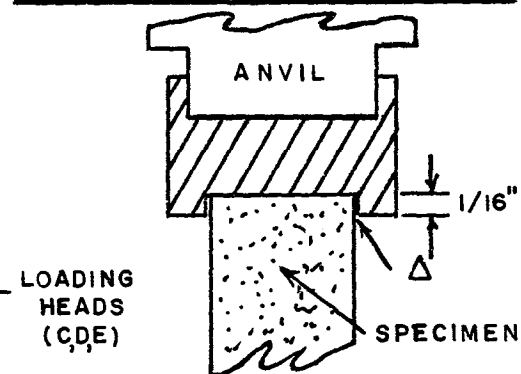
[+] Cermets are materials formed from a mixture of ceramic and metallic powders by the process of compaction and sintering.
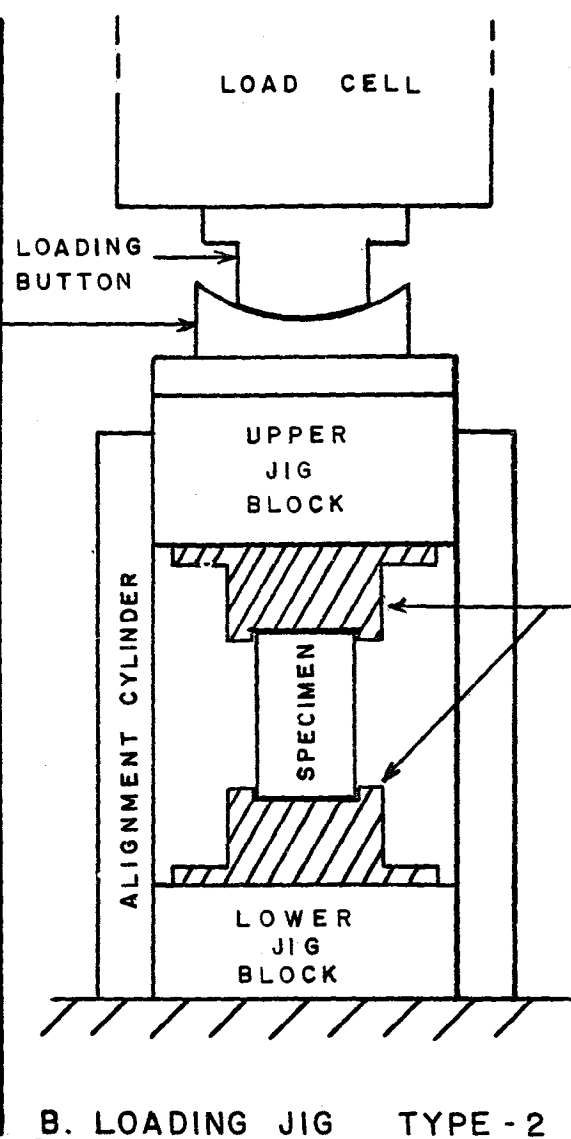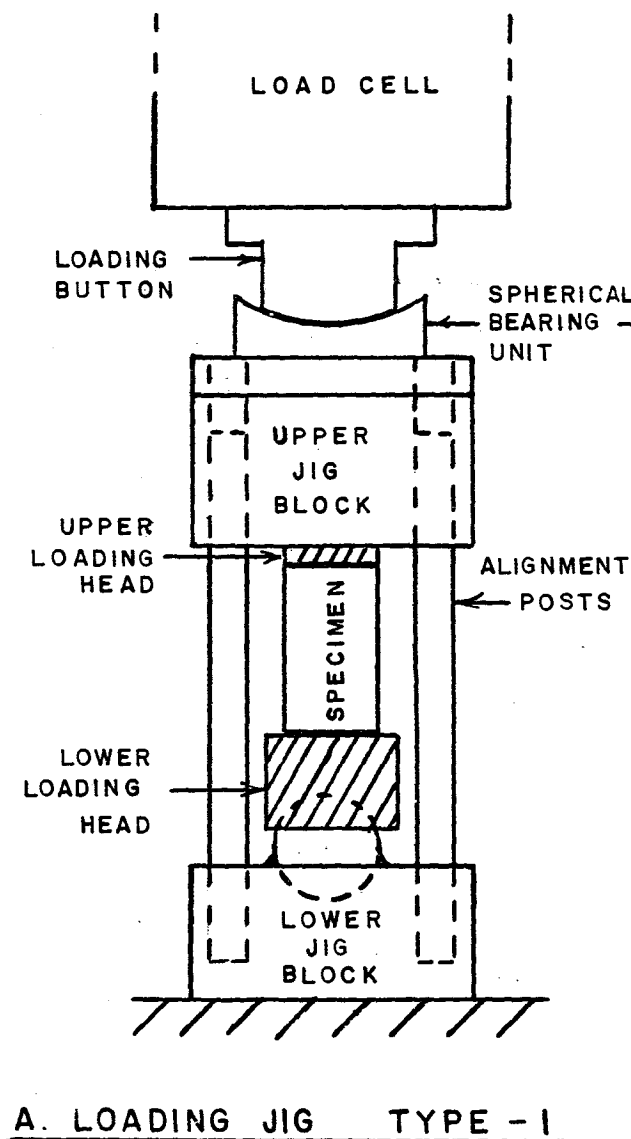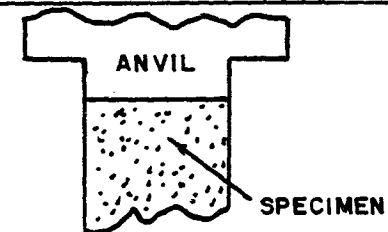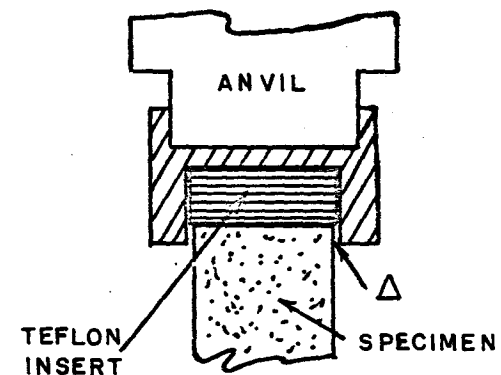
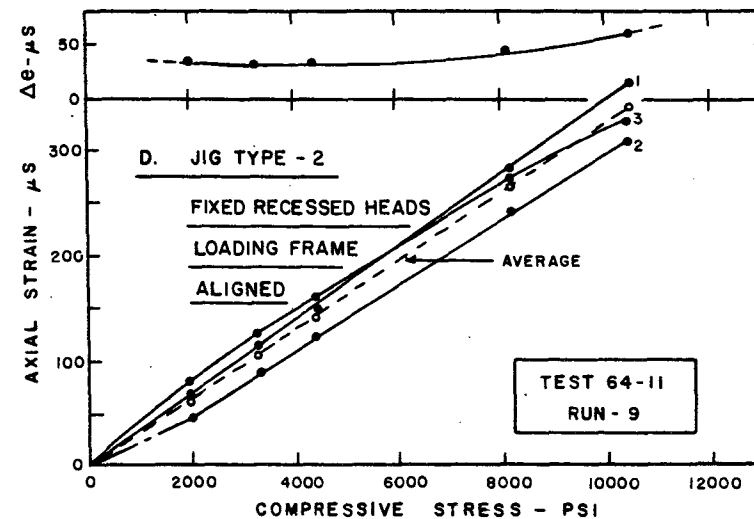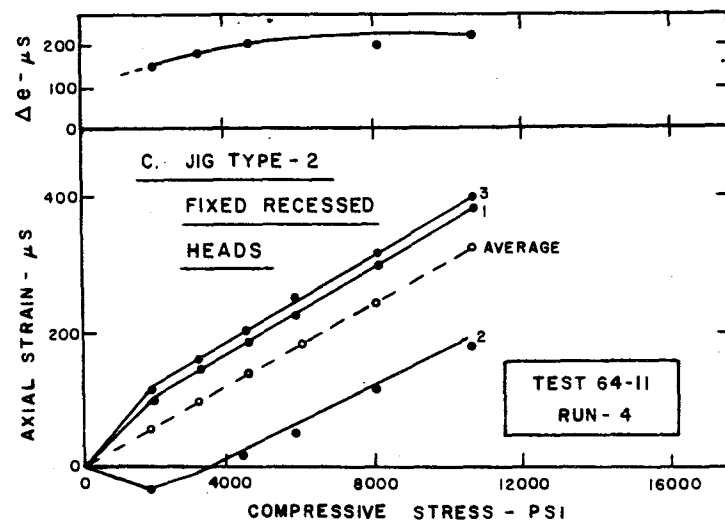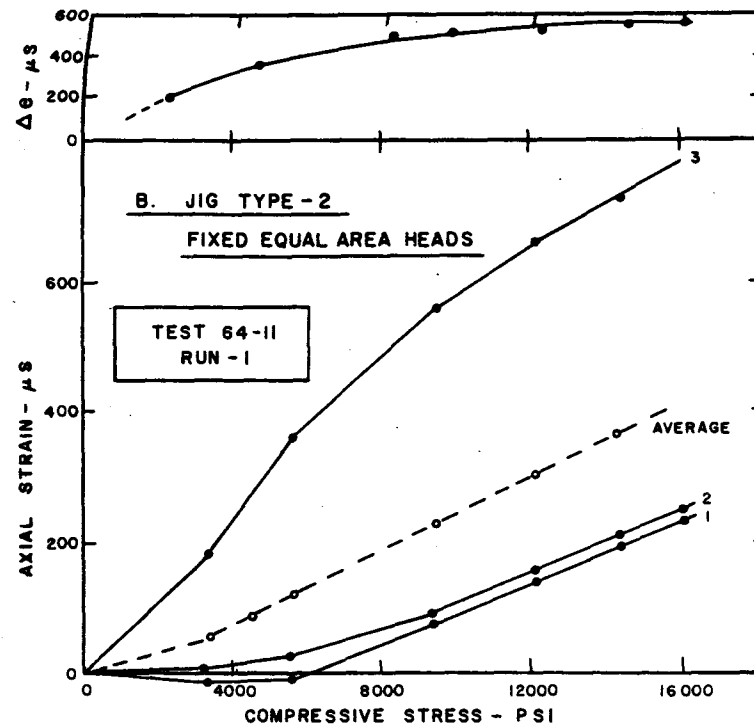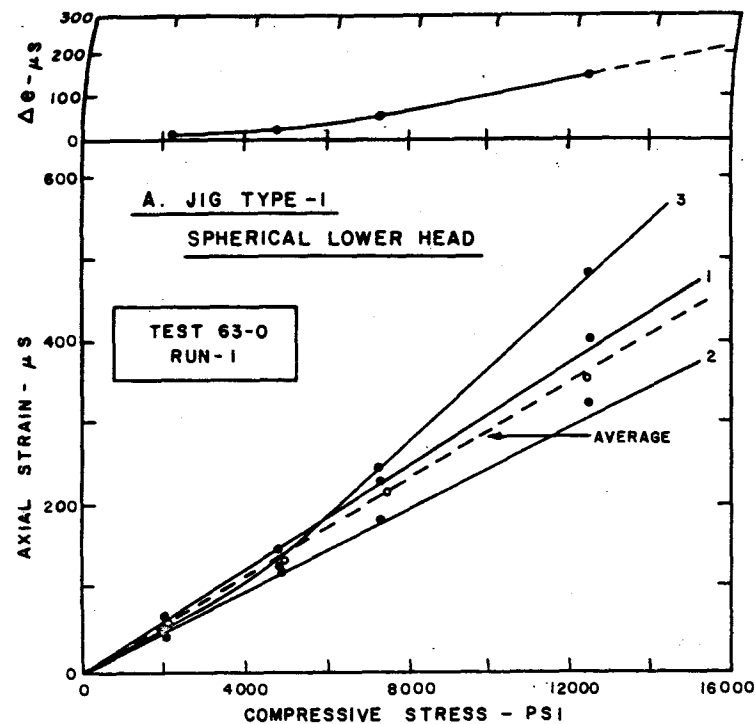FIGURE 64 - Details of Various Types of Specimen Loading Jigs.

FIGURE 65 - Stress-Strain Curves Obtained Using Various Types of Specimen Loading Jigs.

satisfactory loading was obtained using a well aligned testing machine and precision finished fixed loading heads consisting of short, hollow, thick-walled tool steel cylinders, shrunk-fitted onto a length of the actual test material somewhat larger in cross-section than the test specimen. Such an arrangement was not considered practical for testing of geologic materials.

1.8.2 Fixed Loading Heads

Next it was decided to carry out a number of experiments with fixed loading heads and a jig that would provide a degree of forced alignment. The jig arrangement is shown in Figure 64B and consisted of a cylindrical upper and lower jig block (3 inches in diameter) held in alignment by an outer cylinder. A centering hole and a series of threaded holes in the jig blocks allowed various loading head arrangements to be attached. All surfaces were ground finished and the end surfaces of the jig blocks were accurately ground normal to their axis. Initially a set of anvils with a diameter equal to that of specimen was employed. This arrangement is shown in Figure 64C. A series of three experiments was conducted using this arrangement (64-11 (1, 2, 3)) and Figure 65B illustrates the results for Test 64-11 (1), which is typical. The average strain curve appears relatively linear (although it does not pass through zero), but the curves for the individual gages are non-linear and differ greatly in magnitude. Gages 1 and 2 show a very low sensitivity, with Gage 1 initially indicating a tensile strain. The deviation (Δe) between gages increases with stress, but $d(\Delta e)/d\sigma$ appears to decrease up to a stress of approximately 8000 psi, after which it remains nearly constant.

The results of the previous series of tests suggested that, since the anvils and the test specimen were of the same diameter, it was probably difficult to ensure that the specimen was in contact with the anvils over its complete end-surface. To check on this, a set of precision-ground loading caps was machined as shown in Figure 64D. These were designed to be a "close sliding fit" to the anvils and to have a diametric clearance to the specimen of 0.005-0.006 inch, thus allowing the specimen to be aligned to within 0.003 inch of the jig axis. A series of three experiments was run using this arrangement (64-11 (4, 5, 6)). Figure 65C illustrates the results for Test 64-11 (4), which is typical. The average strain curve is linear and passes through zero; however, one of the gages (No. 2) goes initially into tension. As in the previous set of tests the deviation (Δe) increases with stress, but $d(\Delta e)/d\sigma$ approaches a limiting value after a stress of approximately 4000 psi.

Results to this stage using modified jigs had not been very encouraging, and it was decided to check on the effect of very accurately aligning the loading frame itself. Using a micrometer dial gage, accurate to $\pm$ 0.0001 inch, the four posts of the loading frame were adjusted so that the top and bottom plates of the loading frame were parallel to within an angle of less than 2 minutes (0.0051 inch over a span of 10 inches). A series

of three experiments (64-11(7, 8, 9)) similar to (64-11(4, 5, 6)) was then run. The results for Test 64-11(9), which is typical of this series, are shown in Figure 65D. In these tests no gages indicated tensile strains and the deviations (Δe) at low stresses were considerably smaller (being only 35.4 μs at 3147 psi in comparison with 294 and 185 μs for Tests 64-11(1) and 64-11(4)). Figure 66 illustrates the variation of the average strain (e_a) and the deviation (Δe) as a function of stress for Test 64-11(1, 7, 9). It is interesting to note how closely the average strain curves agree, even in cases where Δe was large.

Although the alignment of the loading frame had improved the situation considerably, Δe was still far too large, necessitating further consideration of a more effective loading jig. A number of workers in the past have utilized pads of various materials between the ends of the specimen and the loading plattens in an attempt to develop uniform loading. Obert et al. (34) found in studies of compressive strength of rocks that, although such pads did tend to reduce the deviation in test results, they also reduced the apparent strength of the material. Kerper et al. (28) studying the compressive strength of cermets found that this technique did not significantly reduce the induced bending strains produced by non-uniform loading. Recently studies have been undertaken by Gill (10), Paquin (36), Shih (43) and others at McGill University on the effect of various end-pads and end-lubrication, but as yet no definite solution to the loading problem has been obtained. It should be noted in most cases where end-pads have been employed they were merely placed between the specimen and the loading fixture and during compression were free to extrude laterally.

In soil mechanics flat inflated rubber diaphragms filled with water or other liquid are often located between specimen and the loading plattens in an attempt to obtain uniform end loading. Harboe (17) describes a similar arrangement using instead a thin metal diaphragm. Handin has recently suggested (see Paquin (36)) that one solution might be obtained by loading the specimen ends using direct hydraulic pressure. Cross (6) has used this method to obtain relatively uniform stress patterns in photostress plastic patches attached to short brass cylinders under compression. Hydraulic loading however has a number of disadvantages; first, the specimen ends must be sealed against penetration by the hydraulic fluid and secondly the specimen ends must be fitted with O-rings, which under pressure may cause high shear stresses to develop across the ends of the specimen; thirdly, if high axial stresses are required, the end-loading attachments required to withstand the necessary fluid pressures become bulky.

As part of an experimental investigation of the yield stress of pure lead, Loizou and Sims (33) have described an interesting method for reducing the frictional forces between the compression plattens and the test specimen. Concentric grooves 0.002 inch deep were machined on each end of the specimen and during compressive loading oil with a free fatty acid additive was entrapped in these grooves. It was found experimentally that
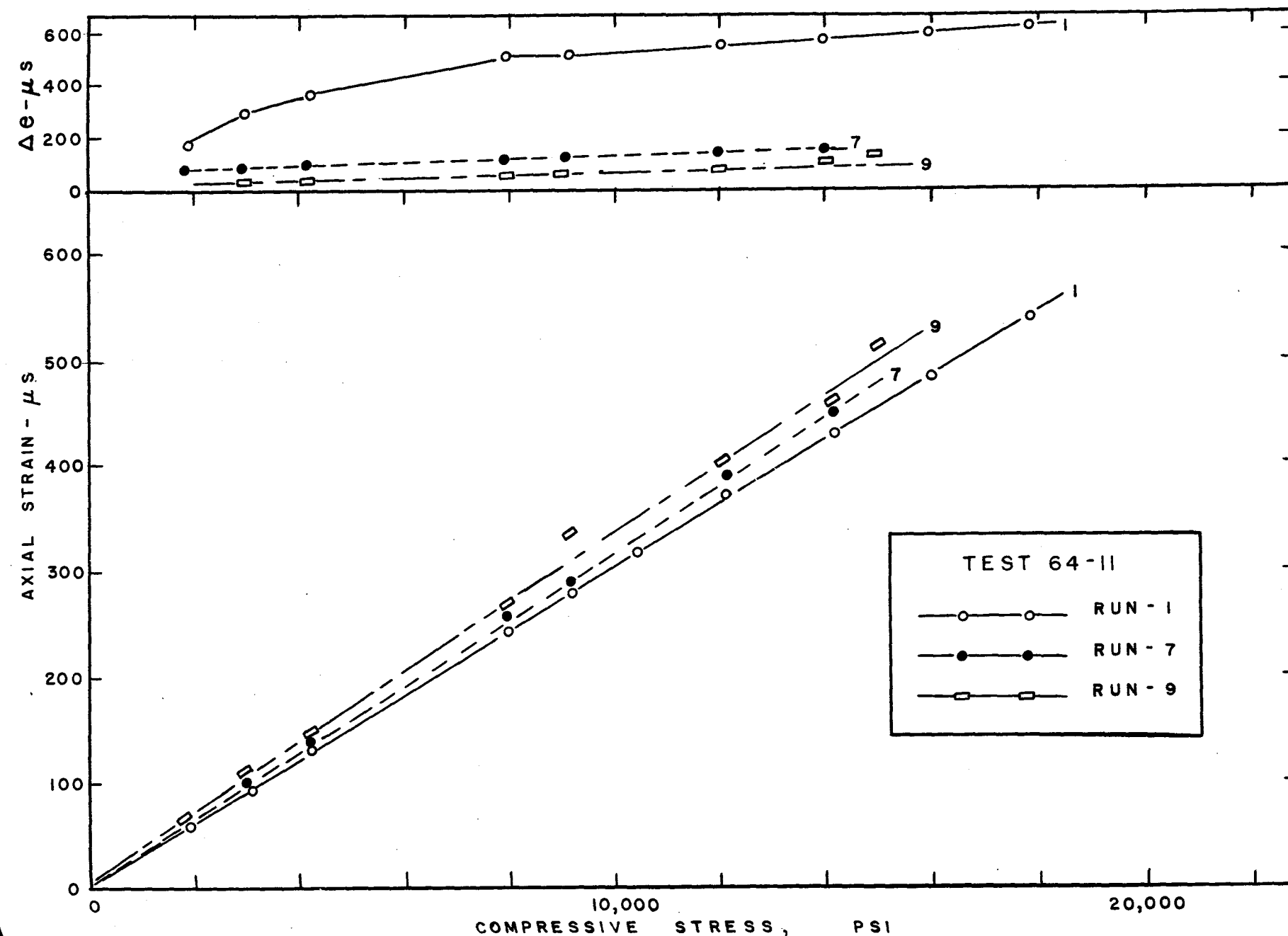
FIGURE 66 - Average Stress-Strain Curves Obtained Using Various Types of Specimen Loading Jigs.

with a spacing of 32 grooves per inch barrelling of the specimen was elimi-nated. Studies on specimens with D/H ratios of 1.5 and 0.75 showed that the yield stress was independent of the D/H ratio only when specimens with grooved ends were used. A similar method of end-preparation might be applied to rock specimens used in compression tests.

1.8.3 Loading Heads with Deformable Inserts

It was decided to study the effect of loading the specimen through a pad of some relatively deformable material that was contained laterally in a hollow loading head. Such an arrangement has some of the advantages of fluid-type loading but none if its disadvantages. A set of hollow loading heads was designed to fit the existing anvils on the loading jig as shown in Figure 64E. The hollow ends of these heads were machined to have a small diametric clearance (0.003 inch) with the test specimen and were fitted with removable, short, cylindrical Teflon inserts. Figure 67 gives further details of this loading arrangement. Two tests (64-11(11, 12)) were carried out using this arrangement. The results for the individual gages from Test 64-11(12) are shown in Figure 68 and the curves of average strain (e_a) and the deviation (Δe) against stress for both experiments are shown in Figure 69. The curves for the individual gages as well as the average were found to be linear and passed through zero. The maximum deviation (Δe) up to a stress level of 25,000 psi was 10 μs and appeared to be independent of stress level. It is also important to note the very close agreement between the two tests. Since the loading jig was completely disassembled after Test 64-11(11) and reassembled for the following test, this agreement indicates the excellent reproducibility and uniformity of the loading technique.

Examination of the Teflon insert after loading showed that a fine lip about 1/64 of an inch high had developed on the insert in the dia-metric clearance between the specimen and the loading head. The insert however was easily removed and appeared otherwise undamaged. It was decided however to use a new set of Teflon inserts for each test to prevent any misalignment due to the presence of the lip.

A series of experiments using this jig was later conducted on a geologic material*. It was found that, although the apparent load uniformity was not as good as with the steel specimen, the per cent devia-tion rarely exceeded 10%. This poorer uniformity is probably due in part to the fact that the material itself has a larger grain size and is not as homogeneous as the steel specimen previously studied. Figure 70 shows the individual stress-strain curves for Specimen WO-3 and Figure 71 shows the average stress-strain and deviation curves for the same specimen.

---

* Experiments were conducted on specimens of Wombeyan marble (WO-2 to WO-7).

UPPER
ANVIL

1.000
+.0000
-.0005

1.001
±.0005

UPPER
LOADING HEAD

7/8

3/8

1/8

.755
±.001

.750
±.001

1.500
±.001

STRESS EQUALIZERS
(TEFLON INSERT)
3/8 X .750 ±.001

SPECIMEN

NOTES

1. DRAWING SCALE
   1" = 1/2"

2. ALL SURFACES
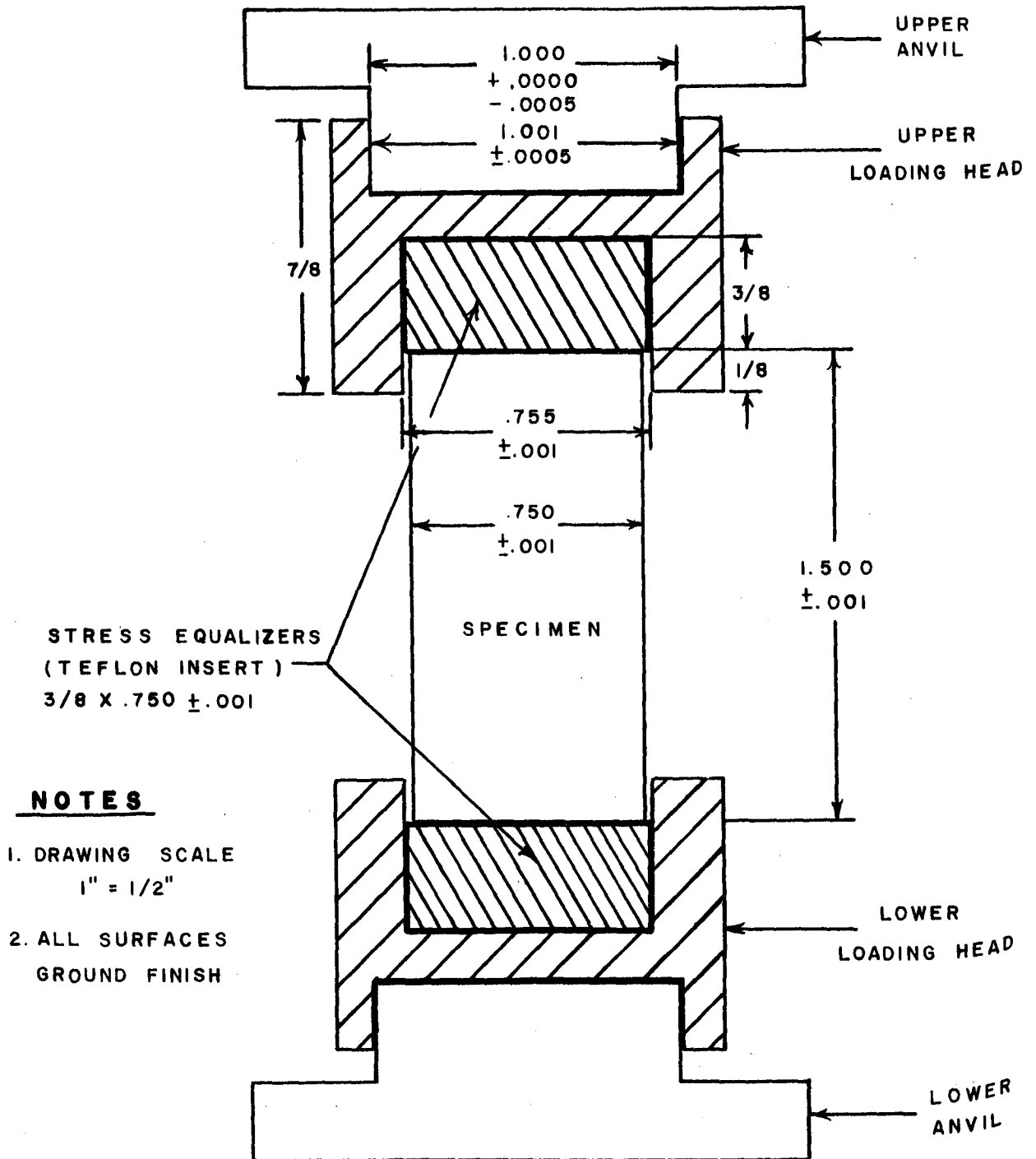   GROUND FINISH

LOWER
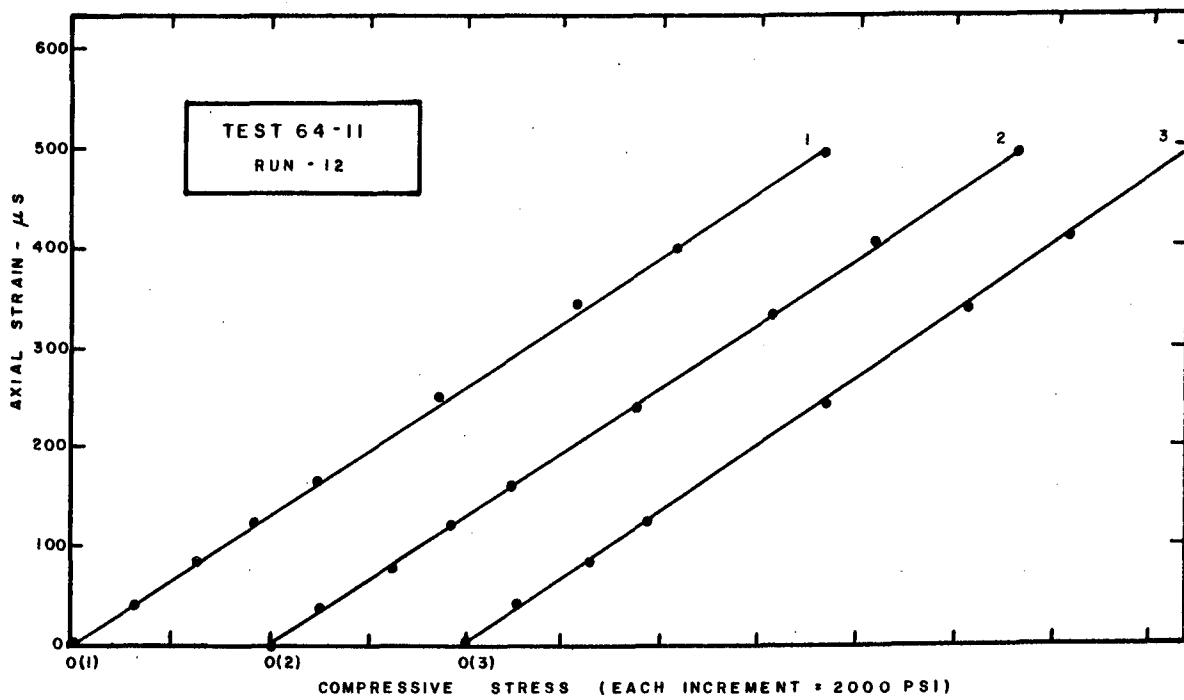LOADING HEAD

LOWER
ANVIL

FIGURE 67 - Details of Deformable Insert Type Loading Heads.

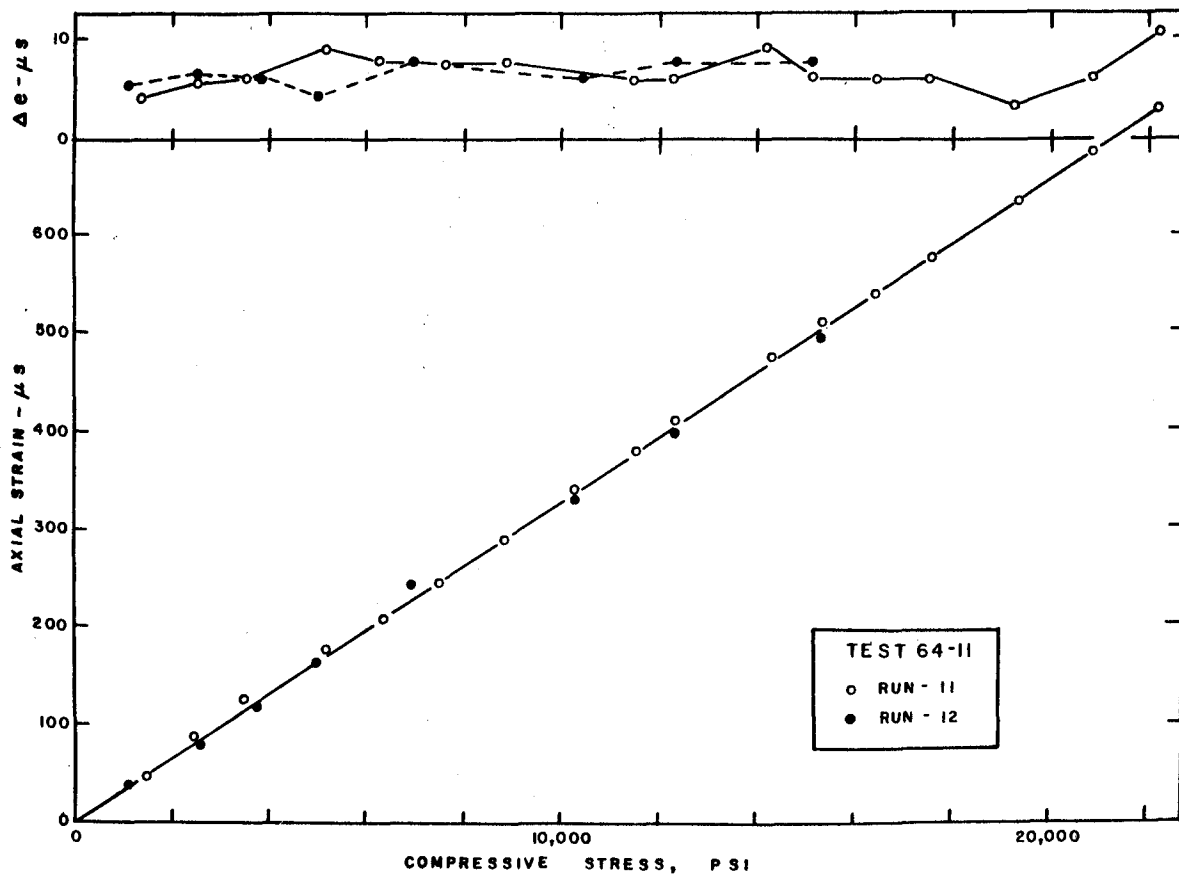FIGURE 68 - Individual Stress-Strain Curves for Steel Specimen.
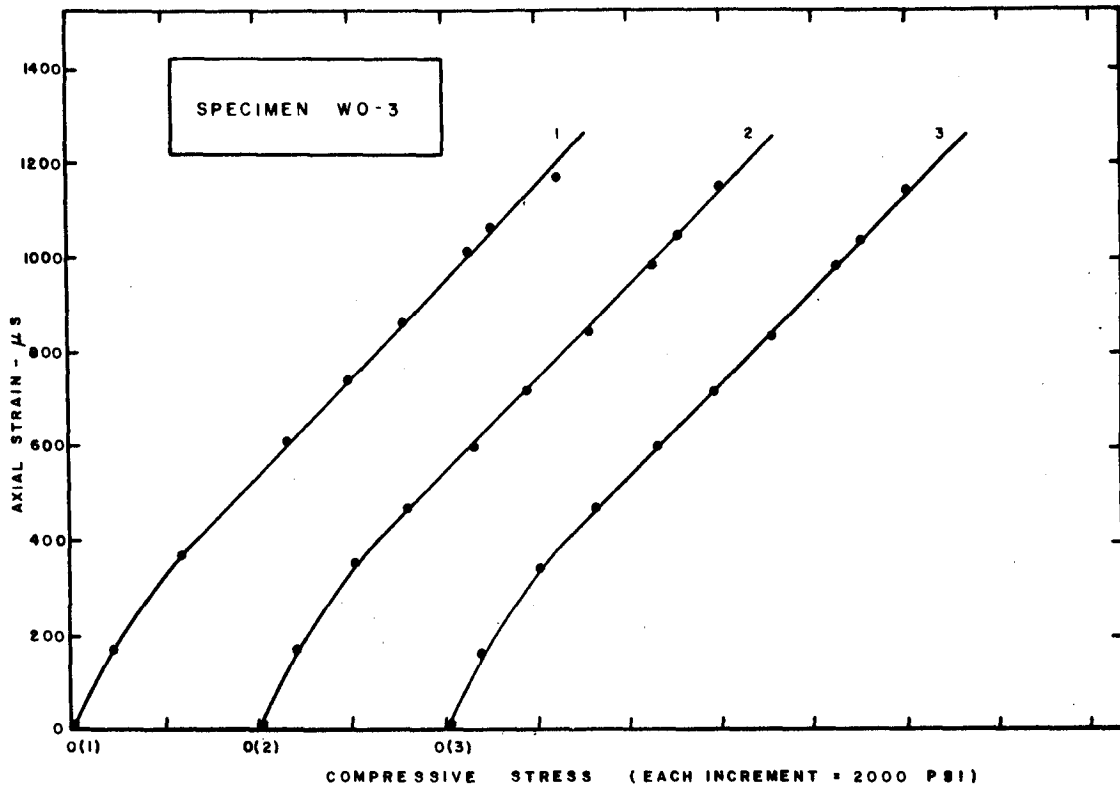

FIGURE 69 - Average Stress-Strain Curve for Steel Specimen.

FIGURE 70 - Individual Stress-Strain Curves for Wombeyan Marble.
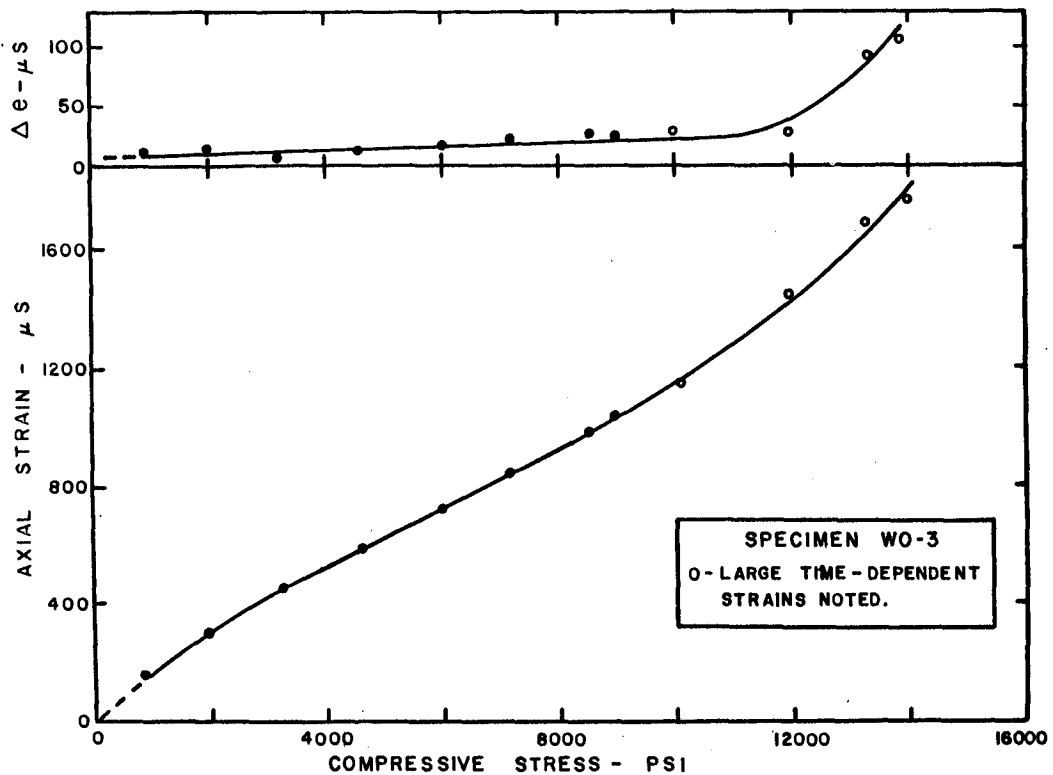
FIGURE 71 - Average Stress-Strain Curve for Wombeyan Marble.

This type of loading jig makes it possible to apply extremely uniform loading to the test specimen and as a result makes it possible to carry out very refined deformation experiments. Figure 72 shows two views of the loading jig in the form presently employed. A number of refinements to this design are planned in the future.

1.8.4 Loading Jig Friction

A secondary problem that arises when using a jig that introduces forced alignment is that of friction between the upper moving piston and the walls of the alignment cylinder. Originally this factor was neglected since the piston and cylinder were machined to a smooth finish and under zero load the piston could be freely rotated within the cylinder. However, during initial deformation experiments on Wombeyan marble the strain versus time curves were found to contain a series of step-like variations that appeared to develop each time the load control system brought the load up to the control point. A typical section from one of these strain versus time curves, illustrating a series of these variations at A, B, C and D is shown in Figure 73A. Originally no apparent reason could be found for their presence. Later in these experiments a series of incremental loading/unloading tests was carried out and the results indicated that only a fraction of the instantaneous elastic strain developed during loading appeared to be recoverable. Figure 73B indicates a typical example. Here the application of an incremental load (equivalent to a stress of 1030 psi) at A results in the instantaneous strain AB. However, the removal of the same load at C results in the recovery of a strain of only CD. A series of the characteristic step-like variations is also noted at E and F. At first it was thought these two phenomena were associated with the material itself, but the same phenomenon was observed when a calibrated steel cylinder replaced the rock specimen. To check on this anomalous behavior further, the applied load was cycled over various ranges and stress-strain curves for the steel specimen recorded directly on an X-Y plotter. In all cases an open-looped stress-strain curve was obtained similar to that shown diagrammatically in Figure 73C. As the stress increased from zero, $de/d\sigma$ was initially small up to C where it suddenly increased and remained constant with increased loading. If at some higher stress (Point D) the stress was decreased, $de/d\sigma$ became initially small again until at Point E it increased and remained constant during the remainder of the unloading. Furthermore, if the stress was only partially reduced to some Point F and then increased again, the strain followed the path F-G-D-H. These observations verified the fact that the phenomenon was definitely frictional, and led to the conclusion that the friction between the upper loading piston and the alignment cylinder was responsible. A rough estimate of this frictional force indicated that it was equivalent to 100 to 300 lb ram thrust, or 260 - 790 psi specimen stress. This frictional effect easily explained the earlier anomalous behavior that had been noted.
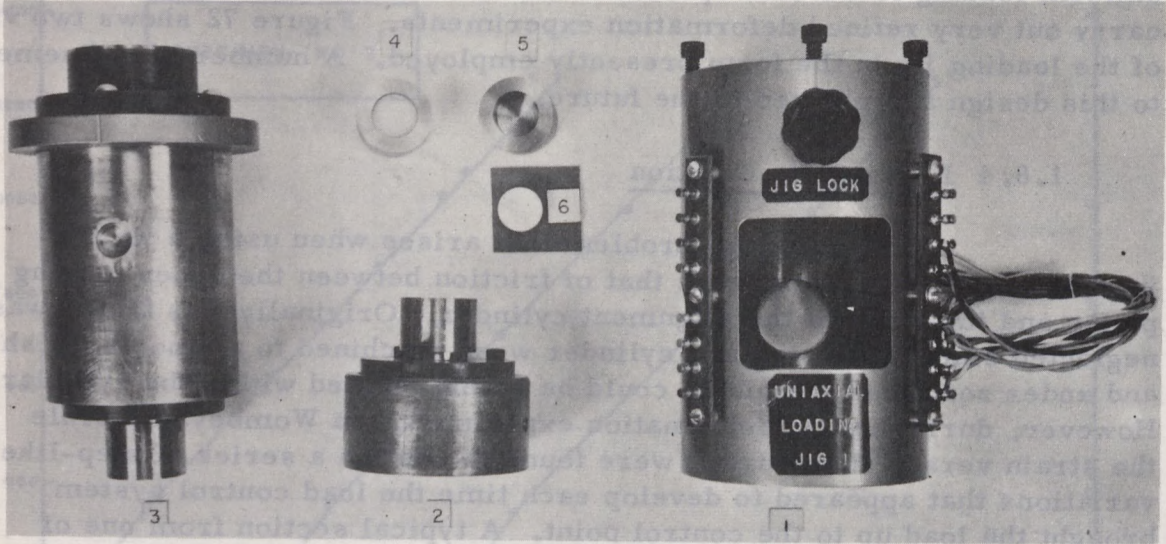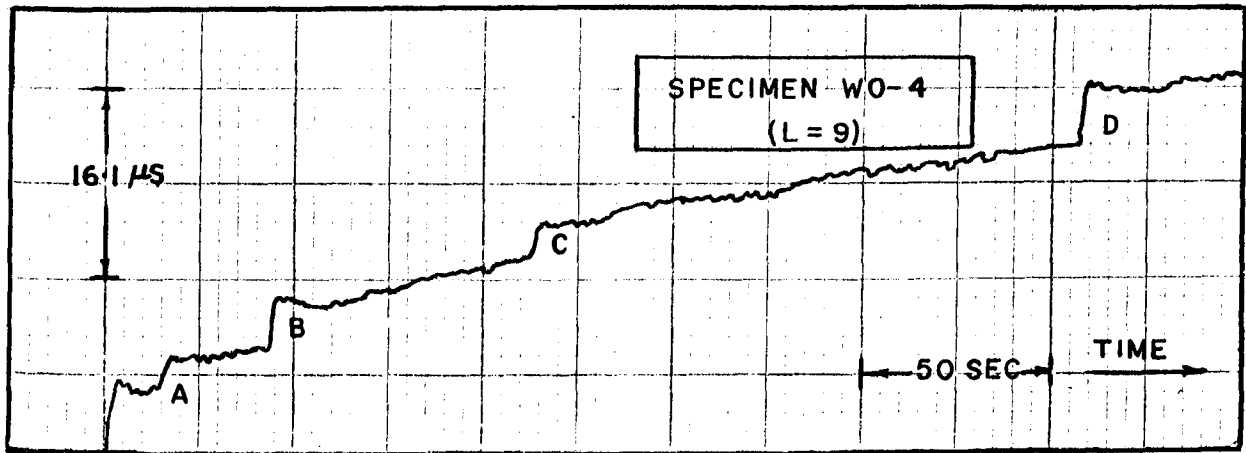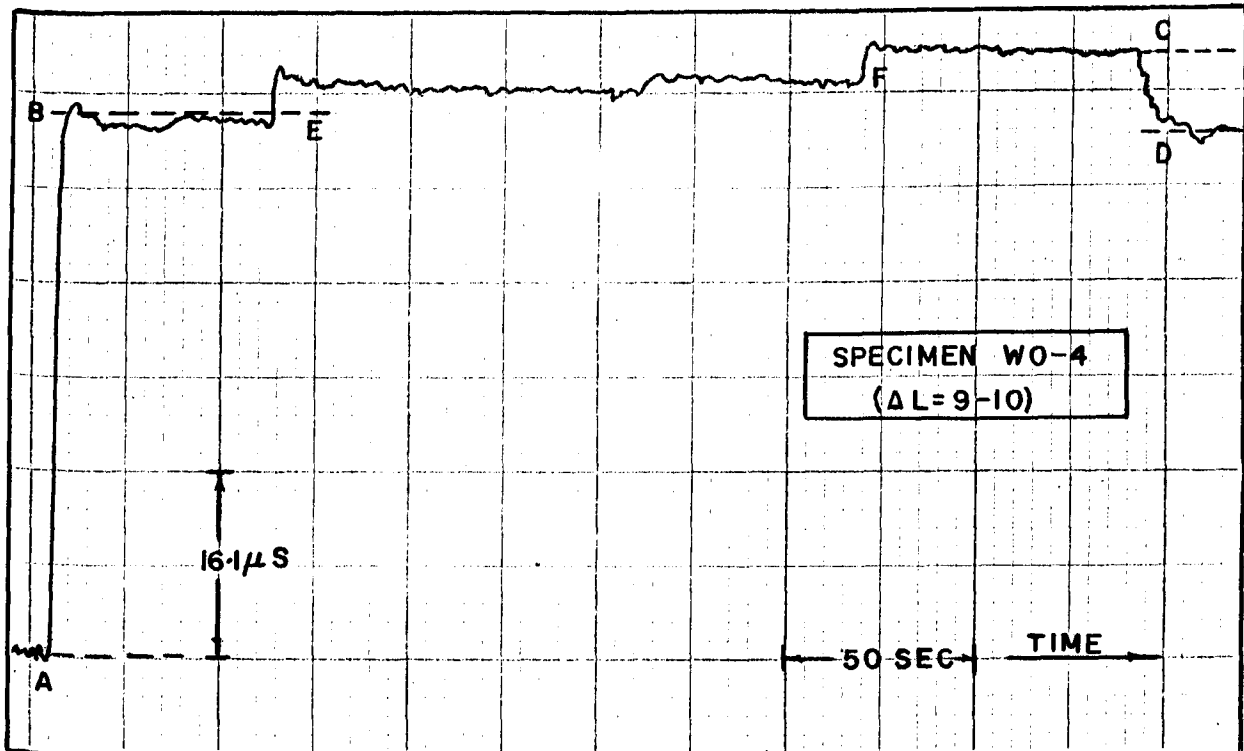
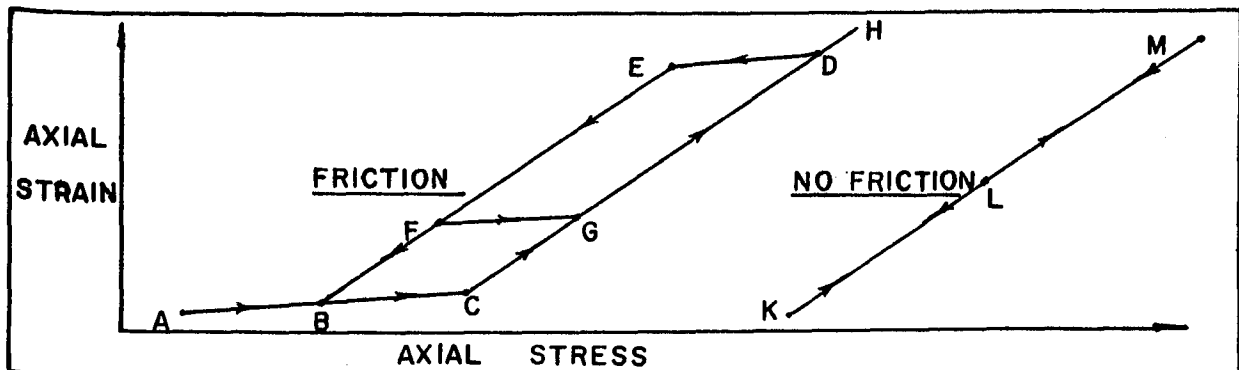A. **Parts of Specimen Loading Jig.**
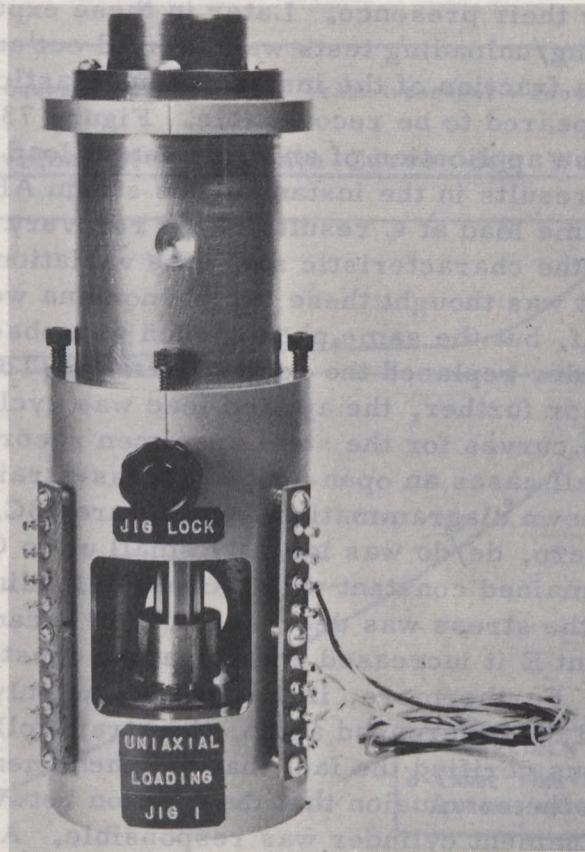
B. **Loading Jig Assembled.**

Figure 72 - <u>Photographs Showing Two Views of Loading Jig.</u>

A. STEP-LIKE VARIATIONS

B. EFFECT OF INCREMENTAL AND DECREMENTAL LOADING

C. EFFECT OF FRICTION

FIGURE 73 - Curves Showing the Effect of Friction in the Specimen Loading Jig.

To eliminate this effect, the loading procedure was modified to the following: (a) the specimen was placed in the assembled loading jig and the jig located in position in the loading frame; (b) a small preload was applied to the specimen to ensure alignment of the specimen in the loading heads; (c) the set screws holding the alignment cylinder to the lower jig block were loosened and the alignment cylinder was slid upwards along the upper jig block until it eventually became free of the lower block; (d) the alignment cylinder was locked to the upper block in the raised position; (e) the test was then continued with the specimen effectively free of the jig. Figure 73C illustrates diagrammatically a stress-strain curve KLM for the steel specimen under these conditions. It was found to be completely closed and repeatable. Using these modified loading conditions, it was found that the step-like variations in the strain versus time curves were absent and all the instantaneous strain developed during incremental loading was recovered when the load increment was removed.

1.9 Discussion

The facility has been in operation for a period of fifteen months. During that time the results of tests conducted on various systems of the facility and the results of a number of deformation experiments, conducted on specimens of geologic material, indicate that both the facility and the associated experimental techniques are satisfactory.

These studies indicate that it is possible to maintain the laboratory temperature to within $\pm$ 1/5°C, to control the axial compressive load on the specimen to within $\pm$ 1/10 per cent and to measure the resulting specimen strains to within $\pm$ 0.5 μs. Using a special loading jig it is possible to load the test specimen uniformly to such a degree that the maximum deviation of the three axial strain gages, mounted at 120° around the specimen, rarely exceeds eight per cent. The experimental method developed for rapid incremental loading and unloading was found to be satisfactory. It was found possible to make incremental stress changes of up to 1000 psi in less than three seconds, corresponding to a stress rate of approximately 300 psi/sec.

Future experiments are planned to investigate the inelastic behavior of geologic material under confinement. To date most of the facilities for these experiments have been completed. These include a triaxial test vessel and confining pressure supply that will allow experiments to be conducted at confining pressures up to 10,000 psi. A convenient method of specimen jacketing has been developed for sealing the test specimen from the confining pressure fluid. It is hoped that these experiments will commence later this year.

1. 10 Acknowledgements

1.11 References

1. Ahrendt, W.R., and Savant, C.J., Jr., "Servomechanism Practice", McGraw-Hill Book Company, Inc., New York (1960).

2. Brace, W.F., private communication, Dunbar Geophysics Laboratory, Harvard University (October 1962).

3. Brace, W.F., "Brittle Fracture of Rock", International Conf. on State of Stress in the Earth's Crust, Santa Monica, California (May 1963).

4. Brown, A., "Ground Stress Investigations in Canadian Coal Mines", AIME Trans. 211, 879 (1958).

5. Cermi, R.H., and Foster, L.E., "Instrumentation for Engineering Measurement", John Wiley and Sons, Inc., New York, pages 136-142 (1962).

6. Cross, H., private communication, Mining Research Laboratories, Mines Branch, Canadian Department of Mines and Technical Surveys, Ottawa (June 1964).

7. Donath, F.A., private communication, Geology Department, Columbia University (May 1962).

8. Evans, R.H., and Wood, R.H., "Transverse Elasticity of Natural Stones", Proc. Leeds Phil. Lit. Soc., 3 (5), 340 (1937).

9. Fairhurst, C., "Laboratory Measurement of Some Physical Properties of Rock", Proc. Fourth Symp. on Rock Mechanics, Bull. Mineral Industries Experiment Station, No. 76, page 105, Pennsylvania State University (1961).

10. Gill, D., private communication, Mining and Geophysics Department, McGill University (December 1963).

11. Gill, D., and Paquin, J.A., private communication, Mining and Geophysics Department, McGill University (February 1964).

12. Griggs, D.T., "Deformation of Rocks Under High Confining Pressures", Jour. Geol. 44, 541 (1936).

13. Griggs, D.T., and Handin, J., "Rock Deformation (Symposium)", Geol. Soc. Amer., Memoir 79 (1960).

14. Grosvenor, N.E., "Specimen Proportion-Key to Better Compressive Strength Tests", Mining Engineering, 15, 31 (1963).

15. Handin, J., "An Application of High Pressure in Geophysics - Experimental Rock Mechanics", Trans. ASME, 75, 315 (1953).

16. Handin, J., private communication, Shell Development Company, Houston, Texas (February 1960).

17. Harboe, E.M., "A Loading System for Compressive Creep Studies on Concrete Cylinders", Report C-1033, Concrete and Structural Branch, U.S. Bureau of Reclamation, Denver, Colorado (1962).

18. Hardy, H.R., Jr., "The Design and Testing of Apparatus for the Experimental Determination of the Time-Strain Characteristics of Mine Rock", FRL-234, Fuels and Mining Practice Division, Mines Branch, Canadian Department of Mines and Technical Surveys, Ottawa (1956).

19. Hardy, H.R., Jr., "Standardized Procedures for the Determination of the Physical Properties of Mine Rock Under Short-Period Uniaxial Compression", TB-8, Mines Branch, Canadian Department of Mines and Technical Surveys, Ottawa (1959).

20. Hardy, H.R., Jr., "Time-Dependent Deformation and Failure of Geologic Materials", Quarterly Colorado School of Mines, 54, 134 (1959).

21. Hardy, H.R. Jr., "A Design of Instrumentation for the Measurement of Time-Dependent Strain in Stressed Rock Specimens", ISA Transactions, 1, 147 (1962).

22. Hardy, H.R., Jr., "Development of Apparatus to Study the Strain Rate Sensitivity Factor in Copper Single Crystals by Incremental Transient Creep Experiments", M.Sc. Thesis, Physics Department, University of Ottawa (1962).

23. Hardy, H.R., Jr., "New Rock Mechanics Program Underway by Canadian Government", Mining Engineering, 17, 62 (1965).

24. Hardy, H.R., Jr., and Larocque, G.E., "An Electronic-Pneumatic Load Maintaining System" (report in preparation).

25. Hardy, H.R., and MacLean, M.J., "Measurement of the Coefficient of Linear Thermal Expansion of Mine Rock" (report in preparation).

26. Hetenyi, M., "Handbook of Experimental Stress Analysis", John Wiley and Sons, Inc., New York, pages 160-238 (1957).

27. Hunt, C.A., "The Development of Apparatus to Determine the Time-Dependent Properties of Rock Salt and Their Measurement on Several Specimens", IR FMP-62/60-MIN, Fuels and Mining Practice Division, Mines Branch, Canadian Department of Mines and Technical Surveys (1962).

28. Kerper, M.J., Mong, L.E., Stiefel, M.B., and Holley, S.F., "Evaluation of Tensile, Compressive, Torsional, Transverse, and Impact Tests and Correlation of Results for Brittle Cermets", Jour. Res. Nat. Bur. Standards, 61 (3), 149 (1958).

29. Larocque, G.E., "Measurement of the Mechanical Properties of Eight Rock Types as part of the Jet Piercing Project", IR FMP-60/37-MIN, Fuels and Mining Practice Division, Mines Branch, Canadian Department of Mines and Technical Surveys (1960).

30. Leeman, E.R., and Grobbelaar, C., "A Compressometer for Obtaining Stress-Strain Curves of Rock Specimens Up to Fracture", J. Sci. Instrum., 34, 279 (1957).

31. Leeman, E.R., and Grobbelaar, C., "A Lateral Extensometer for the Determination of Poisson's Ratio of Rock", J. Sci. Instrum., 34, 503 (1957).

32. Lion, K.S., "Instrumentation in Scientific Research", McGraw-Hill Book Co. Inc., New York, pages 167-176 (1959).

33. Loizou, N., and Sims, R.B., "The Yield Stress of Pure Lead in Compression", Jour. Mech. Phys. Solids, 1, 234 (1953).

34. Obert, L., Windes, S.L. and Duvall, W.I., "Standardized Tests for Determining the Physical Properties of Mine Rock", RI 3891, Bureau of Mines, U.S. Department of the Interior, College Park, Maryland (1946).

35. Papirno, R., "Elevated Temperature Extensometer using a Differential Capacitor Sensor", Tech. Report SM-60-2, Eng. Res. Division, New York University (1960).

36. Paquin, J.A., "Some Aspects of Uniaxial Compression in Rocks", Proc. Second Canadian Rock Mechanics Symposium, Queen's University, page 73 (December 1963). (Published by Mines Branch, Canadian Department of Mines and Technical Surveys, 1964.)

37. Peterson, R.E., "Stress Concentration Design Factors", John Wiley and Sons, Inc., New York (1953).

38. Phillips, D.W., "Tectonics of Mining", Colliery Engineering, _25_, 312 (1948).

39. Price, N.J., "A Study of the Time-Strain Behaviour of Coal-Measure Rocks", Int. J. Rock Mech. Mining Sci., _1_, 277 (1964).

40. Robertson, E.C., "Experimental Study of the Strength of Rocks", Bull. Geol. Soc. Amer., _66_, 1275 (1955).

41. Robertson, E.C., private communication, U.S. Geological Survey, Silver Spring, Maryland (February 1959).

42. Serdenzecti, S., and Boozer, G.D., "The Effects of Strain Rate and Temperature on the Behaviour of Rocks Subjected to Triaxial Compression", Proc. Fourth Symp. on Rock Mechanics, Bull. Mineral Industries Experiment Station, No. 76, page 83, Pennsylvania State University (1961).

43. Shih, T., "Investigation of the Physical Properties of a Gaspé Skarn", Proc. Second Canadian Rock Mechanics Symp., Queen's University, page 75 (December, 1963). (Published by Mines Branch, Canadian Department of Mines and Technical Surveys, 1964.)

44. Sokolnikoff, I.S., "Mathematical Theory of Elasticity", McGraw-Hill Book Co., New York (1956).

45. Solvason, K.R., private communication, Building Research Division, National Research Council, Ottawa (1961).

46. Thaler, G.J., and Brown, R.G., "Analysis and Design of Feedback Control Systems", 2nd Edition, McGraw-Hill Book Co. Inc., New York (1960).

47. Truxal, J.G., "Control Engineers Handbook", McGraw-Hill Book Co. Inc., New York (1958).

48. Udd, J.E., private communication, Mining and Geophysics Department, McGill University (February 1964).

- - - -

HRH:DV